PREPARATION AND PROPERTIES OF KNbO$_3$-BASED PIEZOELECTRIC CERAMICS

THÈSE N^O 3856 (2007)

PRÉSENTÉE LE 31 AOÛT 2007

À LA FACULTÉ DES SCIENCES ET TECHNIQUES DE L'INGÉNIEUR

Laboratoire de céramique

PROGRAMME DOCTORAL EN SCIENCE ET GÉNIE DES MATÉRIAUX

ÉCOLE POLYTECHNIQUE FÉDÉRALE DE LAUSANNE

POUR L'OBTENTION DU GRADE DE DOCTEUR ÈS SCIENCES

PAR

Evelyn HOLLENSTEIN

ingénieur en science des matériaux diplômée EPF
de nationalité suisse et originaire de Bichelsee-Balterswil (TG)

acceptée sur proposition du jury:

Prof. H. J. Mathieu, président du jury
Prof. N. Setter, Dr D. Damjanovic, directeurs de thèse
Dr M. Demartin-Maeder, rapporteur
Prof. H. Hofmann, rapporteur
Prof. P. Nanni, rapporteur

EPFL

ÉCOLE POLYTECHNIQUE
FÉDÉRALE DE LAUSANNE

Suisse
2007

Abstract

During the last several years, new lead-free piezoelectric materials have been developed to replace the lead-based materials, such as PZT. Presently, the family of lead-free ceramics showing the most promising piezoelectric properties is based on potassium sodium niobate (KNN). The KNN ceramics have been investigated since 1960s, but many problems arise, especially during the synthesis. Potassium and sodium based powders are moisture sensitive leading often to disintegration of samples after sintering and to moisture dependent properties. Another drawback is the poor densification during sintering. Elaborated procedures (hot pressing, special handling of powders) are needed to produce high quality KNN ceramics in a reproducible way, and their properties are inferior to those of PZT. Li, Ta and Sb modified KNN, however, were reported in 2004 to exhibit properties comparable to those of PZT. These modified compositions promise to be a new generation of environmentally safer piezoelectric materials. The goals of this thesis are to prepare selected compositions within this family and examine their properties relevant for applications in medical transducer. The emphasis of the work is on piezoelectric properties and their stability with respect to the temperature, humidity, and preparation conditions.

The unmodified, and lithium $(K, Na, Li)NbO_3$ and the lithium with tantalum modified KNN ceramics, $(K, Na, Li)(Nb, Ta)O_3$ have been produced by the conventional solid state synthesis. The conventional processing steps have been adapted with a goal to obtain reproducible high quality samples without using complex techniques such as hot pressing or special powder handling. In particular, the particle grain size and particle size distribution have been controlled for all the steps; this control starts with the initial powders. To reduce the particle sizes the most efficient milling method has been found to be attrition milling. Another important point is the compositional homogeneity. To improve this homogeneity, a second calcination step has been added to the process. Finally, the sintering step is sensitive, the sintering temperature range in these compositions is as narrow as 5 °C and in some cases, the dwell time is reduced to minimum (several minutes) to avoid grain growth. The densities of the so-obtained ceramics are higher than 95%, but some compositional inhomogeneities have been observed in electron microscopy. The electromechanical properties at room temperature are promising for example $d_{33} = 240$ [pm/V], $k_t = 51\%$, $k_p = 45\%$ with $\varepsilon = 919$ [-] and $\tan\delta = 2.6\%$ for ceramics modified with 7 at% lithium, and $d_{33} = 310$ [pm/V], $k_t = 46\%$, $k_p = 46\%$ with $\varepsilon = 829$ [-] and $\tan\delta = 2.4\%$ for ceramics modified with 3 at% lithium and 20 at% tantalum. These properties are especially enhanced for compositions with the orthorhombic to tetragonal phase transition close to room temperature. Dielectric and piezoelectric (resonance, converse and direct) measurements as a function of temperature have demonstrated that the orthorhombic to tetragonal phase transition is strongly dependent on temperature unlike in PZT, where it is controlled primarily by the composition. The thermal behaviour of ceramics is thus influenced by the presence of the phase transition in the analysed temperature range. The

thermal stability has been analysed in the perspective of medical transducers, which are subjected to sterilisation cycles up to 140 °C. A depolarisation after the first cycle has been observed for all the compositions, the smallest being for the lithium and tantalum modified KNN ceramics. After the second cycle, the properties stabilise, being the best for the compositions $(K_{0.465}Na_{0.465}Li_{0.07})NbO_3$ and $(K_{0.485}Na_{0.485}Li_{0.03})(Nb_{0.80}Ta_{0.20})O_3$. As the enhanced piezoelectric properties of these materials are related to the presence of a phase transition, the determination of the contributions of the domain walls in either phase is then of practical importance. The intrinsic and extrinsic contributions of the piezoelectric response can be separated by analysing the piezoelectric response as a function of the applied stress (direct measurements). It has then been shown that the intrinsic contribution is always higher than the irreversible domain wall motion contribution. This latter contribution is nevertheless higher in the orthorhombic phase than in the tetragonal phase. Finally, as the potassium niobate based ceramics have shown in the past their moisture sensitivity, aging measurements have been done in different atmospheres. Surprisingly, the properties of the modified KNN ceramics studied are not found to be dependent on the moisture and only small aging has been noticed. After 100 days, the $(K_{0.485}Na_{0.485}Li_{0.03})(Nb_{0.80}Ta_{0.20})O_3$ ceramics show a decrease of the electromechanical properties below 10% and the coupling coefficient are almost stable with time. With these electromechanical properties and their time/thermal stabilities the modified KNN ceramics are promising substitutes to lead-based materials, in particular the lithium and tantalum modified ceramics.

Résumé

Durant ces dernières années, de nouvelles céramiques piézoélectriques sans plomb ont été développées afin de remplacer les matériaux à base de plomb, comme le PZT dont la toxicité par rapport à l'homme et à l'environnement a été démontrée. Actuellement, la famille de céramiques sans plomb montrant les propriétés piézoélectriques les plus prometteuses est basée sur le niobate de sodium et potassium (KNN). Bien que les céramiques KNN ont été étudiées dès les années 1960, leur synthèse présente encore de nombreuses difficultés. En effet, les poudres à base de sodium et potassium sont sensibles à l'humidité menant souvent à une désintégration des échantillons après le frittage et des propriétés dépendantes de l'humidité. Un autre désavantage de ce matériau est la faible densification lors du frittage. Des procédures élaborées (pressage à chaud, manipulation spéciale des poudres) sont nécessaires afin de produire des céramiques KNN de haute qualité de manière reproductible et leurs propriétés sont inférieures à celles des PZT. Des céramiques KNN modifiées avec du lithium, du tantale et de l'antimoine ont été rapportées en 2004, affichant des propriétés comparables au PZT. Ces compositions modifiées promettent d'être une nouvelle génération de céramiques piézoélectriques plus sûre du point de vue écologique. Le but de cette thèse est de préparer des céramiques de compositions choisies dans cette famille et d'examiner leurs propriétés en vue d'une application en tant que "transducteurs" dans le domaine médical. L'accent est mis sur les propriétés piézoélectriques et leur stabilité en ce qui concerne la température, l'humidité et les conditions de préparation.

Des céramiques KNN non modifiées et modifiées au lithium (K, Na, Li)NbO$_3$ et au tantale (K, Na, Li)(Nb,Ta)O$_3$ ont été préparées par synthèse conventionnelle en phase solide. Les étapes de la synthèse ont été adaptées avec comme but d'obtenir de manière reproductible des céramiques de haute qualité sans avoir recours à des techniques complexes comme le pressage à chaud ou une manipulation spéciale des poudres. En particulier, la taille des particules et leur distribution ont été contrôlées lors de chaque étape, ce en commençant par les poudres initiales. Afin de diminuer la taille des particules, plusieurs méthodes de broyage ont été testées et le broyage par attrition s'est révélé être la plus efficace. Afin d'améliorer l'homogénéité de la composition, une seconde calcination a été ajoutée dans la synthèse. Finalement, le frittage s'est révélé être une étape sensible, car la plage de température de frittage est très étroite, environ 5 °C, et dans certains cas, le temps de palier à observer doit être très court (quelques minutes) afin d'éviter la croissance exagérée des grains. Les densités des céramiques obtenues sont supérieures à 95%, mais des inhomogénéités ont été observées grâce à la microscopie électronique. Les propriétés électromécaniques à température ambiante sont prometteuses; par exemple d$_{33}$ = 240 [pm/V], k$_t$= 51%, k$_p$= 45%, ε = 919 [-] et tanδ = 2.6% pour des céramiques modifiées avec 7 at% de lithium et d$_{33}$ = 310 [pm/V], k$_t$= 46%, k$_p$= 46%, ε = 829 [-] et tanδ = 2.4% pour des céramiques modifiées avec 3 at% de lithium et 20 at% de tantale. Ces propriétés sont spécialement élevées pour des compositions possédant la transition de

phase de orthorhombique à tétragonale proche de la température ambiante. Des mesures diélectriques et piézoélectriques (résonance, effet direct et converse) en fonction de la température ont démontré que la transition de phase de orthorhombique à tétragonal est fortement dépendante de la température, par opposition au PZT, pour lequel cette transition est contrôlée principalement par la composition. Le comportement en fonction de la température pour de telles céramiques est donc influencé par la présence d'une telle transition dans la plage de température étudiée. La stabilité en fonction de la température a été analysée dans la perspective de transducteurs médicaux, qui sont stérilisés à 140 °C avant chaque utilisation. Une dépolarisation après le premier cycle a été observée pour toutes les compositions, la plus faible étant pour les compositions modifiées avec du lithium et du tantale. Après le deuxième cycle, les propriétés se stabilisent et sont les meilleures pour les compositions $(K_{0.465}Na_{0.465}Li_{0.07})NbO_3$ et $(K_{0.485}Na_{0.485}Li_{0.03})(Nb_{0.80}Ta_{0.20})O_3$. Comme les propriétés piézoélectriques élevées sont reliées à la présence de la transition de phase, la détermination de la contribution des parois de domaine dans chaque phase est d'importance pratique. Les contributions intrinsèque et extrinsèque de la réponse piézoélectrique peuvent être séparées en analysant la réponse piézoélectrique en fonction de la contrainte appliquée (mesures directes). Il a été montré que la contribution intrinsèque est toujours supérieure à la contribution du mouvement irréversible des parois de domaine. Cette dernière est néanmoins plus importante dans la phase orthorhombique comparée à la phase tetragonale. Finalement, comme les céramiques à base de niobate de potassium ont montré dans le passé leur sensibilité à l'humidité, des mesures de vieillissement ont été effectuées à différents taux d'humidité. Etonnement, les propriétés des céramiques KNN modifiées ne montrent pas de dépendance par rapport à l'humidité et un vieillissement très faible. Après 100 jours, les propriétés électromécaniques des céramiques de composition $(K_{0.485}Na_{0.485}Li_{0.03})(Nb_{0.80}Ta_{0.20})O_3$ sont diminuées de 10% et les coefficients de couplages sont quasiment constants en fonction du temps. Avec ces propriétés électromécaniques ainsi que leur stabilité en fonction du temps et de la température, les céramiques KNN modifiées sont des substituts prometteurs pour des matériaux à base de plomb et en particulier les compositions KNN modifiées avec du lithium et du tantale.

Mots-clés: sans plomb, synthèse, piézoélectrique, transition de phase et stabilité.

Acknowledgments

First I would like to thank my two thesis directors, Prof. Nava Setter and Dr. Dragan Damjanovic for offering me the possibility to work in the ceramics laboratory. I gratefully acknowledge Dragan Damjanovic for his support, precious advices and answers during the 4 years and his patience reading and correcting my manuscript.

Special thanks to Paul Bowen, for his precious help for the processing during the first years of the thesis. It was a pleasure to work with you!

I would like to thank my brother and my mother for improving so much the quality of the manuscript, I could almost not recognise what I wrote!

I would like to thank my office mates, Sandrine Gentil, Enrique (Kike) Vasco Matias, Maxim Morozov, Christine Leroy and Guochu Deng for the nice atmosphere, and especially to Sandrine, with whom it's never boring! A special acknowledgement for Samuel Rey-Mermet, now our ways separate... Then to the other members of the laboratory, Marlyse Demartin Maeder, for her help during the first years of my PhD, Jacques Castano, the hot-pressing specialist, Antonin Faes, for the TEM pictures, Matthew Davis, for all the help with experimental setups and the so many discussions, Janine Conde, Brahim Belgacem, Alvaro Artieda, Marko Budimir and so many others.

I would like to acknowledged the members of my thesis jury, Prof Mathieu, Prof. Hofmann, Dr. Demartin Maeder and Prof. Nanni, for their patience reading my manuscript and adding some useful comments.

To "l'equipe", for the coffee and diner breaks, but also the great parties, Fred Kohler, Vincent, the really "old" friends, Fred Gonzales, Stephane Vernede, Olivier Ludwig, Gael Couturier, Christoph Niederberger.

Then to my friends from outside the lab, Beatrice Nussberger, Friederike Ilschner, Swati Rastogi, Julie Bucher, Umar Raad, the Lara family, Bertrand Francey and the badminton team.

Finally, I wish to thank my family to whom I dedicate this thesis and without who it would have never been possible to achieve it: my mother, my father and my brother, you're simply the best, my aunt and uncle Anita and Hans-Jürg Aeschbacher, my cousins Stefan and Tomas Aeschbacher, my goodfather Theo Dubler and Elisabeth, y mi familia en Argentina.

At last, but not at least, Enrique, for your constant patience and love during these years!

Contents

Chapter 1

Introduction

Piezoelectric materials are nowadays widely used as transducers, actuators or sensors. They are found in many applications like in medical ultrasonic transducers or filters in mobile phones. In this part a review of the existing piezoelectric materials is presented, and in particular lead-free materials.

Lead-based ceramics are the most used compounds because of their superior piezoelectric properties [1]. These properties of lead-based materials can be related to a phase transition between two different crystallographic structures. However, one severe drawback of these compounds arises from the high toxicity of lead. Indeed, it is well known that lead based derivatives have harmful effects on human beings and the environment since even low-level lead exposure can cause a number of adverse health effects.

In order to circumvent this drawback, extensive research is focused on the quest for alternate piezoelectric materials. In that respect, the most promising lead-free piezoelectric materials are potassium niobate based compounds and in particular the modified potassium sodium niobate ceramics. In these materials, promising electromechanical properties are found for compositions near a phase transition. However, the potassium sodium niobate ceramics present many problems in particular related to their tedious manufacturing.

1.1 Piezoelectric materials

A great breakthrough in the search of new piezoelectric materials was the discovery of lead zirconate titanate solid solutions by B. Jaffe and co-workers in 1954 [2]. This finding has initiated exciting developments and led to an enormous field of applications based on piezoelectric materials. Nowadays, lead zirconium titanate, also called PZT, is the most widely used piezoelectric material. Nevertheless it should be kept in mind that these lead-based compounds can contain up to 60% of lead in weight [3].

Another type of lead based materials, namely the ferroelectric-relaxor families $Pb(Zn,Nb)O_3$-$PbTiO_3$ (PZN-PT) and $Pb(Mn,Nb)O_3$-$PbTiO_3$ (PMN-PT), display the highest known piezoelectric coefficients. For some particular compositions and crystal orientations, the piezoelectric coefficient can reach 2500 pC/N and the thickness coupling coefficient 97% for single crystals [4]. These high piezoelectric properties are related to a so called "morphotropic phase boundary" (MPB). This MPB can be defined as a "change in the structure of a crystal occurring when the replacement of one of its chemical constituents by another reaches a certain critical level"(Oxford English Dictionary). The $PbZrO_3$ - $PbTiO_3$ system was the first binary system to show such a phase transition (see Figure 1.1).
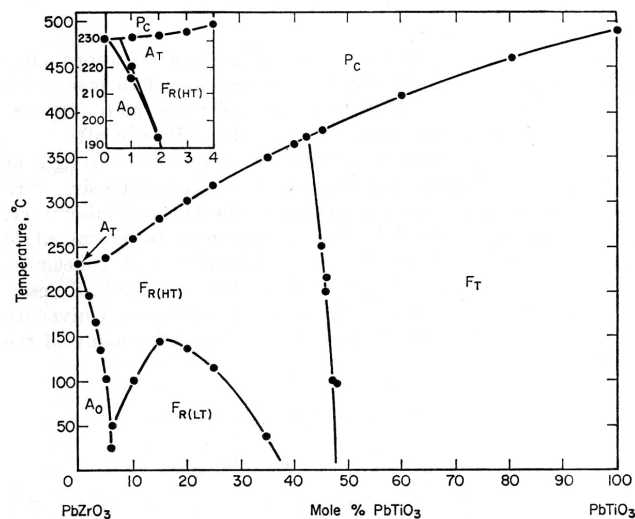
Figure 1.1: Phase diagram of the $PbZr_{1-x}Ti_xO_3$ system [1].

The MPB in the $PbZr_{1-x}Ti_xO_3$ system clearly separates the rhombohedral structure adopted for zirconium rich compounds (on the left-hand side of the diagram) from the tetragonal structure found for titanium rich systems (right-hand side) at around 52% zirconium while at room temperature. This system features a large dielectric constant at the morphotropic phase boundary, as well as high electromechanical properties, as shown in Figure 1.2.
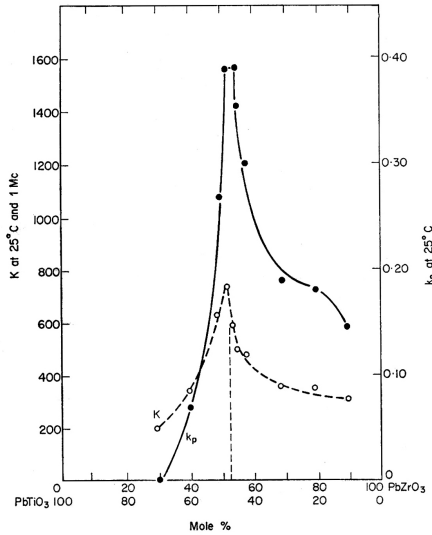
Figure 1.2: Permittivity (K) and planar coupling coefficient (k_p) as a function of the composition in $PbZr_x Ti_{1-x}O_3$ [1].

In the vicinity of the phase transition from tetragonal to rhombohedral phases in PZT, an intermediate monoclinic phase has been discovered by x-ray powder diffraction [5], as seen in Figure 1.3, which schematises the modified phase diagram for lead zirconate titanate. The high piezoelectric properties are due to a polarisation rotation, which is probably facilitated in the presence of this monoclinic structure [6].
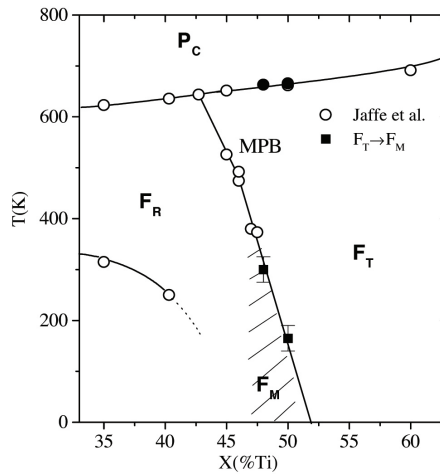
Figure 1.3: Phase diagram of the $PbZr_{1-x}Ti_xO_3$ system including the monoclinic phase [7].

In the $PbZr_{1-x}Ti_xO_3$ system, this MPB has the characteristic to be nearly vertical, i. e. to be temperature independent, which is not the case for other systems like PMN-PT or PZN-PT. Nevertheless, the electromechanical properties of such systems also reach maximal values around the phase transition, as shown in Figure 1.4.

3

Figure 1.4: Piezoelectric k_{33} and d_{33} for the $Pb(Zr,Nb)O_3$-$PbTiO_3$ system [8, 9].

To optimise the properties for specific applications, the properties of PZT ceramics are modified by introduction of dopants, being either donor (of higher charge than that of the ions they replace), or acceptor type (of lower charge than that of the replaced ions). In the first case, the introduced dopants are compensated by cation (A-site) vacancies and in the second case by oxygen vacancies, whose mobility is higher [10]. The donor doped PZT ceramics (with Nb^{5+}), which are called "soft" PZ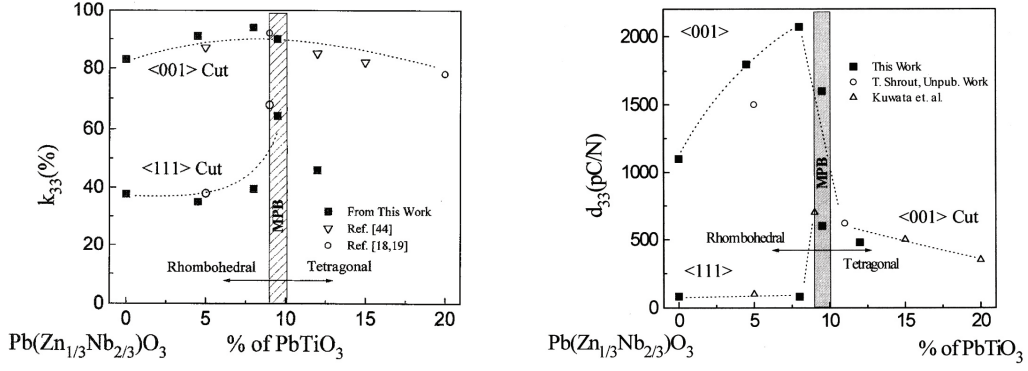T, show increased piezoelectric properties, small aging effects, but also increased dielectric losses compared to acceptor doped PZT ceramics (with Fe^{3+}), which are called "hard" PZT. The high losses are mainly due to the movement of the domain walls [1].

Typical electromechanical properties of commercially available soft (Pz27) and hard (Pz24) PZT ceramics are given in Table 1.1.

Table 1.1: Electromechanical properties of commercial PZT-based ceramics from Ferroperm Piezoceramics [11].

Properties	Pz24	Pz27
ε [-]	425	1800
$\tan\delta$ [-]	0.002	0.017
T_c [°C]	330	350
k_p [-]	0.49	0.59
k_t [-]	0.51	0.47
k_{31} [-]	0.29	0.33
k_{33} [-]	0.66	0.70
d_{31} [pC/N]	-58	-170
d_{33} [pC/N]	149	425
ρ [g/cm^3]	7.7	7.7
$\nu_{12}{}^E$ [-]	0.300	0.389

Based on the properties shown in Table 1.1 it becomes apparent that soft PZT derived piezoelectric ceramics show low losses (lower than 2%), with typical piezoelectric coefficients d_{33} around 400 pC/N and thickness coupling coefficients k_t of about 50%.

The concept of morphotropic phase boundary can be used to design new materials with increased electromechanical properties, and in particular for the development of lead-free

ceramics based on potassium sodium niobate (KNN). This concept is schematised in Figure 1.5.
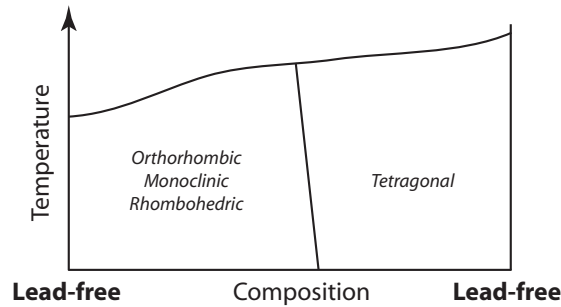

Figure 1.5: New design of lead-free ceramics based on the MPB concept found for Pb(Zr,Ti)O₃.

In this figure, the choice of the component on the right of the MPB can be modified, as the component on the left, with orthorhombic structure, is set to potassium sodium niobate. The choice of this component should nevertheless not be restricted only to tetragonal structures.

1.2   Lead-free vs lead-based piezoelectric ceramics

Lead-based materials have a high lead content (around 60% in weight), which has impacts on the human health and the environment. Since biocompatibility, for example, could be a requirement while choosing a material, these toxic effects of lead derivatives restrict their applicability.

Low concentrations of lead and lead derivatives can be highly toxic if the substances are ingested or inhaled. Furthermore, a constant exposure leads to a gradual accumulation of lead in the human body. These toxic substances are absorbed by the red blood cells (causing high blood pressure) and circulate through the body where they accumulate in lipids of soft tissues. In general lead can damage almost every organ system, with the most prone to damage being the brain, the nervous system, the kidneys, and the blood. For children, the exposure to high lead concentrations can cause slowed growth, behaviour disorders or learning disabilities [12].

During the processing of lead-based materials, lead oxide vaporises, leading to a difficult control of the content but above all, a dissemination of lead in the environment. It is well known that lead remains in the environment for a long time and it is therefore important to solve the problem of recycling of lead-containing devices, as for example computers. Indeed, the recycling of microelectronic devices generates an important quantity of lead-containing waste and thus, the quest for lead-free ceramics is of primal importance in this field.

1.3   Lead-free ceramics families

In this section, two types of lead-free piezoelectric ceramics will be considered, namely the ceramics with good electromechanical properties (including the $(K,Na)NbO_3$, $BaTiO_3$

and (Bi,Na,K)TiO$_3$ families) and the ceramics for high temperature applications (the Bi$_4$Ti$_3$O$_{12}$ family, LiNbO$_3$ and LiTaO$_3$), which display lower piezoelectric properties at room temperature. Some low lead-containing ceramics also have good properties (BiScO$_3$-PbTiO$_3$), but won't be described in this thesis.

1.3.1 Lithium tantalate and niobate

For high temperature applications, LiNbO$_3$ and LiTaO$_3$ crystals are interesting, as their Curie temperatures are high compared to other piezoelectric materials, respectively 1210 °C and 660 °C (T$_c$(PZT) $\approx$ 350 °C, T$_c$(KNbO$_3$) $\approx$ 420 °C). The Curie temperature is the temperature above which the ferroelectric materials have no more a spontaneous polarisation, i.e. the material is in the paraelectric state.

Their crystal structure at room temperature is similar to ilmenite, which is similar to the perovskite structure. For LiTaO$_3$, the coupling coefficient can reach 50% and even higher for LiNbO$_3$ (0.68), but the piezoelectric coefficients are for both inferior to 10 pC/N. They are mostly used in surface acoustic wave devices due to their low acoustic losses.

1.3.2 Bismuth titanate based

Bismuth titanates display high Curie temperatures (e.g. T$_c$(Bi$_4$Ti$_3$O$_{12}$) = 685 °C and T$_c$(Bi$_3$TiNbO$_9$) = 940 °C), making them interesting for high temperature piezoelectric applications [13]. Bismuth titanate Bi$_4$Ti$_3$O$_{12}$ has pseudo-perovskite layers stacked between bismuth oxide layers. The presence of these layers confers an anisotropy to the piezoelectric properties of this compound. Furthermore, the highest piezoelectric properties are observed in the *ab* plane, in which the ceramic platelets grow and where the polarisation is maximal. However, a drawback of pure Bi$_4$Ti$_3$O$_{12}$ is the high conductivity in this *ab* plane, this problem becoming more important with increasing temperature, and thus making them difficult to pole. A way to decrease the conductivity is to introduce niobium into the titanium site, leading to a piezoelectric coefficient d$_{33}$ = 20 pC/N for 7% Nb [14]. SrBi$_4$Ti$_4$O$_{15}$ has also a high Curie temperature (T$_c$ = 530 °C) and the piezoelectric properties of this compound are stable over a wide range of driving conditions (linear, non hysteretic, no frequency dependence). These materials are used in high temperature applications, where a thermal stability is required, but with the disadvantage that their piezoelectric properties are low.

As the piezoelectric properties are highly anisotropic, templating the ceramics is a way to increase them. Indeed, CaBiTi$_4$O$_{15}$ (T$_c$ = 820 °C) ceramics have been synthesised by reactive templated grain growth (RTGG), showing d$_{33}$ $\approx$ 45 pC/N and k$_t$ $\approx$ 0.50 [15], which are 3 times higher than for non-textured ceramics.

1.3.3 Barium titanate

Historically, BaTiO$_3$ was the first piezoelectric ceramic developed on a large scale, before the use of PZT. Barium titanate has a perovskite crystallographic structure and goes through various phase transitions as a function of the temperature. Indeed, at temperatures near 0 °C (i.e. near working temperature) a change from orthorhombic to tetragonal phase is observed, whereas a transition from tetragonal to cubic (paraelectric

phase) occurs at 120 °C. Low Curie temperatures and slightly below room temperature tetragonal to orthorhombic phase transitions narrow down the temperature range available for applications of these materials, especially since the electromechanical properties often drastically vary near to the phase transitions. In order to work at temperatures significantly different from those of a phase transition, the transition temperatures can be modified by chemical substitutions.

Despite these low transition temperatures, barium titanate ceramics made out of ultra pure powder produced by hydrothermal synthesis and manufactured by microwave sintering showed high electromechanical properties d_{33} = 350 pC/N, k_p = 0.36 and ε_{33} = 4200 [16]. These properties are nevertheless influenced by the grain size, density and defects in the structure. The reproducibility of the processing is then an important issue.

1.3.4 Bismuth sodium potassium titanates

Bismuth is relatively non toxic for humans compared to other heavy metals. But bismuth has been related to disorders of the nervous system and studies have shown that the toxicity of this element varies between individuals and is not directly related to the exposure time or the quantities inhaled. As a consequence, the acute and chronic toxicity of bismuth is not well established [17]. The use of bismuth in piezoelectric materials can be considered less harmful than lead for example, but it's not well established when the toxicity should restrict its use.

The bismuth sodium titanate ceramics of composition $(Bi_{0.5}, Na_{0.5})TiO_3$ called BNT are quite difficult to pole because of a high coercive field and high conductivity but they have good piezoelectric properties compared to other lead-free ceramics (d_{33} = 125 pC/N, k_{33} = 0.40, k_p = 0.15, k_t = 0.58 and ε_r = 500 [18]). Another drawback of bismuth based ceramics is bismuth ion vaporisation during the sintering process (the sintering temperature of BNT is around 1200 °C). Compared to BNT, bismuth potassium titanates $(Bi_{0.5}, K_{0.5})TiO_3$ or BKT of 50-50 composition show lower piezoelectric properties (d_{33} = 69.8 pC/N and k_{33} = 0.28 [19]).

Solid solutions of BNT-BKT show a phase transition from rhombohedral (BNT) to tetragonal (BKT) at around 16 to 20% potassium. The piezoelectric properties seem to reach a maximum for compositions near this phase transition, since for instance, k_p = 0.31, k_t = 0.42, a ε_{33} = 1030 and d_{31} = 46.9 pC/N were observed at a potassium content of 16% [20].

The substitution of BNT in $BaTiO_3$ (also with BKT, but piezoelectric properties are lower in this case) leads to an increase of the Curie temperature of $BaTiO_3$, thus enabling an easier poling of the resulting ceramics as compared to pure BNT ceramics. The electromechanical properties are maximised around a phase transition located at 6% BNT, where d_{33} = 180 pC/N and k_p = 0.28 [21]. BNT-BT ceramics have also been produced by RTGG using $SrTiO_3$ templates. The Berlincourt-type measurements showed a small increase compared to conventionally sintered samples, with best values of d_{33} = 200 pC/N [22, 23] for near phase transition compositions. For high electric fields, the samples showed high strain, leading to high piezoelectric coefficients (d_{33} = 520 pC/N), confirming that a substantial fraction of the piezoelectric response measured in unipolar strain curves is associated with domain wall motion. For the BNT-BKT-BT system, the best current properties are found for the tetragonal composition near the phase transition

composition aBNT-bBT-cBKT (85.2, 2.8, 12): $d_{33} = 191$ pC/N, $k_{33} = 0.56$, $\varepsilon_{33} = 1140$, with $T_c = 301$ °C [24].

Starting again from the BNT-BKT system, potassium and sodium can be substituted with lithium. High electromechanical properties for such lithium modified materials were obtained recently, with the best being $d_{33} = 231$ pC/N, $k_p = 0.41$ and $k_t = 0.50$ [25].

1.3.5 Potassium niobate family

Potassium niobate goes through the same series of phase transitions as $BaTiO_3$ but with higher transition temperatures [26], since the Curie temperature is 434 °C and the transition from orthorhombic to tetragonal 224 °C for pure potassium niobate. The different temperatures of the phase transitions of $KNbO_3$ [26, 27] are shown in Figure 1.6.
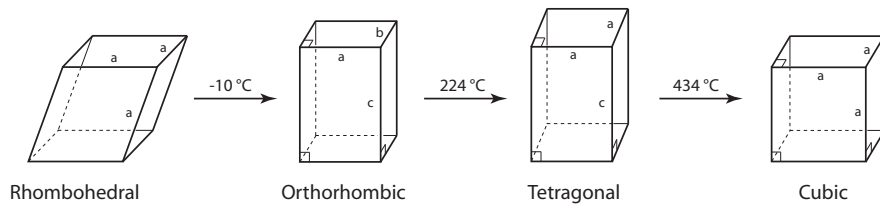
Figure 1.6: Phase transitions for potassium niobate as a function of the temperature [26, 27].

The $KNbO_3$ single crystals can exhibit high piezoelectric coefficients [26, 28, 29] depending on the crystal cut and the poling direction, for example the $[001]_c$ poled crystal shows $k_t = 0.70$ and $d_{33} = 90$ pm/V [28, 30]. Considering this high coupling coefficient, the low permittivity and the low density, this material becomes interesting for high frequency transducers.

$KNbO_3$ ceramics can be synthesised from K_2CO_3 and Nb_2O_5 in a stoichiometric manner, as shown on the phase diagram in Figure 1.7.
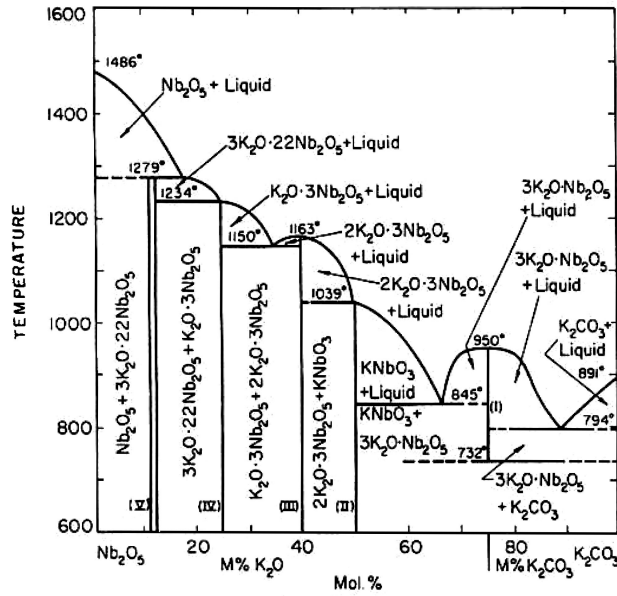
Figure 1.7: Phase diagram of the K_2O - Nb_2O_5 system [31].

Many initial powders can be chosen, $KHCO_3$ [32], K_2CO_3, KOH [33] or K_2O [31]. For $KNbO_3$ it is important to keep the right stoichiometry during the processing, because near 50% K_2O and 50% Nb_2O_5, many hygroscopic phases coexist. Leaching with a potassium carbonate solution or NH_4OH and HCl to remove the secondary phases was applied in the synthesis of potassium niobate powders [34]. The vaporisation of potassium oxide above 840 °C [35] can also lead to off-stoichiometry. The first synthesis of pure $KNbO_3$ ceramics has been reported by Flueckiger *et al* in 1977 [35]. Another difficulty is the obtaining of ceramics with high densities by conventional sintering processes. In order to improve the densification, the defect concentration can be increased and in this context many dopants have been investigated:

- <u>Pb</u>: Introducing up to 3% Pb promotes the appearance of a liquid phase during the sintering. The obtained densities are improved up to 97% of the theoretical density (4.62 g/cm^3 [36]). In this case, however, the sintering times are quite long (40 hours) but lead to a high coupling coefficient value ($k_p = 0.40$).

- <u>$LaFeO_3$</u>: The piezoelectric properties are increased by introduction of a small amount of $LaFeO_3$ into $KNbO_3$ [37, 38, 39]. The optimum concentration of $LaFeO_3$ was 0.2%, showing $d_{33} = 98$ pC/N and $k_p = 0.17$. The densification was improved and densities around 98% have been reported.

- <u>$Bi_{0.5}Na_{0.5}TiO_3$</u>: The sintered ceramics showed good densities but the electromechanical properties were not improved [40].

Sodium niobate can also be introduced in potassium niobate. The solid solution system of $KNbO_3$-$NaNbO_3$ contains several morphotropic phase boundaries, the most important one being at around 50% $KNbO_3$ and 50% $NaNbO_3$. At this composition, usually called KNN, two different orthorhombic structures coexist (Fo_1 and Fo_2), as shown in Figure 1.8.
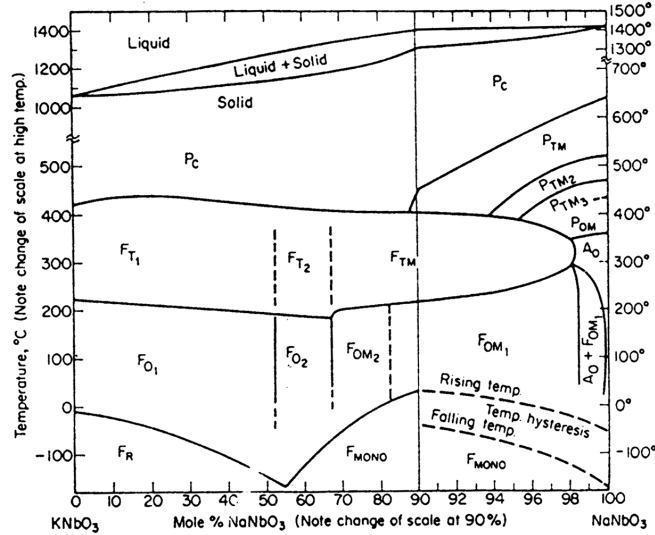
9

Figure 1.8: Phase diagram of the $KNbO_3$ - $NaNbO_3$ system [27, 41].

This phase transition between two orthorhombic structures can be compared to the morphotropic phase boundary found in $Pb(Zr,Ti)O_3$ between a rhombohedral and a tetragonal structure, but keeping in mind the similarity of the two orthorhombic structures involved. The piezoelectric properties seem to be increased around this composition [42, 43], as seen in Figure 1.9.
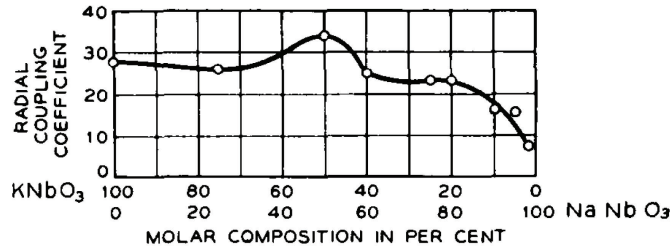
Figure 1.9: Room temperature radial coupling coefficient for $K_{1-x}Na_xNbO_3$ ceramics [42].

In function of the temperature, the KNN ceramics undergo multiple phase transitions as was observed in the case of $KNbO_3$. The Curie temperature of KNN is similar to the one of pure $KNbO_3$ (430 °C) and the transition between orthorhombic and tetragonal is around 200 °C [44]. Thus, a good stability of the properties at room temperature can be expected for KNN ceramics.

One important issue for potassium sodium niobate is the densification step, since, and in analogy to potassium niobate, ceramics produced by the conventional mixed-oxide route have low densities. One way to obtain denser, i.e. up to 99% [45] (theoretical density 4.51 g/cm^3 [46]), homogeneous and fine grained ceramics is to replace the conventional sintering by a hot-pressing step or plasma spark sintering (SPS). The hot-pressed samples show better properties, a higher coupling coefficient k_p, a higher dielectric permittivity and a smaller aging rate [45]. Nevertheless, hot-pressing is not suitable for high volume productions. A summary of reported properties of KNN ceramics is presented in Table 1.2 [47].

10

Table 1.2: Reported properties of KNN ceramics.

Properties	Air-sintered Jaeger [45]	Air-sintered Kosec [46]	Air-sintered Birol [47]	Hot-pressed Jaeger [45]
ρ [g/cm^3]	4.25	4.20	4.30	4.46
d_{33} [pC/N]	80		110	160
d_{31} [pC/N]	21		43.4	49
k_p [-]	0.36	0.23	0.39	0.45
k_{31} [-]	0.22		0.23	0.27

Another method to increase densities is to introduce a dopant, the consequence being the creation of defects in the structure. The effects on the electromechanical properties of KNN of common dopants reported in the literature are the following:

- Excess of Nb^{5+} or incorporation of Mg^{2+}: High density KNN ceramics have been obtained for small added amounts. Magnesium doped ceramics have a slightly better coupling coefficient ($k_p = 0.45$) and a lower permittivity ($\varepsilon = 450$) [46] than pure KNN ceramics, which might be due to the effect of A site vacancies on the densification.

- CuO, Ta_2O_5, Al_2O_3: The sinterability of KNN ceramics has not been improved by the introduction of these additives in concentrations up to 1% [40]. In another report [48], the sinterability of the KNN ceramics was improved with the addition of CuO combined with an excess of the B site cation, which forms the $K_4CuNb_8O_{23}$ phase. Coupling coefficients were then slightly improved.

- Ba: The grain growth during sintering is inhibited by the addition of barium and higher densities are obtained. The limit of solubility of barium in KNN is 1.5 mole% [49] and the addition of barium lowers the phase transitions and the piezoelectric coefficient is slightly increased to $d_{33} \approx 100$ pC/N.

- ZnO: Dense ceramics have been obtained [50] as well as a small increase in the electromechanical properties ($d_{33} = 121$ pC/N, $\varepsilon_{33} = 500$, $k_p = 0.4$ for 1% mole ZnO).

- Mg^{2+}, Ca^{2+} and Sr^{2+}: Alkaline-earth dopants helped to increase densities of the ceramics up to 95%, showing $\varepsilon = 500$ and $d_{33} = 95$ pC/N for Ca^{2+} and Sr^{2+} doped ceramics [51].

- $K_4CuNb_8O_{23}$ (KCN): The KCN complex helps in the sintering stage by introducing a liquid phase during sintering and therefore promoting the densification. In this case, densities reach 97% and by adding 0.5% of KCN, the electromechanical properties are increased to $k_p = 0.39$ and $d_{33} = 180$ pm/V with a high induced strain of 0.09%, but with a decreased Curie temperature [52].

- $K_{5.4}Cu_{1.3}Ta_{10}O_{29}$ (KCT): As for KCN doping, the densities compared to pure KNN have been increased. The ceramics with 0.38% mole KCT show $k_p = 0.42$, $d_{33} = 190$ pC/N and a high induced strain of 0.09% and also a lower Curie temperature [53].

In summary, many dopants help to increase the densities of KNN ceramics, but only a few really increase significantly the electromechanical properties, the exceptions being the two complex KCN and KCT sintering aids.

1.3.6 Modified potassium niobate family

The design of new lead-free materials has to consider the concept of compositional or thermal phase transition, due to the observed enhancement of the electromechanical properties close to these particular phase transitions in many lead-based systems. Indeed, in the cases of PZT and the ferroelectric-relaxor families like PMN-PT or PZN-PT, the importance of this transition has been shown to be crucial in order to maximise these electromechanical properties, as previously mentioned (see Figure 1.5).

For medical applications where biocompatibility is important, KNN ceramics are interesting. In addition, KNN based ceramics show high coupling coefficients, which can be related to the bandwidth and the sensitivity of the transducers. The dielectric losses and permittivity of KNN ceramics are low, which is important for electrical impedance matching at high frequencies. Finally, the design of thicker elements is enabled by the high longitudinal wave velocities of KNN ceramics (5700 m/s [54]), but also by their low density (4.51 g/cm^3), thus rendering the processing and machining easier which is important in the field of high frequency transducers.

The interest for the KNN ceramics has been increased by the discovery in the Toyota Research Laboratories of modified KNN ceramics with improved piezoelectric properties. These ceramics, with the general composition (K, Na, Li)(Nb, Ta, Sb)O$_3$ [55, 56], display new phase transitions involving structures other than orthorhombic (in KNN there is an MPB between two different orthorhombic structures). A notable distinction between the methods shown so far which were aiming at the improvement of the density and electromechanical properties of pure KNN with the new approach is the high concentrations of the inserted atoms. The following compositions and additives have been reported:

- [Li$_x$(K$_{1-y}$, Na$_y$)$_{1-x}$](Nb$_{1-z-w}$, Ta$_z$, Sb$_w$)O$_3$: This general system has been published both as a patent [56] and as an article in Nature by Saito *et al* from Toyota Central R&D Laboratories [55]. Additional substitutions comprising almost the whole periodic table are also covered by the patent. The piezoelectric properties reported for conventionally sintered samples are above 300 pC/N and sometimes even above 400 pC/N for RTGG textured ceramics as depicted in Figure 1.10. With such properties, lead-free ceramics based on potassium sodium niobate are considered as promising lead-free piezoelectric ceramics.
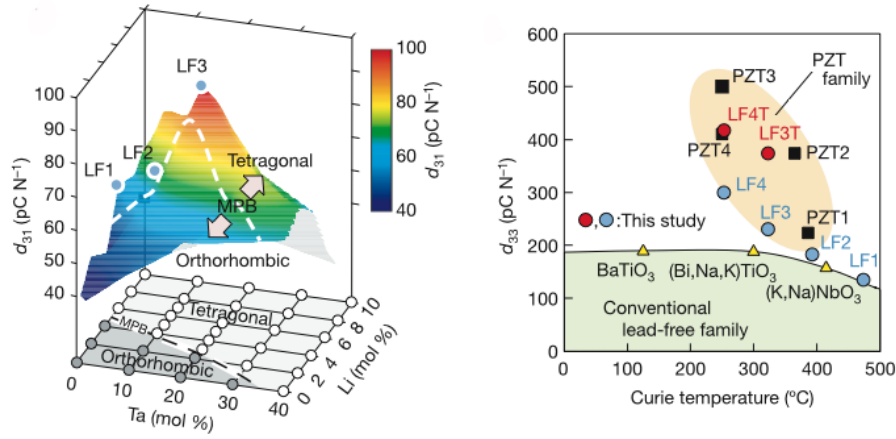
Figure 1.10: Piezoelectric properties as a function of the composition and the Curie temperature compared to other piezoelectric families [55].

- LiNbO$_3$: A morphotropic phase transition from orthorhombic to tetragonal around 6% lithium is reported [57] and was shown to lead to an increase in electromechanical properties. The highest piezoelectric properties were obtained for 6% lithium (d$_{33}$ = 235 pC/N, k$_p$ = 0.42 and k$_t$ = 0.46), with densities being high regardless of the composition. However, for concentrations higher than 8%, secondary phases seem to appear.

- LiTaO$_3$: This case is very similar to the LiNbO$_3$ substituted KNN ceramics, since a phase transition from orthorhombic to tetragonal structure is observed at around 5-6% LiTaO$_3$. Moreover, the piezoelectric properties are increased around this phase transition, giving the best values d$_{33}$ ≈ 200 pC/N and k$_p$ ≈ 0.36 [58].

- LiSbO$_3$: For 5.2% LiSbO$_3$, the orthorhombic to tetragonal phase transition is near room temperature, leading to high electromechanical properties (d$_{33}$ > 260 pC/N, k$_p$ > 0.5 and k$_{33}$ > 0.6) [59, 60]. These high electromechanical properties are strongly temperature dependent, compared to PZT, where they are nearly temperature independent near the MPB.

- BaTiO$_3$: Phase transitions from orthorhombic to tetragonal (around 6%) and to cubic (around 20%) have been observed [61]. There is no clear improvement in electromechanical properties (d$_{33}$, k$_t$, k$_p$) as compared to pure KNN ceramics. Strain-field measurements have been carried out, showing d$_{33}$(KNN) = 170 pm/V and d$_{33}$(2% BT) = 133 pm/V. At high BaTiO$_3$ amount, the ceramic show a relaxor like behaviour.

- SrTiO$_3$ [62, 63]: The ceramics behave like relaxors at high concentrations due to the cationic disorder on the A and B-sites. At around 4% SrTiO$_3$, the structure changes to tetragonal. The piezoelectric coefficient d$_{33}$ is not increased around this transition but the values for k$_p$ and k$_t$ are slightly increased. A pseudo-cubic phase is stable for compositions ranging from 15% to 25% [64] and such ceramics have sub-micron grains uniformly distributed leading to translucent samples. A phase diagram has been proposed for plasma spark sintered ceramics [65].

- <u>KCT</u>: The (K,Na)(Nb,Ta)O$_3$ ceramics with KCT showed a hard behaviour, and by increasing the tantalum content, there is "softening" and an increased electrostrictive effect. For 30% Ta, the electromechanical properties were the best (d$_{33}$ = 270 pm/V and k$_p$ = 0.44) [66, 67].

When high concentrations of new elements (lithium, tantalum, antimony, ...) are substituted in KNN ceramics, the toxicity of these elements should be considered. *Lithium* mainly affects the central nervous system, but also the kidney and the thyroid [68]. *Antimony* derivates on the other hand, can cause severe liver damage, break-down of red blood cells, irritate the mucous membranes and tissues and the central nervous system. In metallic form, *tantalum* is generally harmless but there is some evidence that tantalum derivates can enhance the risk of tumours. However, metallic tantalum should be handled with care due to the fire and explosion hazard caused by its dust [69]. Compared to tantalum, *niobium* and its compounds may be toxic, but there are no reports of human poisoning so far. To conclude, the new substituted atoms can be considered as a good alternative to lead comparing the lower toxicity of all the elements. However, it should be kept in mind that they are not totally harmless either.

The properties of the new KNN based ceramics are promising, but considering the processing difficulties associated with potassium niobate and potassium sodium niobate ceramics, leads us to question of the synthesis of these new compositions.

Other unknown parameters are the origin of their enhanced piezoelectric properties, the nature of the phase transition near the operating temperature and its implication on the stability of the properties. For applications, thermal stability but also the non-linearity and hysteresis behaviour at high driving field of the ceramics should be investigated.

Chapter 2

Statement of the problems

2.1 Open issues

A growing interest is focused on the recently discovered modified potassium niobate ceramics, since these new materials are being considered as replacements of lead-based materials in general, as well as potential candidates for medical applications. Their electromechanical properties are close to those of lead-based ceramics, in particular undoped PZT. Nevertheless, many questions arise since potassium niobate based ceramics show many problems, especially the difficulty to obtain high quality ceramics. The aim of this work is to give answer to these questions and solve the encountered problems listed below.

The processing of potassium niobate ceramics has been for about 50 years the object of many publications, alas only few of the proposed methods proved to be reproducible. The main problem encountered in the processing of KN and KNN ceramics is the poor densification, which has a direct influence on the electromechanical properties of the ceramics and as a consequence their potential industrial use. Many dopants (Li, Ba, Ca, etc ...) have been added in small amounts in order to help the densification process by the introduction of A or B site vacancies. However, reproducible and dense KNN ceramics are difficult to obtain. A good densification of the samples was achieved in a reproducible manner only when techniques like hot-pressing have been applied. Unfortunately, these techniques are not suitable for industrial applications. In this work, the processing of the pure and new modified KNN ceramics is studied, with focus on problems encountered in the pure KNN ceramics processing. For example, the processing steps should be controlled to avoid secondary phases.

Another important point in the processing of KN and KNN ceramics is the sensitivity to humidity of the initial powders (carbonates) and some of the phases found in the K_2CO_3 - Nb_2O_5 phase diagram. In the first reports on the processing of KN ceramics, the presence of hygroscopic secondary phases led to powders and samples that disintegrated in air. These secondary phases were removed by washing out with different types of solutions, which in turn led to the problem of the stoichiometry control. Even stable samples are affected by humidity changes, since it affects for example the dielectric losses. A modification of the chemical composition of the ceramics, for example the lithium and tantalum modified KNN ceramics, could improve their stability towards humidity. This stability with humidity together with the time stability of these materials will be studied.

In the last years, modified KNN ceramics with enhanced electromechanical properties, compared to KNN ceramics have been discovered. Lithium is used as substitute for

potassium and sodium, whereas tantalum and antimony can be used instead of niobium. These chemical modifications lead to ceramics with piezoelectric coefficients d_{33} as high as 400 pC/N for textured ceramics and 300 pC/N after conventional processing. The increased electromechanical response can be related to the presence of a phase transition near room temperature. The understanding of the nature of the phase transition, which can be either compositionally induced (as in PZT) or temperature induced (as in BaTiO$_3$), is essential for applications. Indeed, the thermal stability is better for compositionally induced phase transitions, as small temperature changes can't induce a phase transition. The nature of the phase transition observed in modified KNN ceramics will be studied.

The nature of the phase transition is an important issue for applications since the ceramics should have a good thermal stability. In the case of ultrasonic transducers for medical applications, the stability of the properties should be assured for thermal cycles up to 140 °C because the probes have to be sterilised at such temperatures prior to every use. For some of the newly discovered compositions, this thermal cycle implies going through a phase transition, which is detrimental for the material's properties. Indeed, during the phase transitions, the domain wall configuration is modified, which can lead to a hysteretic behaviour and a partial depolarisation of the samples. Since the phase transition of some of the ceramics showing enhanced electromechanical properties are situated near room temperature, the evolution of the contributions of the movement of the domain walls to the piezoelectric response is important and will be a topic of the present work.

2.2 Structure of the thesis

This thesis work will be divided into the following chapters.

Chapter 3   The experimental techniques used in this work are described briefly. They can be divided into two parts; the first comprises the description of the techniques used to optimise the processing steps. The second deals with the dielectric and piezoelectric characterisations of the obtained ceramics.

Chapter 4   As a result of this work, modified potassium niobate ceramics, with lithium in the A-site and tantalum in the B-site have been successfully synthesised. Each step has been carefully optimised (e.g. the grain size of the initial powders or the sintering parameters like the sintering temperature and time). In the case of the synthesised samples, densities higher than 95% of the theoretical densities have been observed. The microstructures are rather homogeneous and the grain size is comprised between 5 to 10 μm, but basing on results obtained by scanning and transmission electron microscopy, we have observed that within the grains the elements are not homogeneously distributed. The processing still needs further improvement, for example by obtaining finer grained initial powders. Some attempts of milling the initial powders to submicron sizes has not been successful. The electromechanical properties at room temperature of the as-produced ceramics are presented, showing high values around particular compositions.

Chapter 5   In this chapter, results on the study of the dielectric behaviour of the KNN and modified KNN ceramics are presented, as high dielectric losses have been reported in KNbO$_3$. The reproducibility of the pure KNN samples is poor as their dielectric behaviour

is not consistent and in particular a relaxation process is observed at low temperature for some of them. This process is not observed in modified KNN ceramics. In order to understand the origin of the relaxation process, the dielectric response at low frequency was measured, but contact problems have not allowed reproducible results. Qualitatively, the dielectric behaviour at low frequencies seems to be dominated by hopping of charge carriers. As the high losses have been reported to be related to the sensitivity of the potassium niobate ceramics to humidity, measurements with varying humidity have been performed and recorded as a function of time. The modified KNN ceramics show stable properties as a function of time and seem to be independent of the humidity.

Chapter 6 The evolution of the electromechanical properties as a function of the composition and temperature has been investigated using different techniques. In dielectric measurements as a function of the temperature, it becomes apparent that the phase transition is thermally induced. This behaviour is confirmed by direct and converse piezoelectric measurements. In these measurements, the thermal stability of the electromechanical properties is analysed in the point of view of medical applications. With successive thermal cycling, the properties stabilise following a depolarisation after the first cycle. The lithium and tantalum modified KNN ceramics show a better thermal stability than the lithium modified KNN ceramics.

Chapter 7 From direct measurements performed varying the dynamic and static stresses, frequency, temperature and composition of the ceramics, the evolution of the irreversible and reversible contributions have been analysed as a function of the measurement conditions. The modified KNN ceramics show a Rayleigh-type behaviour and a linear d_{33}-stress behaviour at low stresses. From the Rayleigh law, the contributions to the piezoelectric response can be separated. The irreversible contribution is maximal at the temperature of phase transition and is higher in the orthorhombic structure than in the tetragonal structure. Nevertheless, the reversible contribution is always higher than the irreversible contribution. At high static stress, the domain walls can be clamped, as confirmed by the smaller charge-stress hysteresis. This clamping leads to high depolarisation of the samples.

The report is completed by a conclusion and perspective chapter.

Chapter 3

Experimental procedure

In this chapter, the methods and experimental procedures used through out this thesis are presented and have been divided in two categories: on one hand the techniques for processing and characterising powders, comprising the powders characterisation with electron microscopy, x-ray diffraction, and particle size distribution and on the other hand the techniques for the determination of the dielectric, ferroelectric and piezoelectric properties of the ceramics. The methodology applied for the determination of the electromechanical properties by resonance and direct piezoelectric measurements is discussed separately.

3.1 Processing and powder analysis

3.1.1 Dilatometry

A useful tool for the determination of the processing parameters is the dilatometry, where the change in sample size is recorded as a function of temperature. The dilatometer is used for the determination of the temperature of the reactions occurring during heat treatment and leading to the decomposition of the initial powders yielding the final product. However, only the reactions which are associated with a dimensional change can be determined. After the chemical reaction, with further heating, an additional densification associated with a size change can occur, which is useful for the determination of the sintering temperature. In this work, a vertical differential dilatometer *Setaram 2050 DHT* dilatometer was used.

3.1.2 Particle size distribution measurements (PSD)

The particle size distribution and the mean particle size are important characteristics of a powder. These parameters will influence the sintering behaviour, and in the end most of the properties of the samples obtained after sintering.

Many techniques can be used for the determination of the particle size distribution [70]. The *Malvern Mastersizer S* [71] uses the diffraction of a laser beam on a powder suspension (Laser Diffraction Method). When light interacts with a particle, the light is scattered. This phenomenon depends on the size of the particle, the wavelength of the light and the refractive index of the particles and the media in which the particle are. The refractive indexes for our initial powders are given in Table 3.1 [72].

Table 3.1: Theoretical densities and refractive indices of the used powders and solvent [72].

Powder	Density [g/cm^3]	Refractive index [-]
SrCO$_3$	3.7	1.516
Na$_2$CO$_3$	2.532	1.535
K$_2$CO$_3$	2.428	1.531
Nb$_2$O$_5$	4.47	0.981
Isopropanol	—	1.33

In the experimental setup used, application of the Frauenhofer theory of diffraction, corrected by the Mie theory for the diffusion of the particles (for particles <1 μm) [73], enables the calculation of the diffracted light. For the calculations, an ideal model is considered in which the particles adopt a completely spherical shape. For the measurements, the powder is dispersed in a small amount of solvent (depending on the powder, either isopropanol or deionised water) with an ultrasound bath for around 5 minutes to get a homogeneous dispersion. This suspension is directly poured into the solvent circuit of the Malvern apparatus and then goes through the laser beam and the measurement cell. If the powder agglomerates strongly during the drying step, it is possible to carry out the measurement of the suspension directly after milling and thus avoiding this drying process.

The Malvern provides a particle size distribution by volume, noted d_v. For example $d_{v,50}$ is the spherical mean diameter by volume of the particles, i.e. 50% of the particles have a smaller size. Usually, the characteristic diameters $d_{v,10}$, $d_{v,50}$ and $d_{v,90}$ are given by the software controlling to the Malvern apparatus and the particle size distributions are plotted as a function of the particle size as shown in Figure 3.1.
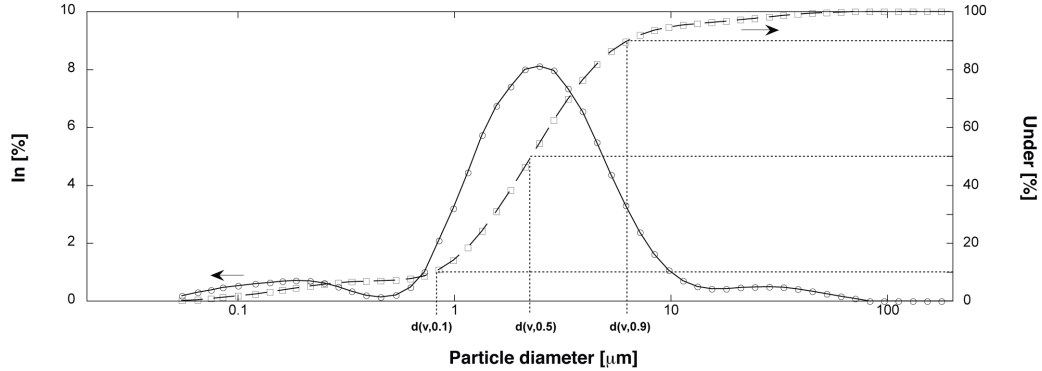

Figure 3.1: Example of particle size distribution and definition of the characteristic particle diameters $d_{v,10}$, $d_{v,50}$ and $d_{v,90}$.

In this work, the PSD measurements were mainly performed on stoichiometric powders, but also on the initial powders. As it will be shown, the initial powders (K_2CO_3, Na_2CO_3, Li_2CO_3, Nb_2O_5 and Ta_2O_5) don't present the same powder characteristics including particle morphology, mean size and particle size distribution. In order to decrease these inhomogeneities, the initial powders were milled in different conditions using the mean particle sizes and particle size distributions to choose the best milling conditions.

3.1.3   X-Ray diffraction (XRD)

X-ray diffraction measurements give information on composition (for example the presence of secondary phases), but also on the crystallographic parameters of the analysed ceramics. A *Siemens Kristalloflex* diffractometer using the K_α wavelength of copper (no distinction between $K_{\alpha,1}$ and $K_{\alpha,2}$) has been used in this work.

Lattice parameters can be determined using XRD. To get a good signal over noise ratio, small fringes (0.3°/0.3°/0.3°/0.05°) and long acquisition times (4-6 seconds) has been used and prior to analysis a sintered sample has been milled to a powder. Once the respective lattice planes for each reflection have been identified, a program based on the trial and error method "TREOR" has been used to calculate lattice parameters. This approach presents some limitations however, especially while dealing with monoclinic structures.

3.1.4   Scanning electron microscopy (SEM)

To determine the particle morphology and size, the *Philips XL30 FEG* electron microscope was used. It has a field emission electron source and is equipped with secondary electron, back-scattered and EDX detectors. Secondary electrons are mostly used for analysis in this thesis, but backscattered electrons can give useful information about the secondary

phases and the composition. For quantitative composition measurements, the microscope is equipped with an EDX detector, with a precision of about 1%.

Powders as well as bulk samples have been analysed. The powders were glued on a conductive tape for observation and special care was taken that the powder is solidly glued to the support, in order to avoid the contamination of the microscope. For an accurate measurement, powders should be covered with a thin layer of gold, deposited by sputtering. Observation of hygroscopic powders like those used in this work is not easy since humidity absorption can be seen during the measurement and because the sampling can be relatively tedious.

The bulk samples can be polished or fractured. On the fractured profiles, grains can be observed, as the fractures go either through the grains or along the grain boundaries. The main advantage of this method is the fast sample preparation. For grain size information on polished samples, a chemical etching should be found in order to create a contrast between the grains and the grain boundary. Polished samples are nevertheless used for chemical analysis using EDX, but without this etching step after polishing and without deposition of a conductive layer.

3.2   Dielectric and piezoelectric properties

Samples are prepared in shape of a disk and electrodes are sputtered on their two major flat sides. Platinum (which should be annealed at 800 °C after deposition), gold or a successive deposition of chrome and then gold (the adhesion of gold being enhanced by a small layer of chrome) was deposited using the *EMS 575X* sputtering system. Silver electrodes can also be considered as an alternative if one uses a silver paste, but as for platinum electrodes they need a densification step at 800 °C.

3.2.1   Dielectric properties measurements

The impedance analysers *HP4194A* and *HP4284A* were used during this work to measure the capacitance, the dielectric loss and the impedance behaviour as a function of the frequency.

Two different setups are available for temperature dependent dielectric measurements, depending on the temperature range and the need of controlled cooling. For temperatures below room temperature, the samples where placed in a *Delta Chamber 9023*, which has a maximal operating temperature of 280 °C and can be cooled with liquid nitrogen down to -150 °C. For higher temperatures (up to 500 °C) an in-house built furnace has been used, with the drawback that no cooling system is available. For temperature dependent measurements the impedance analyser *HP4284A* was used, while for room temperature measurements the *HP4194A* has been chosen. For low frequency measurements (below 100 Hz) the lock-in technique was used.

3.2.2   Ferroelectric measurements: hysteresis loops

The polarisation as a function of an AC field has be measured using a Sawyer-Tower bridge. The charge measurements have been performed with a capacitance placed in series with the sample such as to form a capacitive voltage divider. The instantaneous charge stored on the sample is then related to the instantaneous voltage, the voltage through the

capacity being proportional to the produced charges on the sample. Increasing the applied electric field during the loop measurement, this capacity should be increased. However, it is important to increase the capacity so that it is always larger than the capacitance of the sample, but at levels low enough to ensure a high enough voltage. To minimise the risk of sparking due to the breakdown of air at high fields, the sample was immerged in silicon oil.

3.2.3 Poling

If the material is ferroelectric, the spontaneous polarisation can be reversed by the application of an external electrical field. Unlike crystals, ceramics are composed of randomly oriented grains, which possess identical structures but have a random orientation, resulting in a small or zero net spontaneous polarisation. Therefore, it can be supposed that the properties of the ceramics are isotropic. The application of a high external field to the ferroelectric ceramic in order to get a piezoelectric effect is called poling. The net polarisation is then non-null, as the dipoles of each grain tend to align themselves in the direction of the applied field.

In each crystallographic structure, spontaneous polarisation is oriented along certain crystallographic directions that are equivalent energetically. The number of these equivalent polarisation directions depends on the crystal symmetry. The different equivalent directions of the spontaneous polarisation for tetragonal (4mm) and orthorhombic (mm2) structures are highlighted in Figure 3.2 [74].
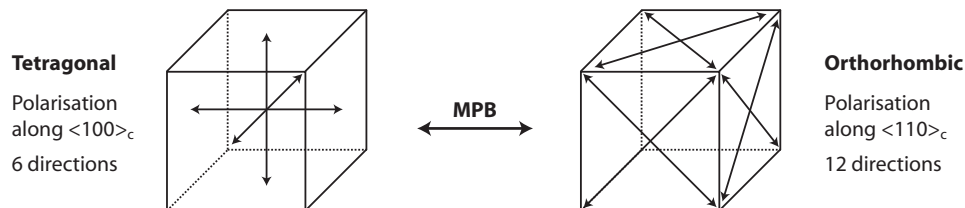

Figure 3.2: Possible polarisation vectors for the tetragonal and orthorhombic structures.

Low dielectric losses at room temperature are important in order to avoid conductivity during the poling process. As an order of magnitude, the losses at 1 kHz of the ceramics should be lower than 5%. To optimise the properties after the polarisation, three experimental poling parameters can be changed: the temperature (if at high temperature, with or without field cooling), the time and the electric field. Initial conditions can be found in the literature for some modified KNN compositions [55, 57, 58].

At higher temperatures, the applied field should be low, in order to avoid breakdown due to higher conductivity. The important point for high temperature polarisation is that during the cooling the field can be conserved through the phase transitions (from orthorhombic to tetragonal for the modified KNN ceramics), that the as-created domain structure is stable over a larger temperature range and that depoling due to the domain switching is avoided. With increasing temperature, the domain switching becomes easier, which means the coercive field decreases, which in turn allows for a poling with a lower field than at room temperature.

For the determination of the optimal polarisation conditions, the piezoelectric coefficient d_{33} (measured with a Berlincourt-type press) and the coupling coefficients k_p and k_t (measured by the resonance technique) are measured after aging of the samples for at least one day. The optimised poling conditions for the modified KNN ceramics have been found to be at a temperature near room temperature (i.e. 50 °C), which means that no phase transition is crossed during the poling process. As a consequence of the low temperature poling, a strong electric field, 50 kV/cm has to be applied. The poling conditions for the different compositions used in this work are shown in Table 3.2.

Table 3.2: Poling conditions for lithium, lithium and tantalum modified KNN ceramics.

Li [%]	Ta [%]	T [°C]	E [kV/cm]	t [min]
1	0	50	50	15
3	0	50	50	15
4	0	50	50	15
5	0	50	50	15
6	0	50	50	5
6.5	0	50	50	15
7	0	50	50	15
7.5	0	50	50	5
3	18	50	50	30
3	19	50	50	15
3	20	50	50	30
3	21	50	50	15
3	22	50	50	15

High dielectric losses or low density samples can show high conductivity during the poling step, demonstrating the importance of the sample quality needed for piezoelectric measurements. For temperature dependent resonance measurements, another polarisation procedure was tested (at 150 °C for 15 min under 30 kV/cm), confirming the choice of low temperature poling. But after thermal cycling, the electromechanical properties are stabilised at similar properties (see Section 6.4.2).

3.2.4 Piezoelectric measurements

The direct piezoelectric effect is defined as the generation of surface charges on a sample, which has been subjected to a mechanical stress and can be expressed as:

$$D_i = d_{ijk}\sigma_{jk} \tag{3.1}$$

where D_i is the electrical field displacement tensor, σ_{jk} is the stress tensor and d_{ijk} is the piezoelectric tensor.

The piezoelectric crystal deforms under the application of an electrical field. The mathematical expression of the converse effect is then:

$$x_{jk} = d_{ijk}E_i \tag{3.2}$$

where E_i is the electrical field tensor, x_{jk} is the deformation tensor and d_{ijk} is the piezoelectric tensor.

The piezoelectric tensor has 18 independent coefficients, and this number can be decreased considering the crystallographic symmetry of the piezoelectric material; for the crystallographic symmetries orthorhombic and tetragonal, the respective number of independent non-zero coefficients are 5 and 3. For those structures, the piezoelectric tensors are shown in Figure 3.3 [75].

$$
\text{a)}\quad
\begin{bmatrix}
\cdot & \cdot & \cdot & \cdot & d_{15} & \cdot \\
\cdot & \cdot & \cdot & d_{24} & \cdot & \cdot \\
d_{31} & d_{32} & d_{33} & \cdot & \cdot & \cdot
\end{bmatrix}
\qquad
\text{b)}\quad
\begin{bmatrix}
\cdot & \cdot & \cdot & \cdot & d_{15} & \cdot \\
\cdot & \cdot & \cdot & d_{15} & \cdot & \cdot \\
d_{31} & d_{31} & d_{33} & \cdot & \cdot & \cdot
\end{bmatrix}
$$

Figure 3.3: Piezoelectric tensor for a) orthorhombic mm2 and b) tetragonal 4mm structures.

The poled ceramics have ∞-fold symmetry in a perpendicular plane to the poling direction and therefore the symmetry of a poled ceramic is ∞mm. In the cases below, the ceramics have the same d tensor as the 4mm structure.

An important coefficient to assess the piezoelectric efficiency of a material is the coupling coefficient, defined as [1]:

$$
k = \sqrt{\frac{E_{mec}^2}{E_{el}^2}}
\tag{3.3}
$$

where E_{mec} and E_{el} are the mechanical and electrical energies implied in the piezoelectric effect.

Converse piezoelectric measurements - high field measurements

The converse measurements were made using a fotonic sensor *MTI-2000*. The fotonic sensor is a fibre-optic measurement system designed for displacement and vibration measurements. The probe consists of optical fibres and half of them emitting light and the other half receiving the light after being reflected on the sample surface. The two types of fibres are randomly distributed throughout the probe. The intensity of light detected by the sensor is a function of the distance between the reflecting surface and the probe. No light is reflected (and thus no signal is observed) when either the probe is in contact with the reflecting surface or when the probe is placed far away from the surface. Between these two extremes, there is a position of maximum intensity. Furthermore, between the maximum in intensity and the contact case, there is a region of linear reflected intensity. By calibrating the position of maximum intensity, the sensor can give an accurate measurement of the distance between the surface and the probe, leading to the deformation of the sample under the applied field.

An in-house experimental setup has been built (see Figure 3.4 [76, 77]) and used for temperature dependent measurement with the addition of a small furnace below the sample. The high field measurements were performed on modified KNN ceramics, of diameter d $\approx$ 5 mm and thickness t $\approx$ 1 mm (with aspect ratio thickness/diameter of 0.2). Since the samples have similar dimensions, the maximal applied voltage was 1000 V

(10 kV/cm). The values of room temperature piezoelectric coefficients are taken as an average of the values of 3 samples. The determination of the temperature dependence of the piezoelectric coefficient was carried out every 5 °C (after stabilising the temperature).
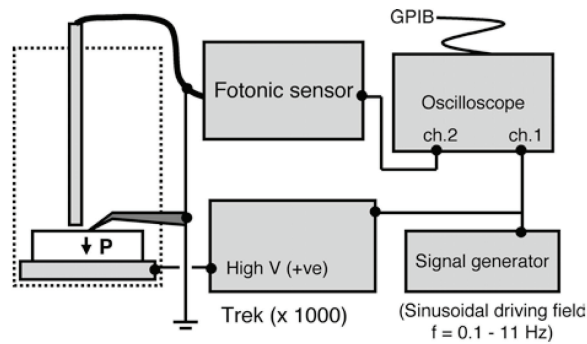

Figure 3.4: Schematic of the use of the Fotonic set-up [77].

Piezoelectric properties measured with this optical technique can be compared to measurements with another high-field method based on magnetic induction using a linear variable differential transformer (LVDT)-based system driven by a lock-in amplifier. This LVDT is an electromechanical transducer that produces an electrical output, which is proportional to the displacement of a separate, moveable, high-permeability core. For more details, see M. Davis PhD thesis [77]. Only few measurements were performed with this setup, because temperature dependent measurements could not be recorded. The two methods have led to values differing by less than 5% for all the studied samples.

The main advantage of the fotonic sensor is that no electronics or special sample holders, which could introduce unwanted phase angles to the measurement, are needed to treat the signal and hold the sample. However, it was difficult to avoid a low level of 50 Hz noise in the fiber-optic measurements, which corresponds to displacements of around 10 nm. As electronic filtering can lead to unwanted phase lags, and therefore spurious hysteresis, a numerical curve "smoothing" procedure was preferred to remove the 50 Hz noise.

Resonance measurements - low field measurements

Under an alternative applied electrical field, a piezoelectric material vibrates. This mechanical behaviour can be explained in terms of the electromechanical properties of the material and the dimensions of the sample. The magnitude of the vibrations is a function of the frequency and at the frequency of natural mechanical resonance, the amplitude of the mechanical vibrations will be maximal. Considering the piezoelectric constitutive equations, the impedance of the sample will show a maximum at the same characteristic frequency. The measurement of the electrical behaviour in combination with the constitutive equations of the piezoelectricity is a method of determination of the electromechanical properties of the material. It is noteworthy to say that by a variation of the sample geometry and poling geometry (the poling direction relative to the position of the electrodes), a complete set of electromechanical coefficients can be obtained.

The theory of wave propagation in a solid is complex and a linear quasi-static theory will be applied according to the *IEEE Standard of piezoelectricity* [78]. This theory

considers that the sample is in thermal equilibrium, the velocities of elastic effects are smaller than of the electrical effects, the material is a perfect insulator and that there is no magnetic field. For a disk with an aspect ratio smaller than 0.1 and for which the major surfaces are covered with electrodes, the electromechanical properties can be calculated using the following equations:

$$s_{11}^E = \frac{K_1^2}{[4R^2\pi^2 f_s^2 \rho(1-\nu^2)]} \tag{3.4}$$

$$s_{12}^E = -\nu s_{11}^E \tag{3.5}$$

where ρ is the density, R the radius of the disk, s_{11}^E and s_{12}^E are the elastic compliances, ν is the Poisson coefficient, f_s is the first serial resonance frequency and $K_i = \omega_{res}R/v_p$ where v_p is the velocity of radial waves.

$$k_p = \sqrt{\frac{f_p - f_s}{f_s} \frac{K_1^2 - 1 + \nu^2}{1 + \nu}} \tag{3.6}$$

where k_p is the radial coupling coefficient and f_p the first parallel resonance frequency.

$$d_{31} = k_p \sqrt{\frac{s_{11}^E \varepsilon_{33}^X (1-\nu)}{2}} \tag{3.7}$$

where d_{31} is the transverse piezoelectric coefficient and $\varepsilon^X{}_{33}$ the permittivity at zero stress.

$$k_{31} = d_{31}\sqrt{s_{11}^E \cdot \varepsilon_{33}^X} \tag{3.8}$$

where k_{31} is the transverse coupling coefficient.

The electric response was measured using an impedance analyser *HP4194*, leading to the values of f_p (frequency at maximum resistance), f_s (frequency at maximum conductance) and the capacity (at low frequency).

As it is assumed that the electroded surfaces are free of stress, electrical contacts as soft as possible should be used. Thin copper wires were glued with silver paste on each electroded surface and during the resonance measurements, the samples were supported only by these wires as shown in Figure 3.5.
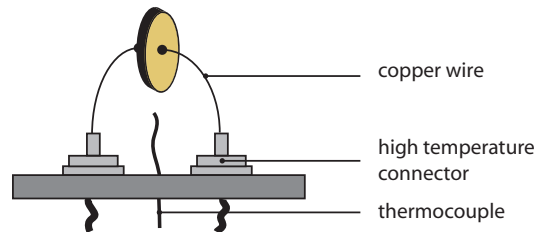

Figure 3.5: Sample setup for resonance measurements as a function of the temperature.

For temperature dependent measurements, the setup was placed in a *Delta Chamber 9023* with a thermocouple as close as possible to the sample. The electromechanical properties were then measured every 10 °C after allowing the system to equilibrate for at least 10 minutes for every given temperature.

Direct piezoelectric measurements

For direct measurements, the aspect ratio (thickness over diameter) of the samples should be as large as possible because the piezoelectric coefficient d_{33} is directly influenced by the aspect ratio. Figure 3.6 schematises a typical plot of d_{33} as a function of the aspect ratio in the case of direct piezoelectric measurements of PZT for 2 different sample geometries. In the case of KNN modified ceramics an aspect ratio higher than 0.4 is used for direct measurements.
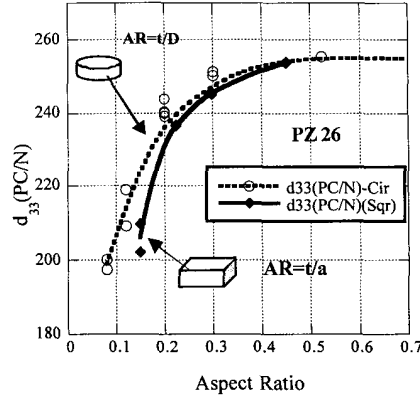

Figure 3.6: Influence of the sample aspect ratio on the piezoelectric coefficient d_{33} of hard PZT [79].

The longitudinal piezoelectric coefficient can be determined by means of a Berlincourt-type press. In this method, the electroded sample is squeezed with a metallic screw on a metal surface, which also acts as an electrical connection to conduct the charges. The charges released by the sample Q_s are defined by:

$$D = Q_s \cdot A \tag{3.9}$$

where D is the charge produced by the piezoelectric effect and A is the electroded area of the sample.

Q_s can be measured using a parallel capacitance C which should be large enough to draw all piezoelectrically-induced charge from the sample or the reference, though not so large that the resulting voltage is too small. The sinusoidal force is applied by a piezoelectric actuator, driven by a signal generator; a reference piezoelectric element with a known piezoelectric coefficient (d_r) is placed mechanically in series with the sample, being then submitted to the same force F as the sample. The charges produced by the piezoelectric reference and the sample, Q_r (Q_s=d_s· F) and Q_s (Q_r=d_r· F), are measured successively by switching the voltages across the parallel capacitance (V_r and V_s respectively), which has then the same value for both measurements. Charges are then given:

$$Q_s = C \cdot V_s \qquad Q_r = C \cdot V_r \tag{3.10}$$

The piezoelectric coefficient of the sample d_s is then given by:

$$d_s = d_r \cdot \frac{V_s}{V_r} \tag{3.11}$$

28

Thus, simply by measuring V_s and V_r and using equation (3.11) will enable us to determine the piezoelectric coefficient for any given sample. This basic setup only allows measurements at sinusoidal driving forces of fixed amplitude and frequency, but the piezoelectric response is dependent on the amplitude and frequency of the driving field (electrical or mechanical). At high driving field, the contribution of the domain wall motion of the piezoelectric response is increasing, due to their facilitated movement.

Non-linear and hysteretic effects are important for any piezoelectric element used in actuators and transducers, especially when high fields are involved. Since the afore described Berlincourt-type of setup can't be used for the determination of these effects, another press was developed in the ceramics laboratory (see Figure 3.7) to circumvent that drawback [76, 77].
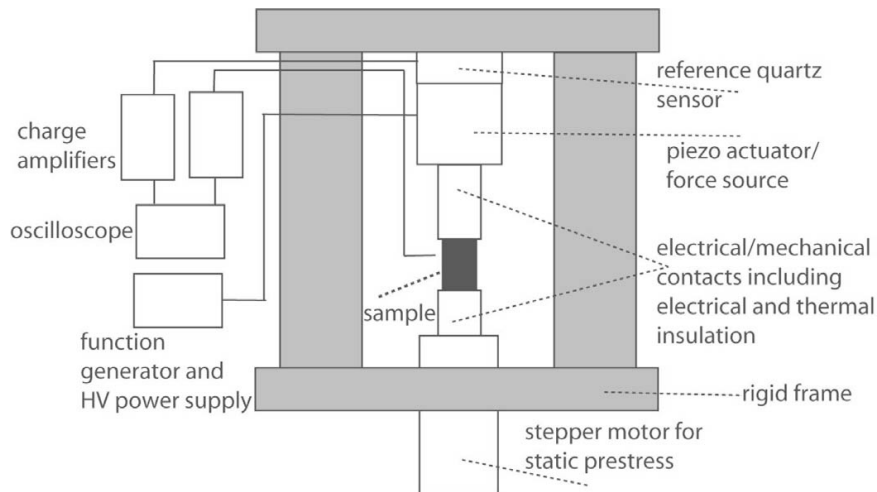
Figure 3.7: Schematic of the Berlincourt-type d_{33} meter used in this work [76].

In this home made press (Figure 3.7), a series assembly of a quartz reference sensor, PZT actuator and sample, mounted between two zirconia columns, is held within a rigid cast iron frame. The sample is placed between the two columns, which end with steel plates, used in this case as electrical, but also as mechanical contact. The force is measured using a quartz sensor and the charge with a charge amplifier, by conversion to an electrical signal, which is fed in to channel one of a digital oscilloscope. The actuator, which applies both static and dynamic components of force, is driven by a signal generator via a high voltage amplifier. The charge produced by the sample is measured by another charge amplifier, which is connected to a second channel of the oscilloscope. Compared to the Berlincourt setup, the frequency, the dynamic and static stresses as well as the temperature can be controlled and varied.

Chapter 4

Ceramics processing

As potassium sodium niobate ceramics are promising lead free piezoelectric materials, a serious endeavour has been focused on the elaboration of these derivatives, but no systematic method has yet been proposed to lead to high quality KNN ceramics in a reproducible way. To overcome the poor densification during sintering, either additives can be introduced or hot-pressing can be used. An important issue is the formation of secondary phases, due to insufficient mixing of the initial powders, which leads to highly humidity sensitive ceramics. Thus, for eventual industrial applications, there is a need to find an acceptable processing method.

In the following section, a systematic methodology and procedure is presented, which allows for the elaboration of dense ceramics in a reproducible way that could be used for industrial purposes. The most important points in the processing are the choice of the initial powders (purity, grain size and powder morphology), as well as the control of the grain size distribution over the whole processing, which can be done by a suitable choice of the milling steps, as well as the introduction of successive calcination steps. Finally the sintering conditions should be carefully optimised. In order to prove the efficiency of the so-obtained processing methodology, electromechanical properties of the ceramics are shown.

4.1   Introduction

In the early 50's, first reports on the processing of potassium niobate crystals were published [31, 34, 80]. The produced crystals showed different colours and the presence of impurities or secondary phases was supposed to be responsible of this change. Based on these observations, the Nb_2O_5-K_2CO_3 phase diagram was determined [31], which has been shown in Figure 1.7. A large number of phases seen in this phase diagram are hygroscopic. It has also been noted that the ceramics swell and disintegrate in air after some time or just after the removal from the furnace because of off-stoichiometry of the ceramics [1]. Initially, these secondary phases were removed by using different techniques, the most popular being the use of a hot solution of potassium carbonate to dissolve the non-perovskite phases, and complemented by the addition of NH_4OH and HCl [34]. After washing with a potassium carbonate solution, the powder was rinsed with distilled water, which reduces the moisture sensitivity of the powder. At this stage, application of this methodology leads to powders of ambiguous stoechiometry, reason why an excess of potassium carbonate had to be added. This method to remove secondary phases in the synthesis of KN ceramics was then applied to KNN ceramics leading to relative densities of up to 97% [42].

For compositions around 50% $KNbO_3$ and 50% $NaNbO_3$, two different orthorhombic structures coexist and the work by Zhang *et al* [43], confirming the results obtained by Egerton *et al* [42], revealed an increase of the electromechanical properties around this particular composition, as shown in Figure 4.1.
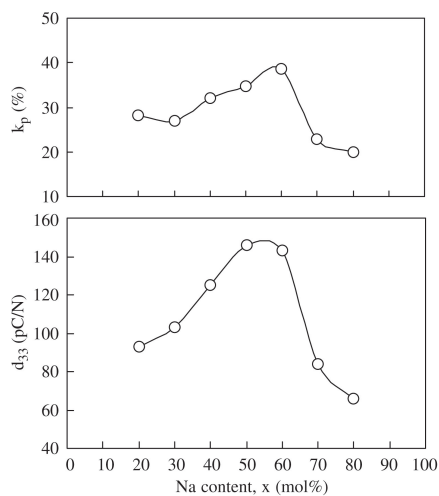

Figure 4.1: Radial coupling coefficient k_p and piezoelectric coefficient d_{33} as a function of the composition $K_{1-x}Na_xNbO_3$ [43].

In another approach for the synthesis of potassium niobate, special care was taken to avoid the secondary phases for example by studying the influence of the evaporation of K_2O above 840 °C and the impact of humidity [35]. However, the most efficient methods towards the elaboration of dense KNN ceramics are by hot-pressing [45] or addition of dopants [46]. Even later works on potassium niobate based ceramics imply the use of dopants to reach high densities [39, 51].

In this work, the standard processing steps have been optimised in order to get dense

samples and in a reproducible way. These steps consist of the mixing of stoichiometric concentrations of the initial powders, the calcination to get the final composition, the powder milling and finally the powder compaction and sintering. However, no additives were used here to improve the densification process, to assure an as simple as possible processing for industrial production. Initially, the aim of the project was to get dense KNN samples but then, during the work progress, new compositions based on KNN were discovered by Toyota Research Laboratories. Because of superior properties of modified KNN ceramics, the focus of the work has been shifted to them. The processing steps for KNN were then just slightly adapted to these new compositions. In the last part of this chapter, the electromechanical properties at room temperature of the so-obtained lithium and tantalum modified ceramics are presented.

4.2   Initial powders

The commonly used method for the processing of KNN ceramics is the solid-state synthesis starting from alkaline carbonates and niobium oxide. The chosen initial powders are the high purity powders, K_2CO_3 99.997%, Na_2CO_3 99.997%, Li_2CO_3 99.997%, $SrCO_3$ 99.999%, Nb_2O_5 99.9985%, Sb_2O_5 99.994% (purchased from Alfa Aesar) and Ta_2O_5 99.99% (obtained from Sigma Aldrich). Two important facts about the initial powders are the nature and amount of the impurities present (usually given by the powder supplier) and the particle characteristics such as the particle size distribution. As we selected high purity powders, the role of the impurities was reduced. The particle size distribution of a powder is an important parameter that influences its properties, handling and domain of application. For an optimal processing of the ceramics, the different components should ideally have a narrow PSD and a small mean grain size, and these properties should be as close as possible one to the other, in order to ensure a homogenous mixing of the components. The powder characterisation is not limited to particle size distribution measurements alone, but microscopy, x-ray powder diffraction and chemical composition analysis can give complementary information [70].

In this work, the volume particle size distribution has been measured by using the laser diffraction technique. For the analysis of the hydrophilic powders (carbonates), the measurements were performed in isopropanol and a good dispersion of the powders in the solvent was obtained by immersing them in an ultrasound bath for 5 minutes (this is crucial for obtaining accurate measurement). For example, it is tedious to obtain a good dispersion of potassium carbonate, since it forms large particles that sediment after the ultrasonic treatment, as shown in Figure 4.2 for two successive measurements.
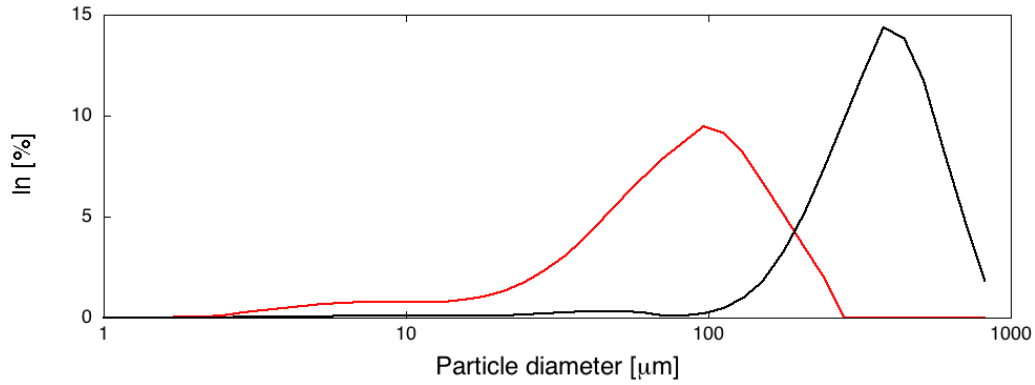
Figure 4.2: Two successive measurements of particle size distribution of the raw K_2CO_3 powder purchased from Alfa Aesar, showing the importance of the sampling.

The particle size distributions of the raw sodium carbonate and niobium oxide are illustrated in Figure 4.3.
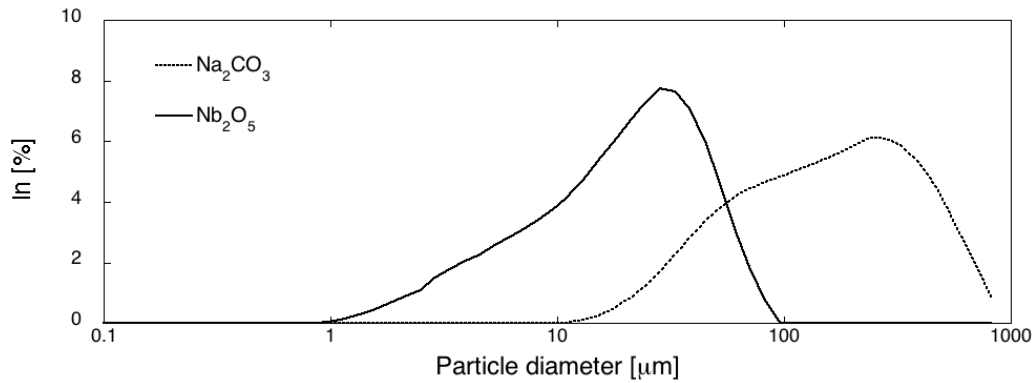

Figure 4.3: Particle size distribution of the raw Na_2CO_3 and Nb_2O_5 powders purchased from Alfa Aesar.

The mean particle sizes $d_{v,0.5}$ of the potassium and sodium carbonates are high (respectively 370 μm and 160 μm), and the PSD is variable, showing the importance of the sampling. Furthermore, some big agglomerates can be seen in lots furnished by the supplier. The niobium oxide has a smaller mean grain size (20 μm), but needs to be reduced for the ceramic processing.

Three powder milling methods are common in ceramics processing, namely ball, mortar and attrition milling. In the ball milling process, a milling medium, consisting typically of zirconia balls, solvent and the powders are mixed in a jar placed between two rolls turning in opposite directions. In attrition milling, the powder, solvent, as well as a similar milling medium as for ball milling are placed in a jar. A shaft equipped with horizontal arms turning into this jar creates shocks between the powder and the milling medium. Due to the high rotation speed (in our case, 650 rpm), the collisions are more frequent than in ball milling, where the rotation speed is lower (about 97 rpm, but depending on the recipient size). Finally, using an agate mortar and container, the powder is milled by hand, usually in dry conditions. For potassium carbonate, the three milling methods have been used to try to reduce significantly the particle sizes, as shown in Figure 4.4.
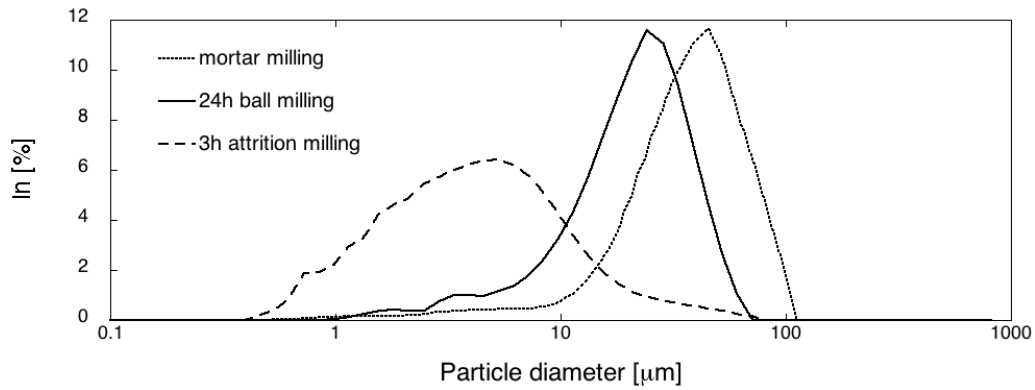
34

Figure 4.4: Particle size distribution of the K_2CO_3 powder after mortar milling, 24 hours ball milling and 3 hours attrition milling.

Attrition milling turned out to be the most efficient method and the milling parameters, specially the milling times were optimised like for potassium carbonate on Figure 4.5. The maximal milling time was fixed to 3 hours to avoid the wearing of the zirconia balls and the consequent contamination of the powder with ZrO_2.
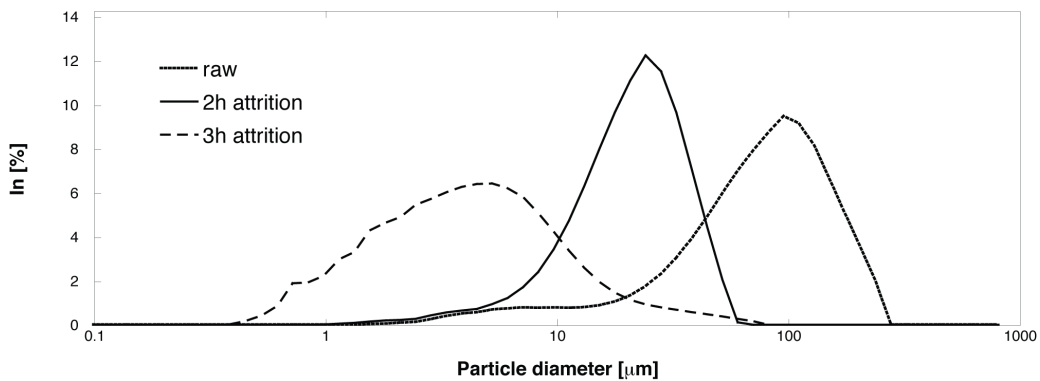

Figure 4.5: Particle size distribution of the raw, 2 hours and 3 hours attrition milled K_2CO_3 powders.

The jar used for attrition milling has a volume of 110 cm³ and the interior is made of Teflon, to avoid contamination with alumina or zirconia (the most common materials found in attrition jars), which can be eliminated during calcination.

The smallest obtained mean grain size for potassium carbonate was 4 μm. It should be noted here, that during ball milling of the different initial powders, which is the first step in the ceramics processing, the grain sizes of the components can be further reduced.

As was already demonstrated for potassium carbonate, and as it is generally assumed, attrition milling is the most efficient milling method. Therefore the other powders were milled using only attrition milling. The best results for potassium and sodium carbonate as well as for niobium oxide are summarised in Figure 4.6.
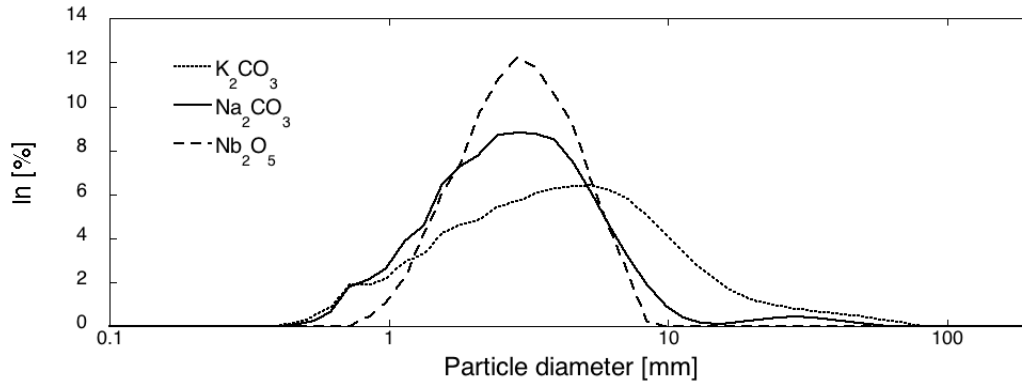
Figure 4.6: Particle size distribution of the K_2CO_3 powder after 3 hours ($d_{v,0.5}$ = 4.08 μm), the Na_2CO_3 powder after 2 hours ($d_{v,0.5}$ = 2.81 μm) and the Nb_2O_5 powder after 3 hours attrition milling ($d_{v,0.5}$ = 2.91 μm), which are the optimal conditions for each powder.

In summary, the mean particle sizes of the starting powders have been significantly reduced and lies in the same order of magnitude for all samples studied: 4.08 μm for K_2CO_3, 2.81 μm for Na_2CO_3 and 2.91 μm for Nb_2O_5. Since other PSD measurements on milled powders gave similar results, this attrition milling can be considered to be reproducible. For dopants such as strontium, which is often used for KNN ceramics, similar particle size reductions have been carried out. An alternative is to buy powders certified to have a grain size below a certain value, for example tantalum oxide Ta_2O_5 which is commercially available with grain sizes under 5 μm. Nevertheless, since spherical particles are considered in the PSD measurements, these results should not be interpreted as real values but rather as qualitative results. This is nicely illustrated in the case of K_2CO_3, Na_2CO_3 and Nb_2O_5 (see Figures 4.7 and 4.8) where the different powders display different morphologies.
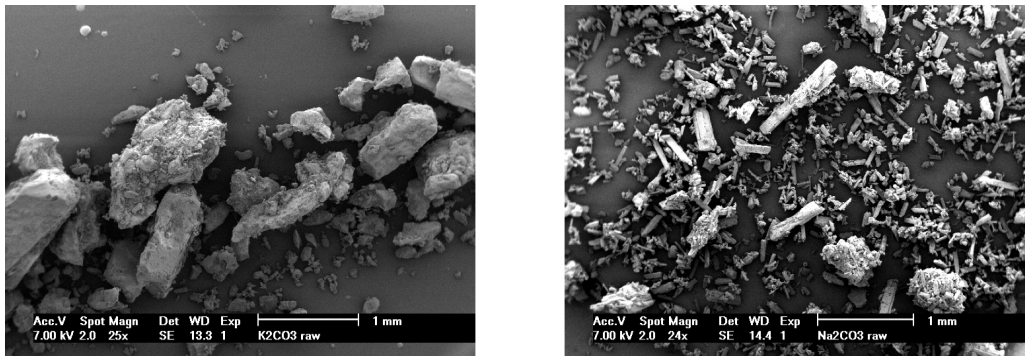

Figure 4.7: SEM picture of the K_2CO_3 and Na_2CO_3 raw powders.

After the grain size distribution, the particle morphology of the different components has to be considered. The morphology of the powders could not be modified since we do not produce the powders in our laboratory. The ideal morphology required is spherical (and the most suited to validate the laser diffraction PSD measurements shown before), and in practice, morphologies not differing too much one from the other. The morphologies of potassium and sodium carbonate have been observed by means of scanning electron microscope and are shown in Figure 4.7.

The different powders show different shapes as well as a variation of the mean grain size. As shown in Figure 4.8, the niobium oxide has a complex shape compared to the needle-like or spherical shape of, respectively, the sodium and potassium carbonates. In this figure, the reduction of the particle size by attrition milling measured by laser diffraction is confirmed.
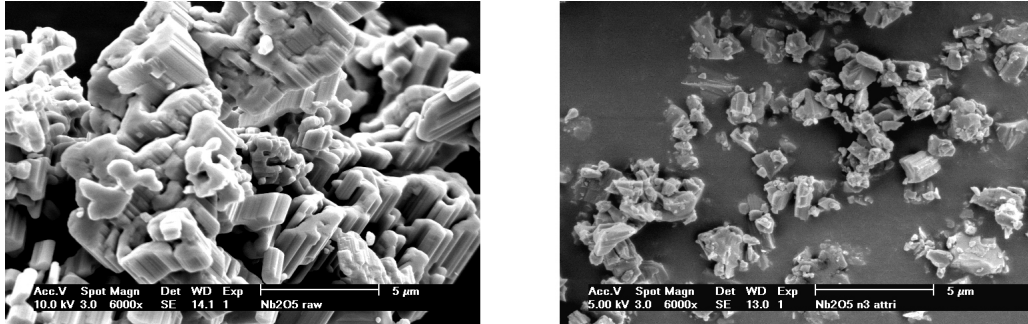

Figure 4.8: SEM picture of the raw and attrited Nb_2O_5 powders.

With the initial milling, the impact of the shape on the final mixing of the different powders is reduced and during the next processing step, i.e. ball milling, the particle sizes are further reduced.

4.3 Synthesis of KNN powders

Once the starting powders are prepared with optimised particle size distributions and mean particle sizes, the processing parameters can be determined. The first step is the mixing of the initial powders in stoichiometric amounts using ball milling. The choice of the milling medium is important to avoid ZrO_2 contamination. Different types of milling media have been tried, changing in composition and shape. The surfaces of two types of ZrO_2 doped balls, yttrium and magnesium doped ZrO_2 are shown in Figure 4.9.
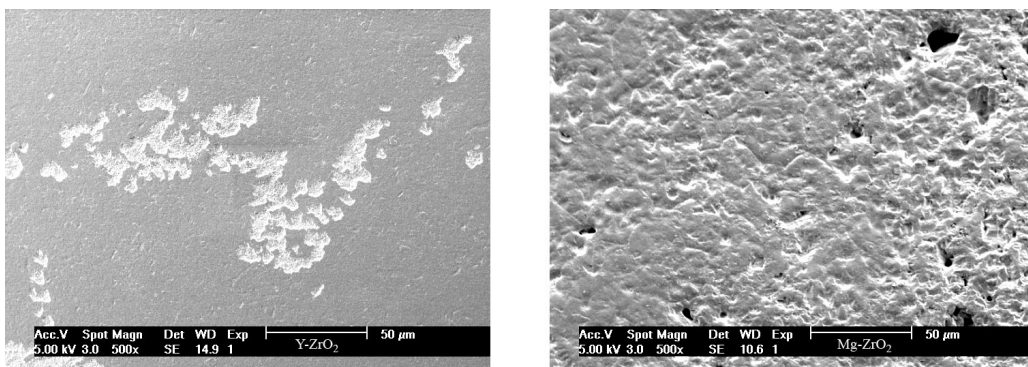

Figure 4.9: SEM picture of the Y-ZrO_2 and Mg-ZrO_2 spherical balls.

The effect of ball milling is different for the two materials, as well as for the different shapes. The best choice is found to be yttrium doped ZrO_2 balls, as it has been noticed that Mg-ZrO_2 balls wear more and as a result a non-negligible amount of ZrO_2 is found in

the ceramics (up to 1% in weight). The balls used for attrition are similar to the Y-ZrO$_2$ medium used for ball milling, differing only by size (2 mm instead of 5.5 mm). No zirconia traces were detected in the produced ceramics using this milling medium.

Typically, ball milling is performed for 24 hours in a solvent such as water, alcohol or acetone. In the case of KNbO$_3$ based ceramics and because a part of the initial powders are hydrophilic, the solvent used is isopropanol or acetone, with a slight preference for isopropanol, due to the environmentally detrimental impact of acetone. Because of their sensitivity to water, the powders are dried prior to milling in a furnace at 200 °C for 24 hours. Once the powders are removed from the furnace, they should be weighed as quickly as possible and inserted into the solvent. To assure a homogeneous mixing of the initial powders, a two step milling is performed. In a first step, the A-site initial powders (K$_2$CO$_3$, Na$_2$CO$_3$, SrCO$_3$, Li$_2$CO$_3$, ...) are mixed together. In the second step, the B-site initial powders (Nb$_2$O$_5$, Ta$_2$O$_5$, Sb$_2$O$_5$, ...) are added to the A-site powders along with more solvent and balls. As an example, the milling conditions for 20 g of powder of (K$_{0.5}$,Na$_{0.5}$)NbO$_3$ doped with 0.5% strontium are given in Figure 4.10.
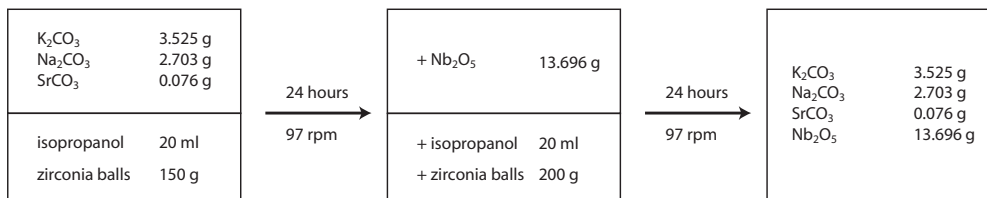

Figure 4.10: Ball milling conditions for (K$_{0.5}$Na$_{0.5}$)NbO$_3$ ceramics doped with 0.5% strontium.

Once the mixing step is finished, the solution is dried prior to calcination. This drying step must be carefully controlled, as stresses produced by differential shrinkage may cause defects in the powder. The solution obtained is dried under an IR-lamp to avoid agglomeration of the particles [81], but an alternative drying method to avoid the agglomeration of the powder would be lyophilisation. The dried powders should be kept at temperatures higher than 100 °C to avoid hydration of the carbonates until they are inserted into the preheated (100 °C) furnace for calcination. The calcination temperature, or the temperature needed to achieve the reaction and to obtain the desired composition, has been determined using dilatometry and XRD. One problem that could appear during the thermal cycle is the loss of potassium oxide K$_2$O, but only above 840 °C [35].

A pellet of a mixture of the different starting powders in the amount required to get a stoichiometric KNN ceramic, has been uniaxially pressed and heated to 850 °C at a rate of 2 °C/min. The dilatometric curve of such a pellet is given in Figure 4.11.
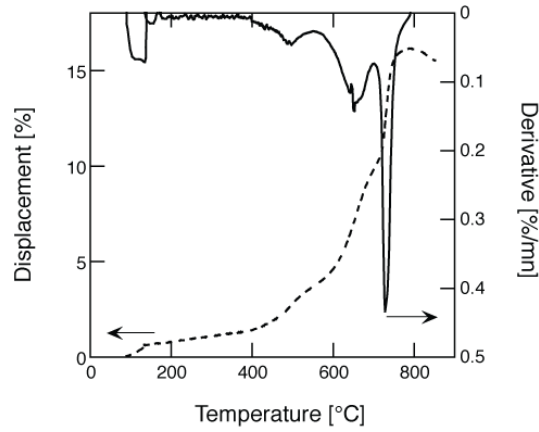
Figure 4.11: Dilatometric curve of a stoichiometric K_2CO_3-Na_2CO_3-Nb_2O_5 pellet.

A reaction occurs between 700 °C and 800 °C, as the sample loses up to 15% of its height and there is also small peak around 650 °C, which is probably due to the formation of a secondary phase. The first peak around 150 °C represents the elimination of the absorbed water.

In order to control the compositional homogeneity or in other words to detect the presence of secondary phases, different thermal cycles have been performed at different temperatures and the obtained ceramics have been analysed using XRD. The results are shown in Figure 4.12. It can be seen that the reaction was completed after the calcination step.
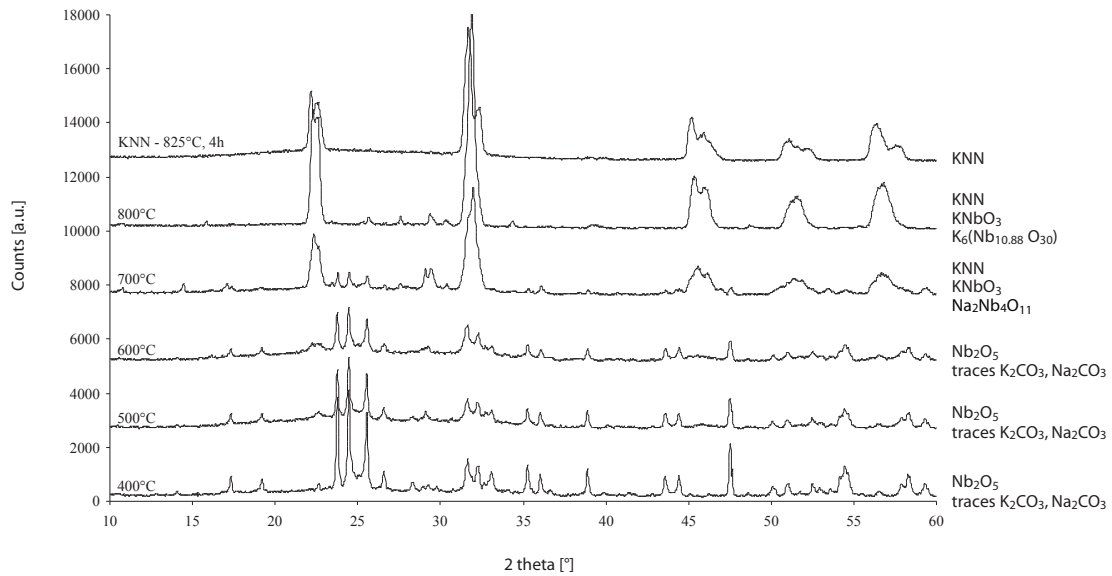

Figure 4.12: Diffraction pattern for K_2CO_3-Na_2CO_3-Nb_2O_5 pellets treated at different temperatures, with the identified compounds at each temperature.

Above 700 °C, no residual peak corresponding to the starting powders can be observed. However, at 700 °C and 800 °C, secondary phases are present. For comparison a KNN powder is superimposed on Figure 4.12. A good mixing can avoid the appearance of

such secondary phases, and a calcination temperature of 825 °C for 4 hours leads to the desired composition [47]. The heating rate is 2 °C/min and the nominal cooling rate 10 °C/min but no cooling system is available to ensure such a cooling rate. Doping the KNN ceramics with 0.5% strontium improves the densification but doesn't change the reaction temperature.

It is possible to calculate the theoretical weight loss that should occur during the calcination step. Considering un-doped KNN ceramics, the ideal reaction that occurs and the theoretical weight loss are both given in Figure 4.13.
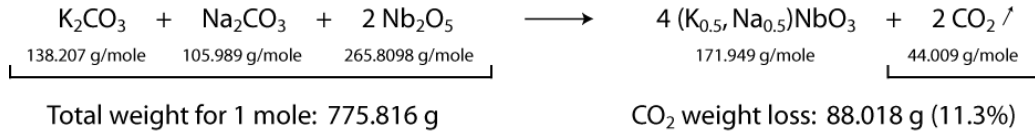
$$K_2CO_3 \quad + \quad Na_2CO_3 \quad + \quad 2\,Nb_2O_5 \quad \longrightarrow \quad 4\,(K_{0.5}, Na_{0.5})NbO_3 \quad + \quad 2\,CO_2 \nearrow$$

138.207 g/mole   105.989 g/mole   265.8098 g/mole   171.949 g/mole   44.009 g/mole

Total weight for 1 mole: 775.816 g CO_2 weight loss: 88.018 g (11.3%)

Figure 4.13: Weight loss during sintering due to CO_2 production.

It is important to weigh the powder after each step in order to understand the synthesis, but one should take into account that the weight loss will be higher than predicted as not all the powder from the crucibles can be removed. In addition, if there is a ZrO_2 contamination due to the milling medium, the weight of the powder after the calcination will be higher than predicted.

The typical PSD and the diffraction pattern (K_α, 10-60°, step 0.04°, 4 sec) after one calcination step are shown in Figures 4.14 and 4.15 respectively.
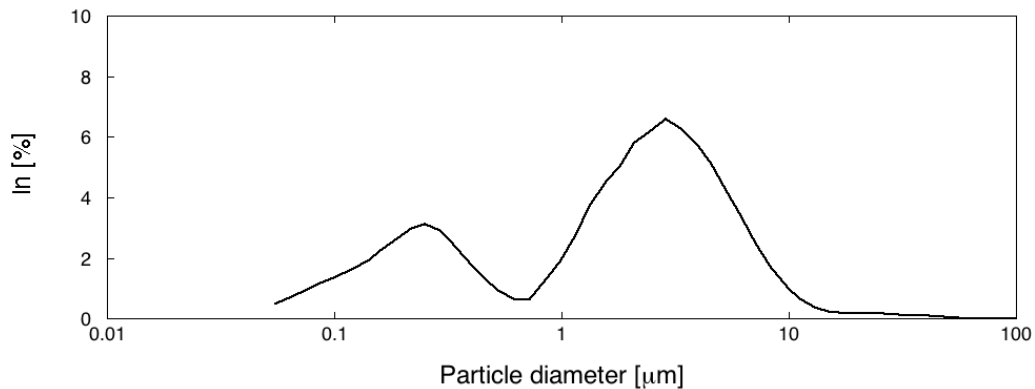

Figure 4.14: Particle size distribution of a KNN powder after one calcination step at 825 °C for 4 hours ($d_{v,0.1} = 0.14\ \mu m$, $d_{v,0.5} = 1.57\ \mu m$ and $d_{v,0.9} = 5.54\ \mu m$).
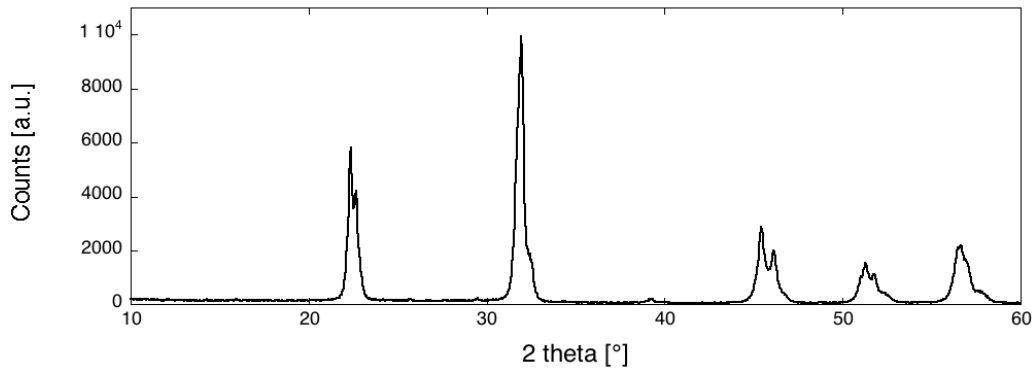
Figure 4.15: Diffraction pattern of a KNN powder after one calcination step at 825 °C for 4 hours.

The mean grain size is about 1.5 μm and the PSD is bimodal. To improve the properties of the ceramics, it is important to reduce the grain sizes and to avoid the PSD distribution tail for the large grain sizes (in the particular example of Figure 4.14 around 5 μm to 20 μm).

Generally, after one calcination, the powder homogeneity can still be increased further since broad XRD peaks are observed, especially at high-angles. Considering a high angle diffraction peak, the right tail represents sodium rich phases and the left tail shows the potassium rich phases. These secondary phases in the sintered samples can be observed using backscattered scanning electron microscopy. The bright spots in Figure 4.16 represent light element-containing phases, and thus, as potassium is the lightest component of our ceramics, the needle-like secondary phase seen below is a potassium rich phase.
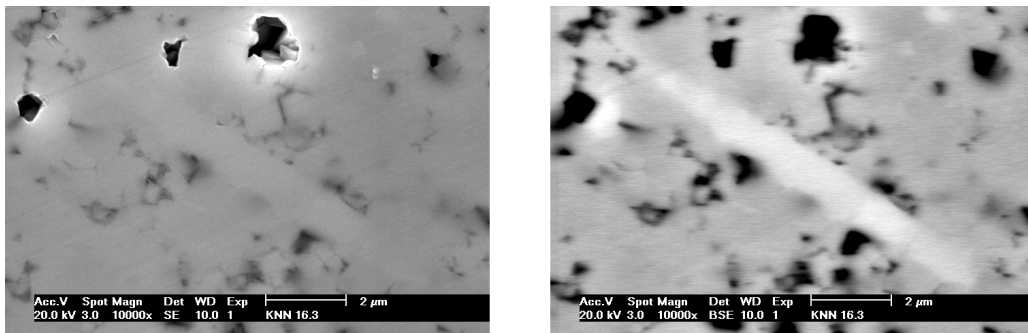

Figure 4.16: SEM image of a secondary phase in a KNN ceramic in secondary electron and backscattered electron microscopy.

After the calcination, the powder is milled and the most common milling procedure at this point of the processing is a ball milling for 24 hours in isopropanol. For comparison, an attrition milling for 3 hours has been done. The obtained particle size distributions after the application of these two milling techniques is shown in Figure 4.17.
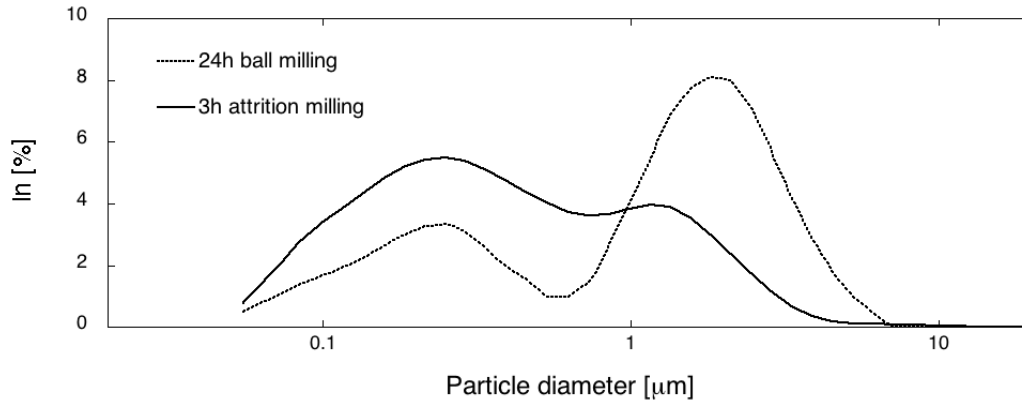
41

Figure 4.17: Particle size distribution of KNN powder after one calcination step and 24 hours ball milling ($d_{v,0.1}$ = 0.15 μm, $d_{v,0.5}$ = 1.34 μm and $d_{v,0.9}$ = 3.09 μm) or 3 hours attrition milling ($d_{v,0.1}$ = 0.10 μm, $d_{v,0.5}$ = 0.36 μm and $d_{v,0.9}$ = 1.67 μm) respectively.

From Figure 4.17 it becomes apparent that the attrition milling is more efficient. In complement to the PSD measurements, it should be mentioned that sintered samples showed a density of under 80% of the theoretical density (4.52 g/cm^3) for the ball milled powder and above 93% for the attrition milled powder. This milling step is important to decrease the particle sizes (mean grain size in attrited powders is typically between 0.5 and 1 μm), as the sintering behaviour of the powder depends strongly on the particle characteristics. The synthesis method should lead to small grain size and in a reproducible way.

A second calcination step, similar to the first calcination (at 825 °C for 4h), is performed to enhance the compositional homogeneity. Figure 4.18 shows the diffraction pattern for KNN powders after one (solid line) and two calcinations (thick line). A net decrease of the high resolution peaks (at high diffraction angles) can clearly be observed, representing a diminution of the sodium rich phases (at the right basis of the peaks) after two calcinations.
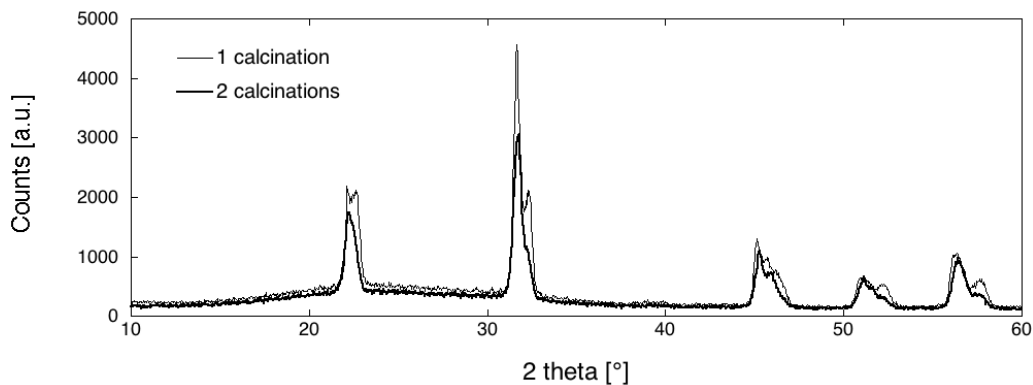

Figure 4.18: Diffraction pattern of KNN powders after one and two calcination steps.

After the second calcination, an attrition milling is performed to reduce the particle sizes. The typical particle size distribution of the final powder after sieving with a 100 μm mesh are shown in Figure 4.19.
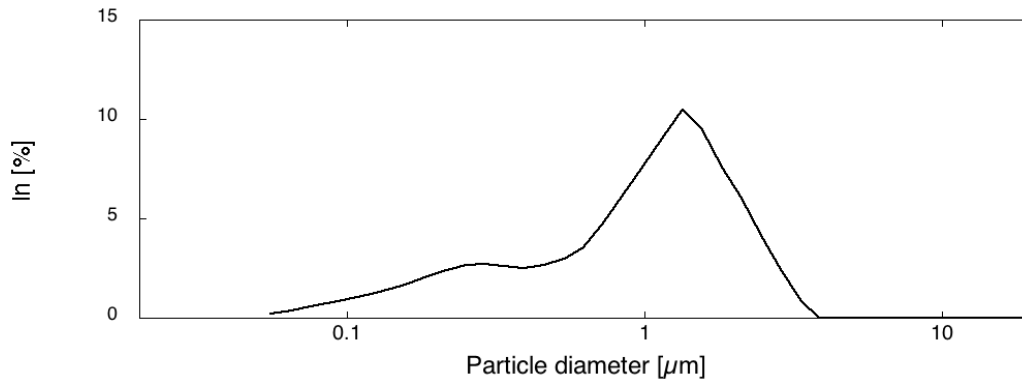
42

Figure 4.19: Final particle size distribution of a KNN powder ($d_{v,0.1}$ = 0.21 μm, $d_{v,0.5}$ = 1.06 μm and $d_{v,0.9}$ = 2.12 μm).

The mean grain size of the final KNN powders is about 1 μm and this value is confirmed by the images obtained by using electron microscopy (Figure 4.20).
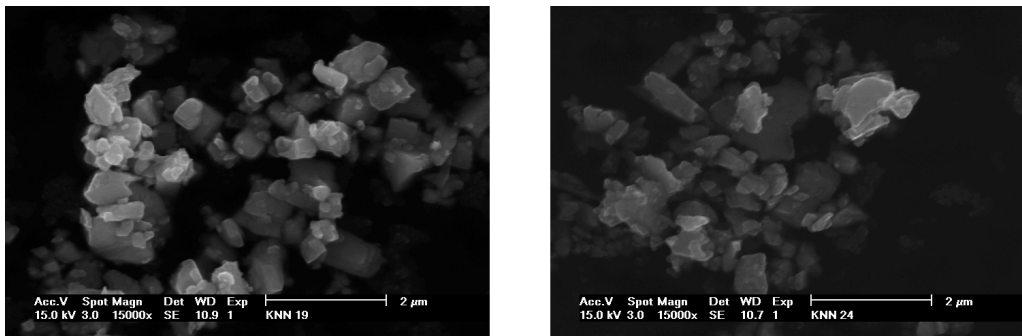

Figure 4.20: SEM image of a KNN powder.

The grain size distributions have been measured during all processing steps and the results are summarised in Figure 4.21. During synthesis most of the processing steps (especially all the milling steps used throughout the synthesis) have been adapted so as to minimise the mean particle size.
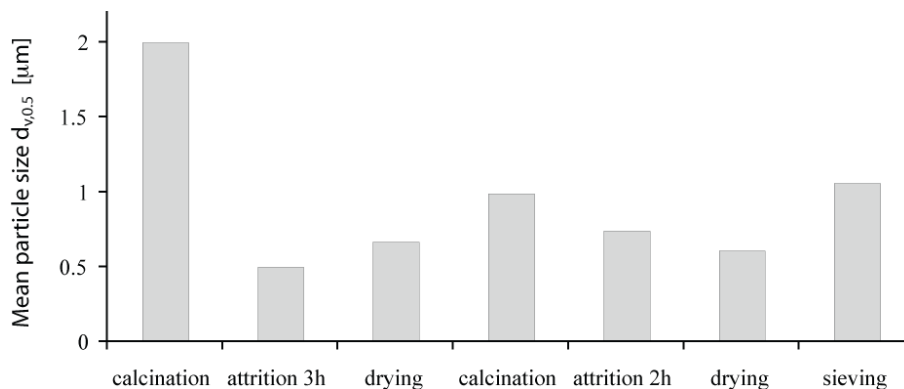

Figure 4.21: Particle size distribution after every processing step of a KNN powder.

It can be noticed that after each calcination step, the mean grain size increases, due to diffusion and agglomeration. Therefore a milling step is necessary after every calcination. At the end of the process, the powders are sieved to avoid particles over 100 μm. After this sieving step, the mean grain size increases slightly, one supposition being the "flying away" of the finer grains during the sieving.

After the sintering of the so-obtained powders, the grain size is typically of a few microns, and homogeneous, which means that no abnormal grain can be noticed, as shown in Figure 4.22.
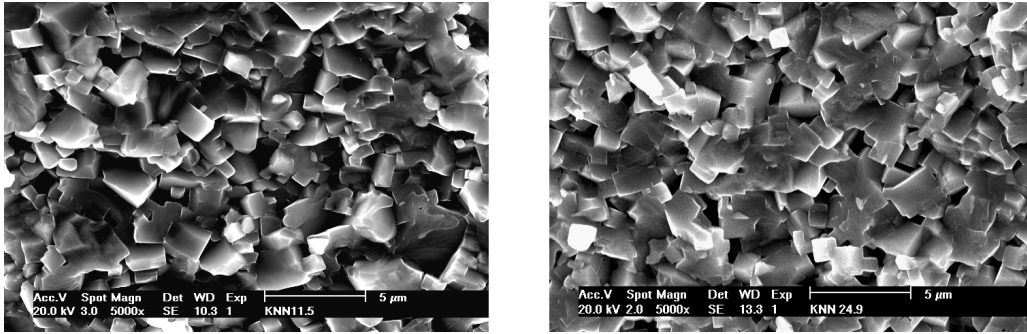

Figure 4.22: SEM image of two KNN samples after sintering.

4.4 Sintering of KNN ceramics

Uniaxial pressing was used to press pellets of different diameters, which are adapted to the properties to be measured. An alternative method, is the so-called isostatic pressing in which the sample is surrounded by a liquid under pressure, thus exerting a homogenous pressure on the entire surface of the powder, but to assure a simple processing, isostatic pressing was not used. For the uniaxial pressing, binders, plasticizers and deflocculants (to aid powder dispersion) can be mixed to the powder prior to pressing. However, these additives require an additional burning out step during the sintering [82], reason why no additives were used in this work.

The pressing conditions should be carefully monitored, for example to avoid cracking inside the sample. The pressing behaviour strongly depends on the sample dimension. For example for high pressures and aspect ratios near to one, density gradients can be found in the sample, as illustrated in Figure 4.23.
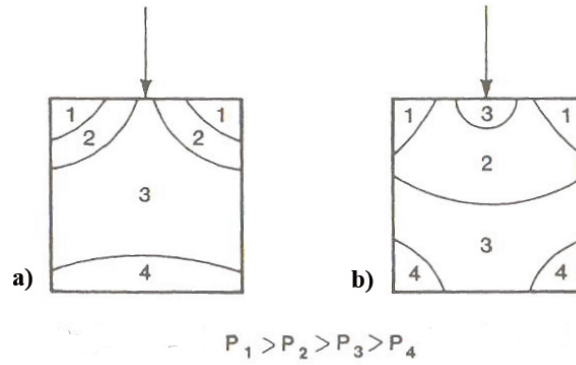
$P_1 > P_2 > P_3 > P_4$

Figure 4.23: Pressure gradients at a) beginning and b) after uniaxial pressing [82].

During conventional sintering, the different parameters that can be optimised are the heating and cooling rates, the sintering temperature and the dwell time. This work was focused on the optimisation of sintering temperature and time. In order to get an initial rough estimate of the sintering temperature, a dilatometric curve has been measured and is given in Figure 4.24.
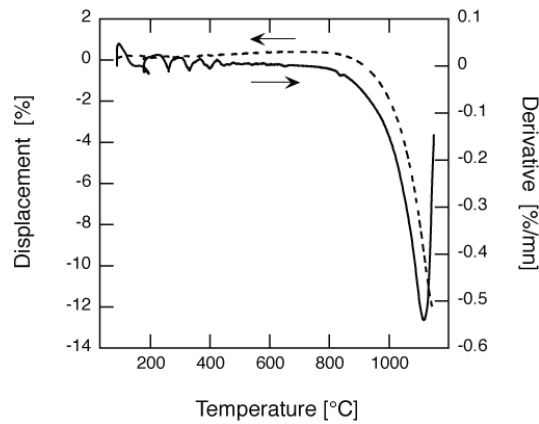
Figure 4.24: Dilatometry curve of a KNN pellet.

The sintering conditions are optimised in order to obtain the highest density and lowest dielectric losses. Low losses are more important for dielectric and piezoelectric properties than high values of density, but both criteria lead mostly to the same sintering conditions. The samples were sintered in a refractory *Lenton* furnace with maximal temperature set to 1450 °C. The optimised sintering conditions for pure KNN ceramics are shown in Figure 4.25.

Figure 4.25: Sintering step for pure and 0.5% Sr doped KNN ceramics.

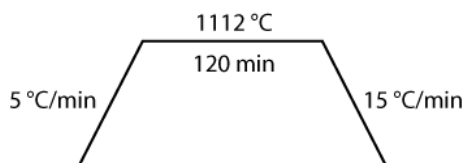It is important to find sintering conditions to avoid abnormal grain growth, a fact that appears easily in potassium sodium niobate ceramics. In the worst cases, the grains can grow up to dozens of microns and incorporate pores, as shown for example in Figure 4.26.
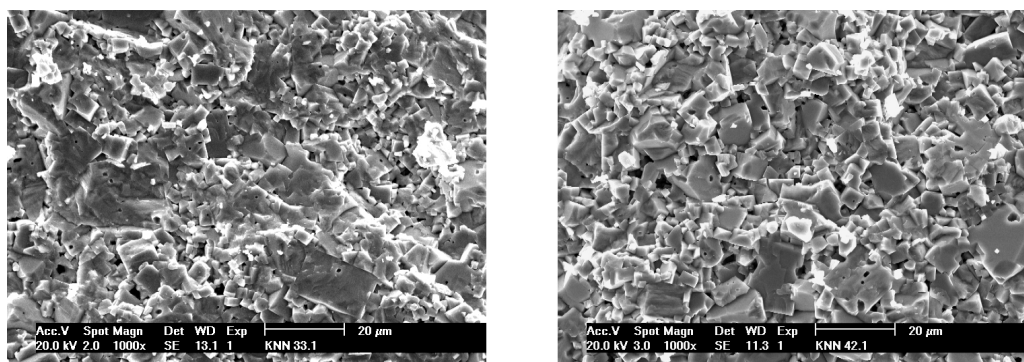

Figure 4.26: SEM image of KNN ceramics showing grain growth.

Densities of around 4.30 g/cm^3 are obtained for doped KNN ceramics with 0.5% strontium in the A site (which corresponds to about 95% of the theoretical density). The temperature range of KNN ceramics sintering is narrow, only about 10 °C; at lower temperature, the diffusion is not efficient enough and at higher temperatures grain growth occurs. Even taking all possible precautions, the dense ceramics are difficult to synthesise in a reproducible way.

For a better understanding of the sintering process, many dopants like alumina (Al_2O_3, material from the crucible), zirconia (ZrO_2, milling media) or niobium oxide (Nb_2O_5) have been introduced in small amounts (0.25-0.5%). In all the cases, the densities of the sintered ceramics were around 95%, but the microstructures were not optimal, as shown in Figure 4.27. The dielectric losses were high, making them useless for dielectric and piezoelectric applications.
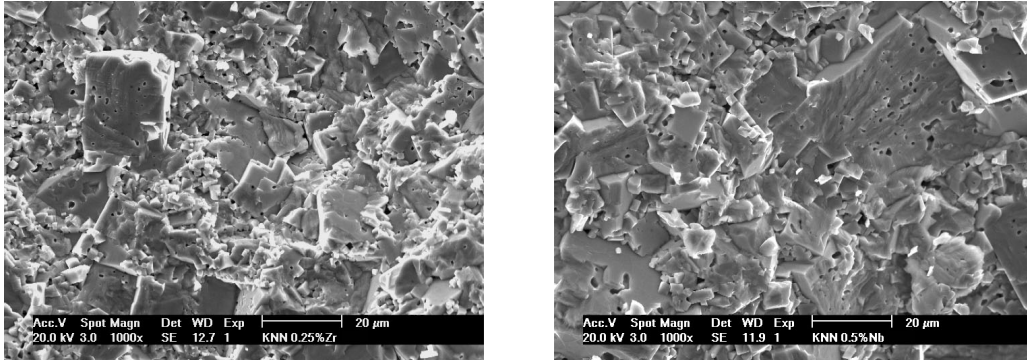
Figure 4.27: SEM image of ZrO_2 and Nb_2O_5 doped KNN ceramics.

To get high densities, hot pressing techniquecan be used, which implies the application of pressure during the sintering cycle. In this method, the driving forces for the densification are the temperature and the pressure, leading often to a reduced grain size compared to conventional sintering. However, the principal problem of this technique is that it is not well suited for industrial purposes. Some other techniques like plasma spark (as example for $SrTiO_3$ modified KNN ceramics [65]) or microwave sintering can also be applied to increase the quality of the ceramics as high heating rate can for example be obtained by these techniques and thus avoiding grain growth, but here, special care was taken to keep the processing applicable in industry.

For hot-pressing, an uniaxially pressed sample is placed in an alumina cylinder, as shown in Figure 4.28. To avoid the sticking of the sample on the alumina after the sintering (at such high temperatures potassium sodium niobate reacts with alumina), the sample is soaked in a zirconia suspension (zirconia powder dispersed in ethanol), to protect the whole surface of the sample with zirconia [45]. A sapphire is placed on both surfaces of the sample in order to avoid the sticking of the alumina piston on sample. Moreover, the adjunction of this sapphire ensures the parallelism of the surfaces of the sample since the piston is smaller than the sample. In this way, the sample can be, after a hot pressing, removed without breaking any part of the set-up.
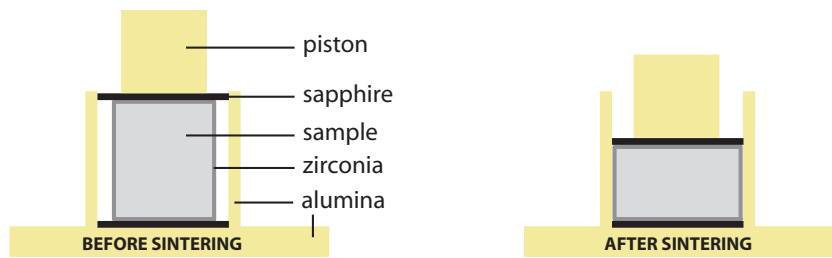

Figure 4.28: Schematic representation of the sample preparation for hot-pressing.

Starting from the sintering cycle used for conventional sintering (at about 1100 °C), the parameters are optimised. The sintering temperature has been gradually decreased as the densification is enhanced due to the application of a pressure. A typical example of

47

obtained microstructures is shown in Figure 4.29 for sintering temperatures of respectively 1100, 1050 and 1000 °C. It has to be mentioned that the pressure is only applied during the dwell time, and not during the heating and cooling steps. The maximum force that has been applied is 3 kN (40 MPa), for about 15 minutes, depending on the sintering temperature.
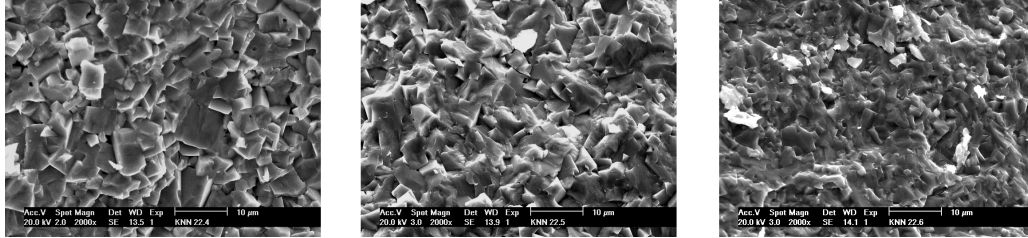
Figure 4.29: SEM picture of KNN ceramics hot-pressed at 1100 °C, 1050 °C and 1000 °C.

The surfaces of the so-obtained ceramics are not perfectly flat, but the samples can be cut and rectified by ultrasound technique to get precise dimensions. The densities of the samples range from 4.47 to 4.50 g/cm^3, which is around 99% of the theoretical density of KNN. The ceramics show smaller grain sizes than the conventionally sintered ceramics as illustrated in Figure 4.29.

A summary of the processing steps to obtain KNN ceramics by conventional sintering is depicted in Figure 4.30.
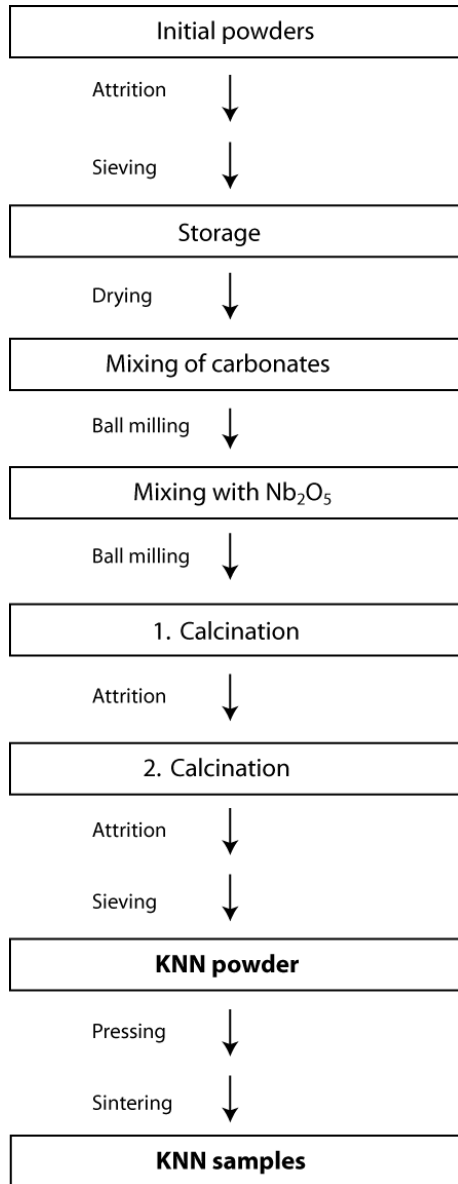
```
                    ┌─────────────────────────┐
                    │     Initial powders     │
                    └─────────────────────────┘
          Attrition              │
                                 ↓
          Sieving                │
                                 ↓
                    ┌─────────────────────────┐
                    │        Storage          │
                    └─────────────────────────┘
          Drying                 │
                                 ↓
                    ┌─────────────────────────┐
                    │   Mixing of carbonates  │
                    └─────────────────────────┘
          Ball milling           │
                                 ↓
                    ┌─────────────────────────┐
                    │    Mixing with Nb₂O₅     │
                    └─────────────────────────┘
          Ball milling           │
                                 ↓
                    ┌─────────────────────────┐
                    │     1. Calcination      │
                    └─────────────────────────┘
          Attrition              │
                                 ↓
                    ┌─────────────────────────┐
                    │     2. Calcination      │
                    └─────────────────────────┘
          Attrition              │
                                 ↓
          Sieving                │
                                 ↓
                    ┌─────────────────────────┐
                    │       KNN powder        │
                    └─────────────────────────┘
          Pressing               │
                                 ↓
          Sintering              │
                                 ↓
                    ┌─────────────────────────┐
                    │      KNN samples        │
                    └─────────────────────────┘
```

Figure 4.30: Summary of the processing steps for KNN ceramics.

A conclusion arising from this adapted process is that the processing route needs to be carefully optimised for each new composition or family of compositions, especially the sintering conditions, which are the most sensitive to impurities, particle size distribution and composition. To avoid any effect of moisture, all the powders had to be stored in desiccators with 15% relative humidity.

4.5 Lithium and tantalum modified KNN ceramics

In our constant efforts to improve the densification and the piezoelectric properties of KNN ceramics, many dopants (i.e. a substance added in small amounts), in particular divalent atoms as barium or strontium have been used. It is assumed that by introducing a divalent atom in the crystallographic lattice, the number of defects leads to higher densities because of an accelerated diffusion through the vacant sites. The densification is

in fact increased with these additions, but properties of such ceramics are not necessarily improved compared to pure KNN ceramics.

As it is the case in PZT and in the ferroelectric-relaxor systems PMN-PT and PZN-PT, the introduction of a compound in high amount can lead to a structural change. The two structures that are usually observed are one hand rhombohedral, orthorhombic or monoclinic and on the other hand tetragonal. It appears that, at the intersection of the two structures the properties seem to be maximised. The design of new lead-free ceramics does use this idea of increased properties around a structural phase transition.

In the case of potassium sodium niobates with orthorhombic structure, it has been reported that the introduction of high concentrations of lithium niobate and/or tantalum is inducing a phase transition from orthorhombic to tetragonal at high concentrations [57, 58]. To improve the piezoelectric properties of pure KNN, (K, Na, Li)(Nb, Ta)O_3 ceramics were synthesised.

Starting from the processing steps for the KNN ceramics, the parameters that have to be adjusted are essentially the different thermal cycles. The preparation of the initial powders is identical to that of KNN ceramics. Tantalum oxide has not to be attrited as the purchased powder has a certified grain size < 5 μm and lithium carbonate is only introduced in small amounts due to its low atomic weight. But introducing lithium and/or tantalum in high quantities can modify the reaction temperatures, as well as the densification processes. The afore described milling conditions (i.e. ball and attrition millings) have not been changed, as the obtained samples had good densities and homogenous microstructures. The calcination and sintering temperatures had then to be optimised for each different composition. Special care had to be given to the optimisation of the sintering temperature, because of its proximity to the melting point.

The first step to the synthesis of modified KNN powders is the determination of the calcination temperature.
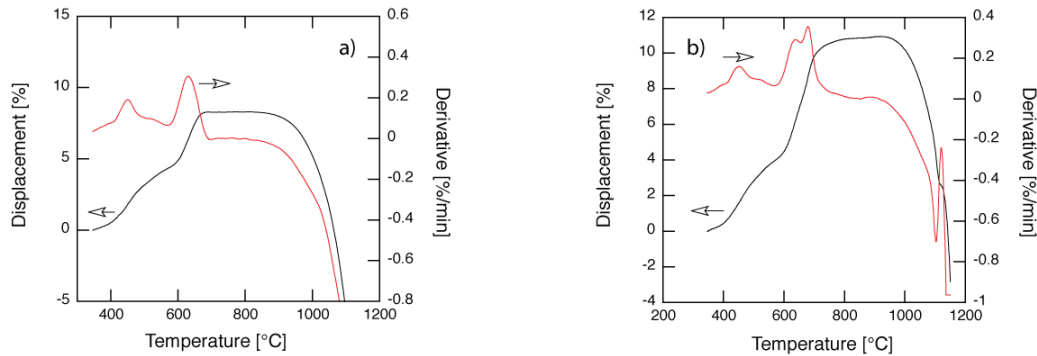

Figure 4.31: Dilatometry curves of stoichiometric pellets of modified KNN with final composition a) 6% lithium and b) 3% lithium with 20% tantalum.

Figure 4.31 shows dilatometry curves for KNN-6% lithium and KNN-3% lithium and 20% tantalum, which are the compositions with the highest expected properties. Basing on these curves, it becomes apparent that the reactions occur between 600 to 700 °C. These reactions occur at lower temperatures than for pure KNN ceramics, because of the high diffusivity of lithium, and thus, the calcination temperature can be kept at 825 °C as was the case for pure KNN. Instead of choosing a different calcination temperature for each composition, a high temperature (825 °C) was preferred. After calcination at

825 °C for 4 hours, the XRD patterns of the new compositions don't show any peaks corresponding to unreacted initial powders.

The powder characteristics of modified KNN ceramics are similar to those of KNN ceramics, the mean grain size being around 1 μm and the particle size distribution being bimodal, as shown in Figure 4.32 for a 6% lithium modified KNN powder.

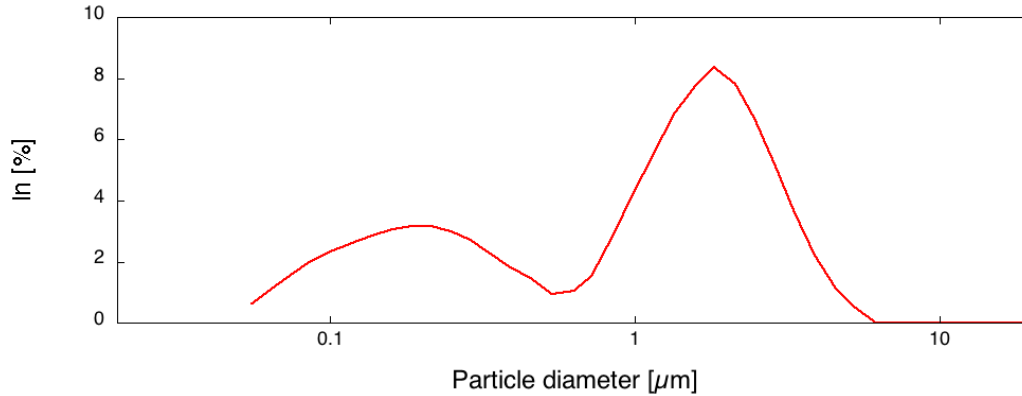*Figure 4.32: Particle size distribution of a 6% lithium modified KNN powder ($d_{v,0.1} = 0.12 \mu m$, $d_{v,0.5} = 1.23 \mu m$ and $d_{v,0.9} = 2.85 \mu m$).*

Despite of the fact that sintering conditions have been reported for these new compositions [55, 57], optimisation of the sintering temperature and time was necessary. It has been observed that the sintering conditions for lithium modified KNN compositions described by Guo *et al* [57] are not the best suited for our lithium modified ceramics, as grain size distribution for example can modify significantly the sintering behaviour of the ceramics. As a consequence, sintering temperatures and especially sintering times have been modified. For example, the effect of the variation of the sintering time on the microstructures of 6% lithium modified KNN ceramics are shown in Figure 4.33.
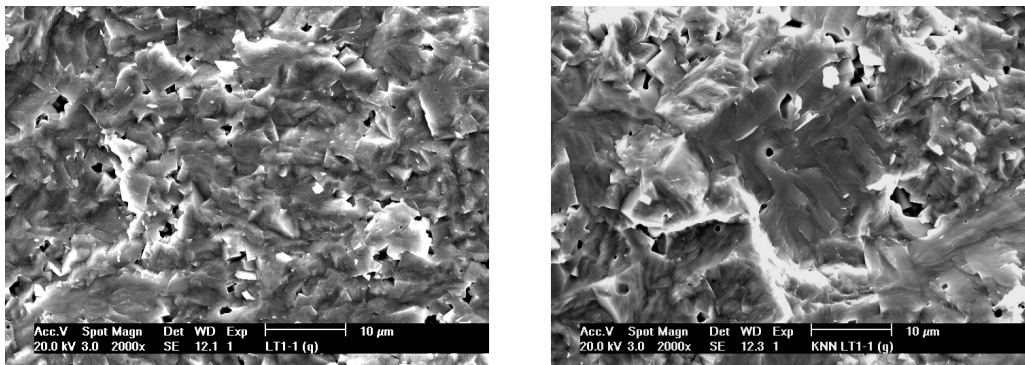

Figure 4.33: SEM image of 6% lithium modified KNN ceramics for 10 and 60 minutes at 1070 °C.

The densification process, especially for lithium modified KNN ceramics, takes place within a narrow temperature range (5 °C). Out of this range, either grain growth occurs at high temperatures or low densities are obtained at low temperatures, due to insufficient driving force for diffusion. Compared to pure KNN powders, which present a difficult

densification process, the introduction of lithium improves, because of its small size, the densification and in particular the diffusion processes. The sintering conditions used in this work for the two families of modified KNN ceramics, on one side the lithium and on the other side the lithium with tantalum modified KNN, are summarised in Figure 4.34. These plots show the variation of the sintering temperatures with lithium and tantalum contents. The ceramics sintered at these temperatures showed the best properties, principally density and dielectric losses.
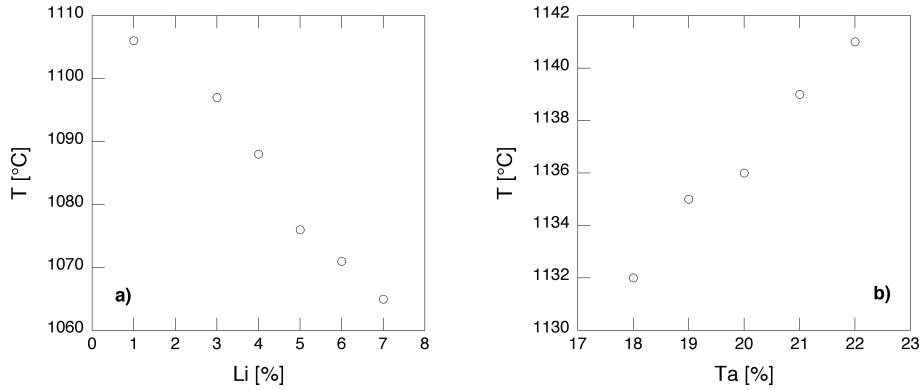

Figure 4.34: Sintering temperatures for a) Li-modified (10 minutes dwell time) b) Li (3%) and Ta-modified KNN ceramics (60 minutes dwell time) used in this work.

As stated previously, the temperature and compositions are not the only crucial factors influencing the densification process. Indeed, the effect of the time required is of importance (and is not shown on Figure 4.34). On these graphs only the sintering temperatures are depicted, but the sintering times should be mentioned. As seen in Figure 4.33, lithium modified KNN ceramics, can show grain growth for long dwell times and as a consequence, the dwell time for all the lithium modified ceramics is decreased to 10 minutes, but with maintaining the sintering temperatures close to the melting point. With these sintering parameters, densities higher than 95% are obtained. This problem of grain growth is not encountered in the case of tantalum modified ceramics, so for this family a sintering time of 60 minutes is sufficient to obtain high densities (higher than 95%), which then allows to sinter at temperatures further away from the melting point and thus reducing the risk of liquid phase sintering.

Grain growth appears at high temperatures, as well as for long sintering times. A compromise between sintering temperature and time had to be found. The effect a very small atom like lithium on the diffusion at high temperature is evident in that context. Lithium and tantalum modified ceramics are less sensitive to grain growth than lithium modified ceramics, which is nicely illustrated in Figure 4.35. This is due to the fact that the lithium concentration used for such compositions is lower (3%) than for lithium modified ceramics near the phase transition (6% lithium). The final grain size of tantalum modified ceramics is much smaller and the grain size distribution is narrower (no grain above 10 μm can be noticed).
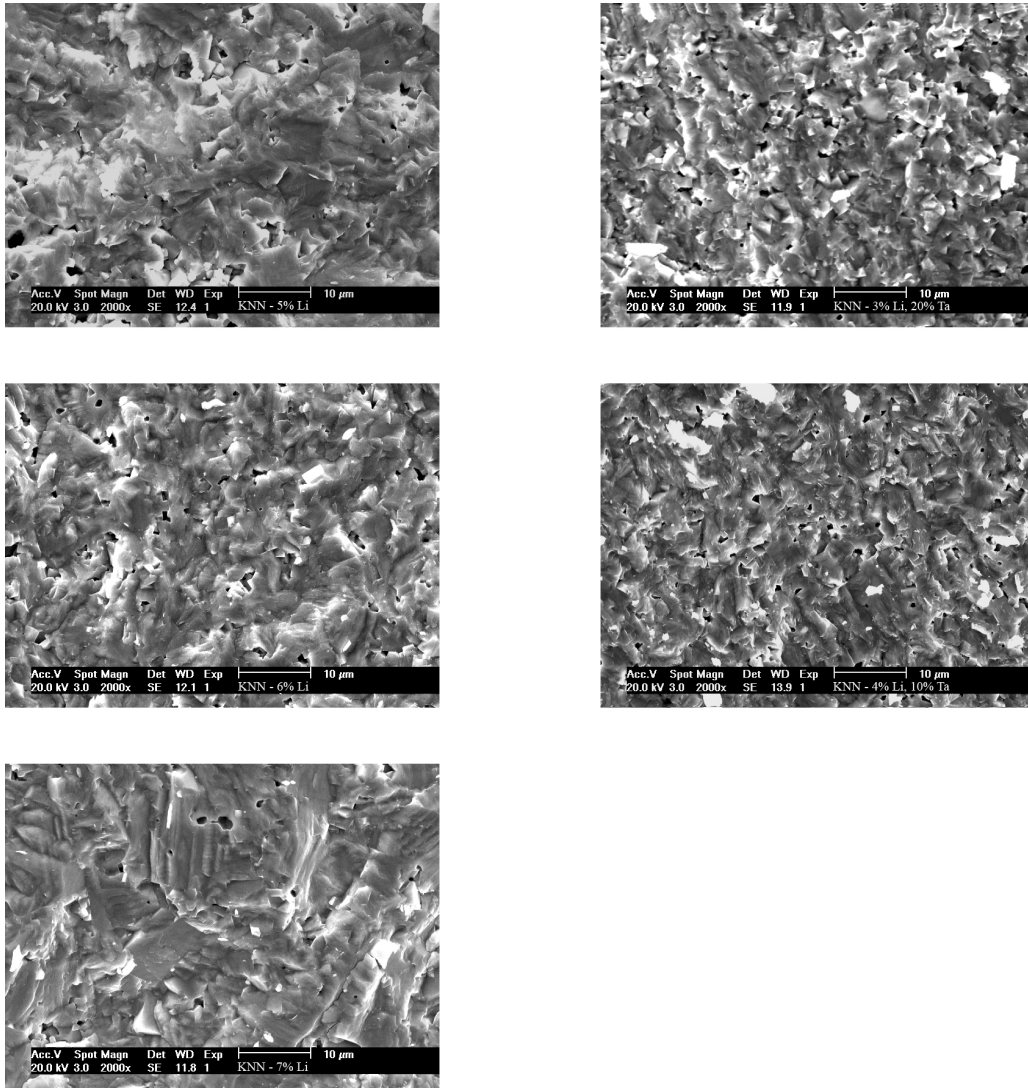
Figure 4.35: From top to bottom, SEM image of 5,6 and 7% lithium modified KNN ceramics on the left hand side and compositions $(K_{0.485}Na_{0.485}Li_{0.03})(Nb_{0.8}Ta_{0.2})O_3$ and $(K_{0.48}Na_{0.48}Li_{0.04})(Nb_{0.9}Ta_{0.1})O_3$ on the right hand side.

The respective lattice planes for each reflection on the XRD pattern have been identified and are shown on Figure 4.36. This indexation is necessary for the determination of the lattice parameters.
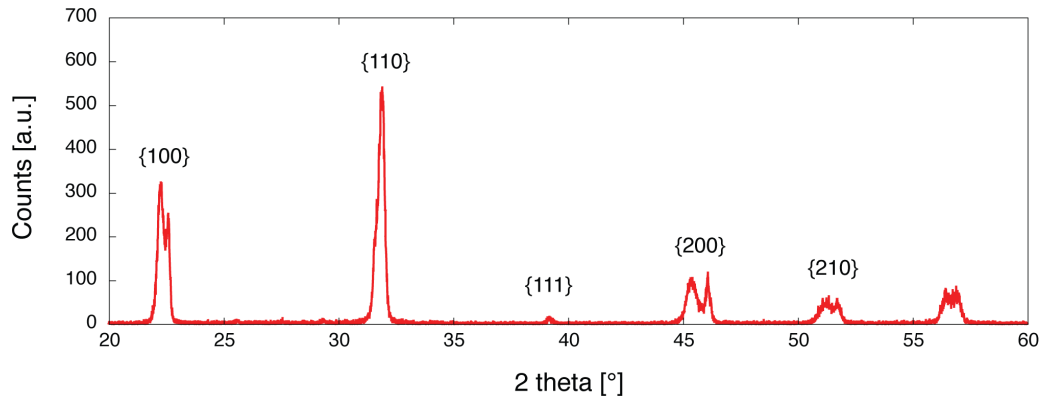
Figure 4.36: Indexed diffraction pattern of a 6% lithium modified KNN ceramic

The relative intensities between the peaks of a same family of planes is modified considering the tetragonal and orthorhombic phases, as it can be seen in the diffraction patterns as a function of the lithium content in Figure 4.37.
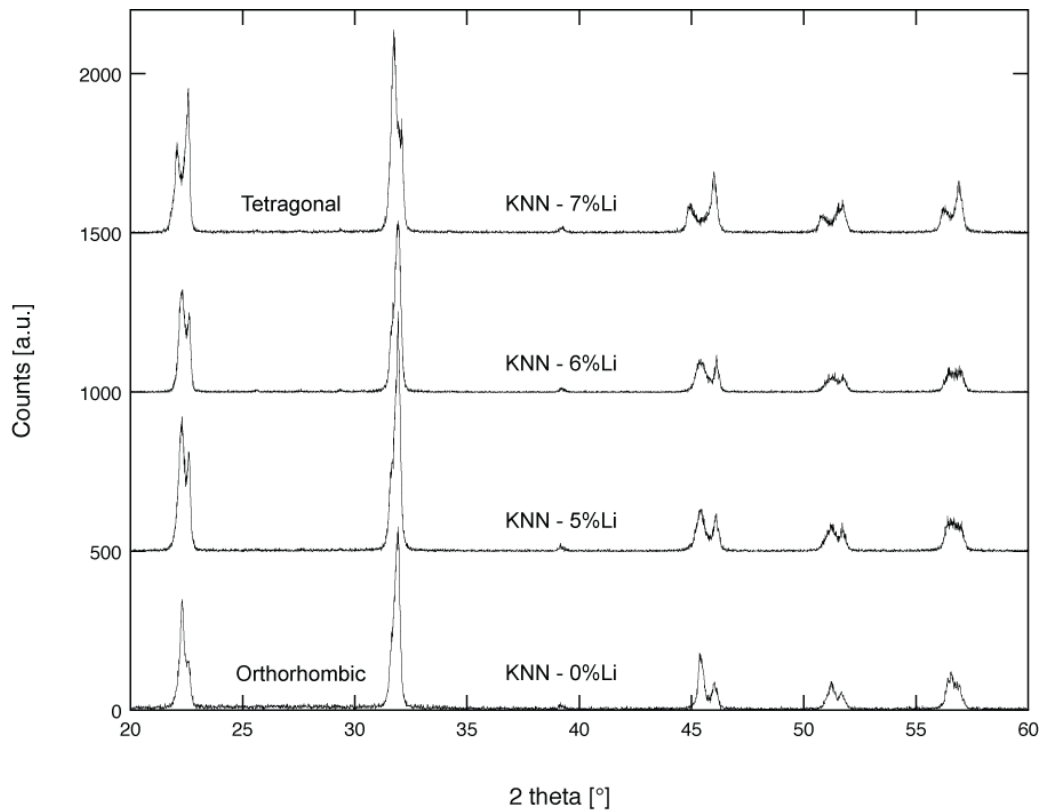

Figure 4.37: Diffraction pattern of modified KNN ceramics with, 0, 5, 6 and 7% lithium.

The phase diagram by Matsubara *et al* [83] reproduced in Figure 4.38 illustrates the phase transitions between orthorhombic and tetragonal structures as well as the tetragonal to cubic phase transition. This phase diagram confirms that the phase transition of the 6% lithium modified ceramics are located at room temperature.
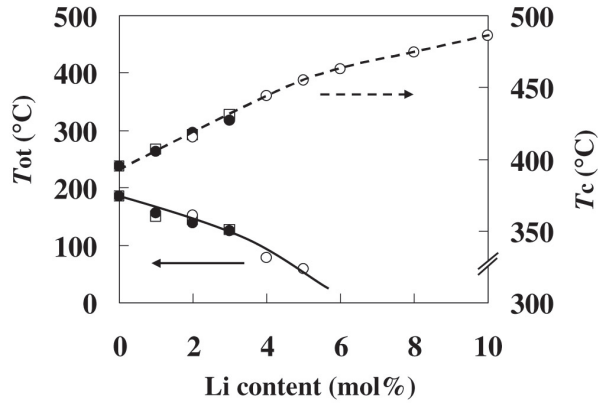
Figure 4.38: Phase diagram for (K,Na,Li)NbO₃ ceramics with 0.38% KCT as sintering aid as a function of the lithium content [83].

Lattice parameters of the $(K_{1-x}Na_x)NbO_3$ and $(K_{0.5-x/2}Na_{0.5-x/2}Li_x)NbO_3$ systems have been reported [57, 84, 85] and as an example the evolution of the lattice parameters as a function of the lithium concentration is shown in Figure 4.39 [57].
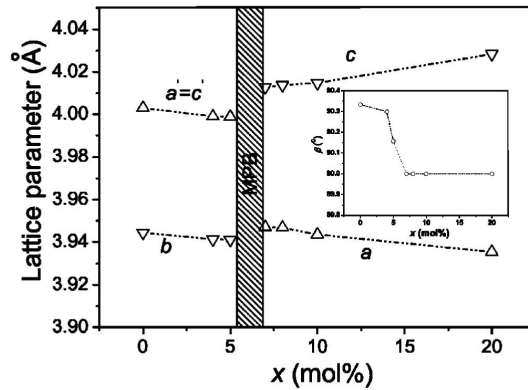

Figure 4.39: Lattice parameters for $(K_{0.5-x/2}Na_{0.5-x/2}Li_x)NbO_3$ ceramics as a function of the lithium concentration [57].

These parameters can be compared to the results obtained in this work using the trial and error method TREOR, with supposition that the structure is either orthorhombic or tetragonal (as KNN is orthorhombic). The lattice parameters have been determined with the lattice planes identified in Figure 4.36. For KNN and lithium modified KNN ceramics, the results of the lattice parameters match reported data [57]. In Figure 4.40, phase transitions are observed around 6% lithium on one hand and on the other hand, for the ceramics family modified with 3% lithium at around 20% tantalum.
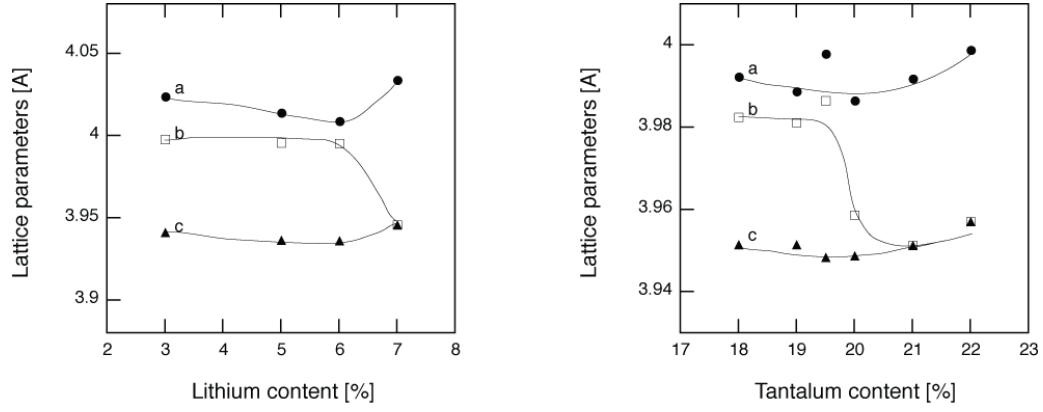
55

Figure 4.40: Lattice parameters a,b and c of lithium and lithium (3%) with tantalum modified KNN ceramics as a function of the lithium and tantalum concentrations respectively.

A summary of the compositions synthesised during this work is shown in Table 4.1.

Table 4.1: The modified KNN compositions synthesised in this work can be classified by the concentrations of elements in the A and B sites of the perovskite structure (ABO_3).

A site			B site		
K [%]	Na [%]	Li [%]	Nb [%]	Ta [%]	Sb [%]
49.5	49.5	1	100	-	-
48.5	48.5	3	100	-	-
48	48	4	100	-	-
47.5	47.5	5	100	-	-
47	47	6	100	-	-
46.75	46.75	6.5	100	-	-
46.5	46.5	7	100	-	-
46.25	46.25	7.5	100	-	-
48.5	48.5	3	82	18	-
48.5	48.5	3	81	19	-
48.5	48.5	3	80.5	19.5	-
48.5	48.5	3	80	20	-
48.5	48.5	3	79	21	-
48.5	48.5	3	78	22	-
49	49	2	80	20	-
48	48	4	80	20	-
48.5	48.5	3	78	20	2
48.5	48.5	3	76	20	4
44	52	4	86	10	4
44	52	4	84	10	6
50	50	-	95.8	0.2	4

These ceramics can be mainly classified into two groups, the lithium modified ceramics and the lithium with tantalum modified KNN ceramics.

56

4.6 Homogeneity

Inductively coupled plasma mass spectroscopy (ICP-MS) has been applied in the laboratory (by N. Klein) to analyse the chemical compositions of the modified KNN ceramics, as many characterisation techniques don't allow to measure the lithium concentration. From these measurements, the composition of the ceramics is in good agreement with the stoechiometry expected, differing of about 0.5% in the worst cases.

As reported by Guo *et al* [57], increasing the lithium content above 7% will lead to the apparition of the secondary phases $K_3Li_2Nb_5O_{15}$. For compositions below 7%, secondary phases can be observed due to an insufficient mixing of the initial powders. An example of secondary phases can be seen in Figure 4.41 for a 3% lithium and 20% tantalum modified KNN ceramic.
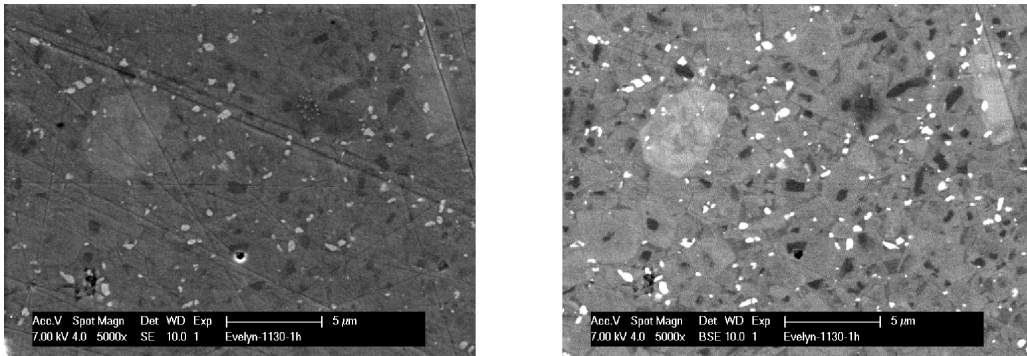

Figure 4.41: SEM images of secondary and backscattered electron microscopy of lithium (3%) and tantalum (20%) modified KNN ceramics showing the compositional heterogeneity.

Similarly to SEM analysis, the elemental mapping obtained by transmission electron microscopy (high resolution Philips CM 300 microscope) using energy dispersing X-ray analysis, is also pointing out the repartition of secondary phases within grains. The major limitation of this method is that the light elements such as lithium can't be detected. These results are highlighted in Figure 4.42.
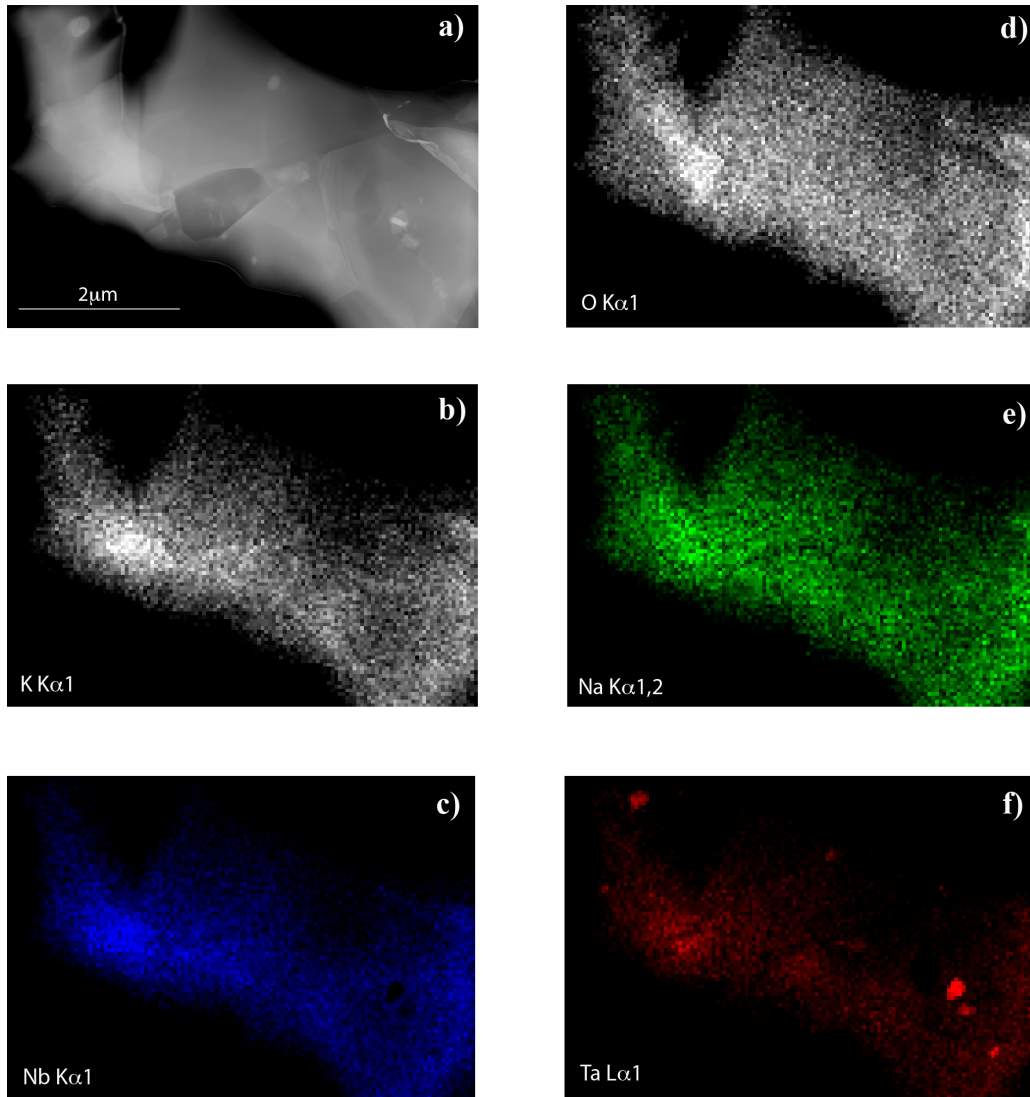
Figure 4.42: EDX mapping in transmission electron microscopy for a 3% lithium and 20% tantalum modified KNN ceramic. a) TEM picture, b) potassium, c) niobium, d) oxygen, e) sodium and f) tantalum distribution within the ceramic.

The control of the initial powders is the most important point in order to increase the homogeneity of the ceramics. If the initial grain sizes are decreased, these inhomogeneities are supposed to decrease. To bypass this particle size problem, spray drying may be used, but for this method to be applicable, the initial powders need to be soluble in a same solvent, which is not the case for our initial powders. The only solvents which dissolve all of the initial powders are strong acids like HF, but these would react with the spray-drying setup. Niobium oxide is almost insoluble (especially in water) compared to the other initial powders, and is also difficult to grind to a mean particle size below 1-2 μm. Interestingly, the properties of the sample are reproducible, despite of the presence of heterogeneities in the micron size.

4.7 Electromechanical properties

The processing steps described above lead to ceramics with densities higher than 94% in a reproducible way. The sintering conditions have been adjusted to optimise the density, but also the dielectric properties. In particular, the dielectric losses are a good indicator of a fine and homogeneous microstructure, leading to good electromechanical properties. Combining resonance and converse piezoelectric measurements, a complete electromechanical characterisation is given in this section for compositions developed by Saito *et al* [55] and Guo *et al* [57].

Piezoelectric resonance measurements on disk shaped samples enable the determination of the elastic, electromechanical coupling coefficients and piezoelectric coefficients $s_{11}{}^E$, $s_{12}{}^E$, k_p, k_t, k_{31}, d_{31} as well as the permittivity. The electromechanical properties at room temperature for lithium and lithium with tantalum modified ceramics are summarised in the Tables 4.2 and 4.3.

Table 4.2: Electromechanical properties of lithium modified KNN ceramics.

Properties	3% Li	5% Li	6% Li	7% Li	7.5% Li	Pz26
permittivity [-]	418	420	480	760	919	1300
losses [-]	0.085	0.022	0.026	0.025	0.026	0.003
$s_{11}{}^E \times 10^{12}$ [m²/N]	10.5	10.5	11.4	12.8	12.9	-
$s_{12}{}^E \times 10^{12}$ [m²/N]	-4.27	-3.60	-4.21	-5.54	-6.04	-
d_{31} [pC/N]	-38	-59	-59	-76	-72.1	-130
k_p [-]	0.348	0.520	0.474	0.486	0.43	0.57
k_t [-]	0.39	0.53	0.49	0.51	0.34	0.47
k_{31} [-]	0.189	0.299	0.266	0.259	0.22	-

Table 4.3: Electromechanical properties of lithium (3%) and tantalum modified KNN ceramics.

Properties	10% Ta*	18% Ta	19% Ta	20% Ta	21% Ta	22% Ta	20% Ta, 2% Sb
permittivity [-]	578	753	762	829	928	973	1184
losses [-]	0.030	0.025	0.033	0.024	0.024	0.028	0.031
$s_{11}{}^E \times 10^{12}$ [m²/N]	11.2	11.0	11.5	10.8	11.3	11.5	12.6
$s_{12}{}^E \times 10^{12}$ [m²/N]	-4.19	-4.53	-4.59	-4.30	-4.75	-4.97	-5.37
d_{31} [pC/N]	-63	-47	-34	-78	-48	-46	-94
k_p [-]	0.47	0.32	0.23	0.46	0.30	0.27	0.48
k_t [-]	0.52	0.32	0.36	0.46	0.31	0.22	0.43
k_{31} [-]	0.26	0.18	0.12	0.19	0.16	0.15	0.26

(* with 4% lithium)

The electromechanical properties at room temperature shown in these tables are in good agreement with previous reports [55, 57], confirming the enhancement of the properties in these composition regions, around 6% lithium for the first family and 20% tantalum

(with 3% lithium) for the second. In particular, coupling coefficients reach values of up to 50% for some particular compositions.

The dielectric permittivity at room temperature increases with the concentration of both lithium and tantalum, thus indicating the decrease of the orthorhombic to tetragonal phase transition temperature as a function of these concentrations. No permittivity maximum is observed in function of the composition, as it is the case for example at the MPB in PZT (see Figure 1.2).

The lithium and tantalum modified KNN ceramics present the best longitudinal and transverse piezoelectric coefficients, especially the ceramics modified with antimony (for 2% Sb, d_{33} = 220 pC/N and d_{31} = -94 pC/N). These ceramics are nevertheless difficult to pole due to high conductivity, even at low temperatures.

For lithium modified KNN ceramics, our previously published values of relative permittivity (950) and losses (0.084) with gold electrodes [86] differ from the values with chrome-gold electrodes (permittivity (760) and losses (0.025)), the electrical contact being improved with a thin layer of chrome (20 nm). The dielectric losses can be decreased previous to polarisation with an annealing at 150 °C.

Converse (strain-field) measurements were made at room temperature using a fibre-optic probe system. The longitudinal converse piezoelectric coefficient, d_{33}, was determined for a series of compositions and it is simply given by the ratio of the maximum strain over the maximum field in the cycle, S_{max}/E_{max}. All the compositions used, are thought, basing on the literature [55, 57], to be near the phase transitions for both the lithium modified ceramics and the lithium with tantalum modified ceramics for different tantalum concentrations. For comparison, the strain-electric field relationship for a commercial hard PZT sample (Pz26, Ferroperm, Denmark) is shown for each composition in Figure 4.43.
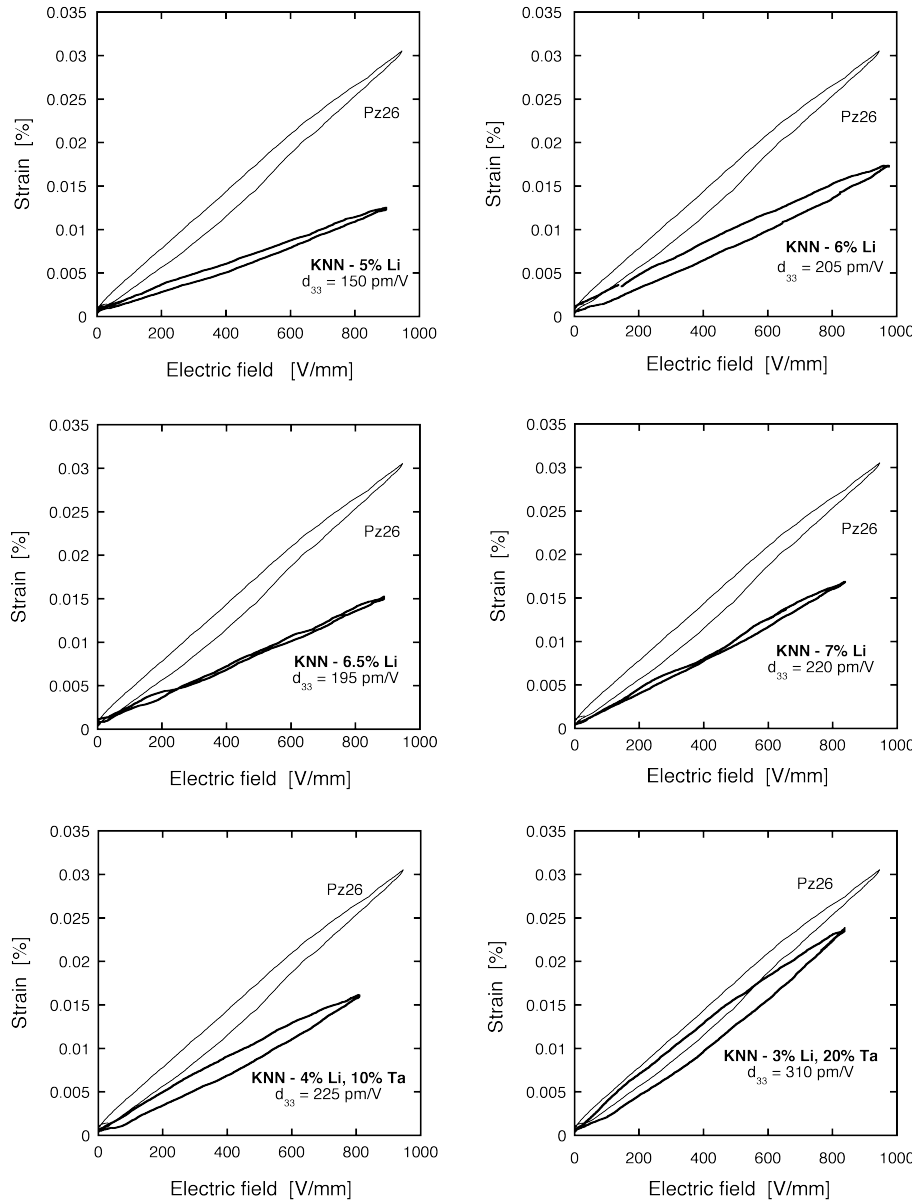
Figure 4.43: Strain versus electric field curves for lithium, lithium and tantalum modified KNN ceramics.

For the lithium substituted ceramics, the properties are improved around the phase transition, located at 6% lithium. The piezoelectric coefficients for lithium substituted KNN ceramics are around 200 pm/V for compositions near this transition and are slightly higher on the tetragonal side of the phase transition. Notably, all of the strain-field curves show a similar amount of hysteresis to the sample of hard PZT, with compositions 6.5 and 7% lithium (tetragonal) being nearly anhysteretic. The position of this phase transition in lithium modified samples reported by Guo *et al.* [57], and confirmed by this work, is different than the one reported by Saito *et al.* [55]. The reason may be that d_{31} and d_{33} do not peak at the same composition, as was previously observed for PZT [1].

The highest value of the piezoelectric coefficient of the measured composition is $d_{33} = 310$ pm/V, for lithium and tantalum substituted KNN ceramics of composition 3% lithium and 20% tantalum, almost reaching the value of that of the Pz26 sample

(d_{33} = 320 pm/V). To confirm these results, the strain-field measurements were repeated using the LVDT system and gave similar values of d_{33}, within experimental error (less than 5%). The lead-free substituted KNN ceramics have therefore converse piezoelectric properties very similar to those of the Pz26 sample both in terms of desirable "hardness", piezoelectric d_{33} and thickness coupling coefficients. It is still unclear whether the high piezoelectric response is related to the proximity of ambient temperature to the orthorhombic-tetragonal phase transition temperature. If so, one can expect instability of the properties with temperature variation. These questions will be treated in the next chapters.

For direct measurements, the aspect ratio of the samples should be at least 50%, since the piezoelectric coefficient is dependent on the aspect ratio (see Figure 3.6 for PZT). This is due to the distribution of the stress and the strain in the sample as a function of the thickness [79], when the surfaces of the sample are clamped in the press. No information about the effect of the aspect ratio in KNN ceramics is known. The polishing step is also important for these measurements, as the two electroded surfaces should be perfectly parallel to collect all the charges.

Piezoelectric coefficients d_{33} were determined using a Berlincourt-type press (section 3.2.4). The piezoelectric coefficients obtained for various compositions are summarised in Figure 4.44. The results shown are an average of at least 3 samples and the broadest spread is found for 6.5% lithium modified KNN ceramics (200, 260 and 280 pC/N).
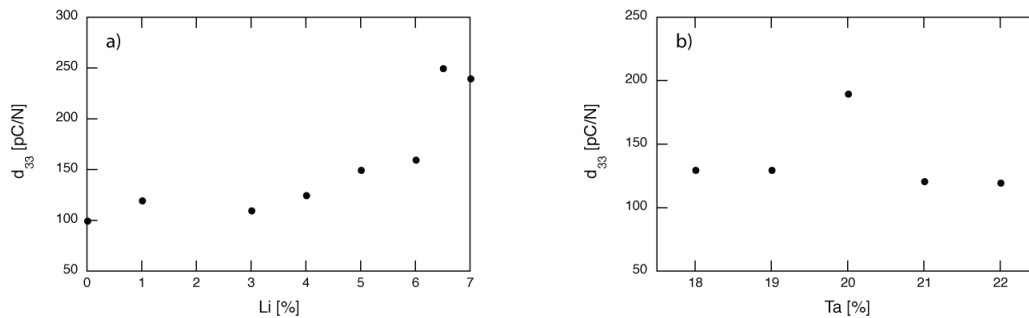

Figure 4.44: Piezoelectric coefficient d_{33} as a function of a) the lithium content and b) the tantalum content (for 3% lithium).

There is a net increase in the piezoelectric coefficient d_{33} near the the phase transitions, confirming the results reported previously [55, 57]. The piezoelectric coefficients obtained with the converse measurements can be up to 60% higher than those obtained by direct measurement. This difference has also be seen in $LiSbO_3$ modified KNN ceramics [59, 60]. There are three possible explanations for this. Firstly, the large fields applied during the converse measurements (up to 1000 V/mm) may actually better pole the samples. Secondly, the domain walls may be more susceptible to displacement under large unipolar electric fields than under uniaxial and weak dynamic compressive pressures. Finally, the aspect ratio of the samples was not well suited to direct measurements. In PZT, for example, d_{33} values measured for samples with aspect ratios of less than 0.5 can be reduced by as much as 30% by effects of lateral stresses at the points of contact [76]. Since we could not pole thicker samples to verify whether they would have large apparent coefficients, we consider the converse measurements, less dependent on sample geometry, to be more reliable. This assumption is confirmed by comparing direct and converse

measurements on Pz26 samples with high aspect ratios, in which case both experimental procedures gave similar values.

These measurements were confirmed by a characterisation carried out at Imasonic (Besançon) for $(K_{0.47}Na_{0.47}Li_{0.06})NbO_3$ and $(K_{0.485}Na_{0.485}Li_{0.03})(Nb_{0.80}Ta_{0.20})O_3$ ceramics and which can be found in Table 4.4.

Table 4.4: Summary of the properties of $(K_{0.47}Na_{0.47}Li_{0.06})NbO_3$ and $(K_{0.485}Na_{0.485}Li_{0.03})(Nb_{0.80}Ta_{0.20})O_3$ ceramics determined by Imasonic, compared to Pz24 from Ferroperm.

Properties	KNN - 6%Li	KNN - 3%Li, 20%Ta	Pz24
Density [g/cm^3]	4.76	4.25	7.70
Acoustic wave velocity [m/s]	6370	6824	4200
Acoustical impedance [MRayls]	30	29	32
Antiresonance frequency f$_p$ [MHz]	3.66	6.69	
Resonance frequency f$_s$ [MHz]	3.42	6.03	
Free permittivity $\varepsilon_{33}{}^T$ at 1 kHz [-]	865	528	425
Clamped permittivity $\varepsilon_{33}{}^S$ at 2f$_p$ [-]	480	233	240
Thickness coupling coefficient k$_t$ [-]	0.39	0.47	0.52
Bar mode coupling coefficient k$_{33}$ [-]	0.67	0.74	0.66

For medical transducers the acoustic impedance matching between the human body and the transducer is important. PZT is the most widely used piezoelectric material for the elaboration of medical transducers. Unfortunately, PZT has an acoustical impedance comprised between 30 and 36 MRayls, whereas the impedance of the human body is of about 1.5 MRayls [87]. To overcome this flaw, matching layers with graded acoustic impedance are placed between the PZT-transducer and the body. More conveniently, a simpler solution would be to replace the PZT by a piezoelectric material with lower acoustical impedance. Potassium niobate crystals as well as KNN ceramics have a reduced acoustic impedance compared to PZT (24 MRayls [54, 88]) and thus might be considered to be promising piezoelectric materials for medical transducer applications. The discovery of modified KNN ceramics with electromechanical properties similar to PZT reinforces this idea. As shown in Table 4.4, the acoustical impedances of lithium and tantalum modified ceramics prepared here are close to PZT. Nevertheless, one relevant advantage of the modified KNN ceramics compared to PZT is shown in Figure 4.45.
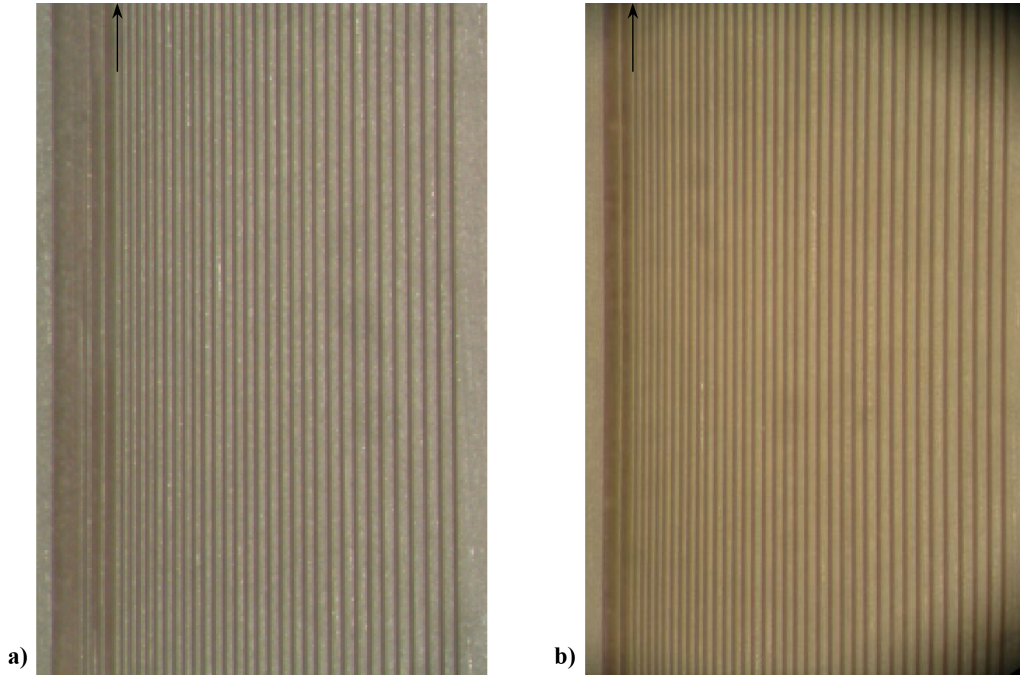
Figure 4.45: Picture of dicing of a) $(K_{0.47}Na_{0.47}Li_{0.06})NbO_3$ and b) $(K_{0.485}Na_{0.485}Li_{0.03})(Nb_{0.80}Ta_{0.20})O_3$ ceramics, the arrow showing the smallest entire slice.

In these images, the dicing pitch was progressively decreased from the left to the right and repeated five times for each size. The arrows show the dicing limit before the breaking of the samples. The limit dicing pitch for the two tested materials is 30 μm, which is significantly less than the 45 μm of commercially available Pz24. It appears that the modified KNN ceramics can be more finely diced than PZT.

Another difference between PZT ceramics and the modified KNN ceramics is the longitudinal wave velocity presented in Table 4.4, which is of interest for high frequency applications. The acoustic wave velocity of modified KNN ceramics is comprised between 6300 and 6800 m/s, which is far superior to the 4200 m/s of commercially available Pz24. As the longitudinal velocity is high, the active transducers elements can be thicker, which is of technical importance. Increased velocities directly contribute to the high values of acoustical impedance of the modified KNN ceramics.

4.8   Conclusions

Pure and modified KNN ceramics have been synthesised by traditional solid state sintering. The conventional processing steps have been optimised for the KNN based ceramics and the most important modifications are the following:

- As the choice of initial powders is crucial for the final quality of the ceramics, high purity carbonates and oxides have been chosen. To control the mean particle size and the particle size distribution during the processing, the initial powders have been milled using attrition milling, which revealed to be the most efficient milling method for these powders.

- To reduce the secondary phases, a second calcination step was introduced. Electron microscopy clearly shows that secondary phases are still present in ceramics produced in this way, but that the heterogeneity seems to be confined in the grains. Furthermore, no traces of secondary phase are found on XRD patterns, which means that the amount as well as the size of the secondary phases are markedly reduced compared to ceramics obtained via a the traditional processing. The reduction of the secondary phases requires a milling of the initial powders and some attempts to further reduce the particle size of the initial powders to sub-micron sizes were unfruitful.

- The sintering is the most sensitive step, as the densification has been reported to be difficult in such materials and because grain growth can easily occur. In this work, no sintering aid has been used, but the obtained densities for all the samples are well above 94%, simply by applying a conventional sintering. Introducing lithium in KNN ceramics, the sensibility of grain growth is even increased compared to pure KNN due to the high diffusivity of lithium. By adapting the sintering conditions, and principally the sintering time, grain growth could be avoided. But it has to be noted here, that the high diffusivity of lithium, even in low concentration, helps the densification.

The method demonstrated here is acceptable for industrial applications, since dense ceramics can be obtained without hot-pressing or addition of compounds that may reduce properties or require a burn-out step. Moreover, the samples have good chemical stability in air and no decomposition has been noticed after sintering. The final powders and samples do not need to be handled with special care, i.e. in a dry box like the initial powders, nor in a controlled atmosphere.

The as-produced ceramics have increased electromechanical properties compared to pure KNN ceramics. The piezoelectric properties, especially of lithium and tantalum modified KNN ceramics, get close to those of hard PZT, since the piezoelectric coefficient d_{33} is as high as 310 pm/V and thickness coupling coefficients k_t of around 0.50 have been measured. Their mechanical behaviour seems even better, as slices as thin as 30 μm can be cut.

Reproducibility is of great importance for industrial applications. The results shown throughout this section are always average values of at least 3 samples. However, experimental errors of up to 30% had to be registered in the case of lithium modified KNN ceramics for some of the measurements. The reproducibility of the lithium and tantalum modified KNN ceramics is far better, since most data lie within an experimental error of 15%. It is unclear here how and to what extent the reproducibility of the electromechanical properties is influenced by the lithium distribution in the ceramics and the coarser-grained microstructure of the lithium modified ceramics.

Chapter 5

Instability of materials with respect to humidity and time. Dielectric loss and conductivity.

In the previous chapter, the hygroscopic nature of the KNN based ceramics has been discussed and pointed out. This sensitivity, which is supposed to be the cause of the high losses observed at room temperature, can be linked to either the presence of hygroscopic secondary phases or to the microstructure (for example high porosity).

Dielectric relaxation processes in function of temperature have been noticed in pure KNN ceramics. To investigate on the origin of these relaxations, the dielectric properties of the pure KNN ceramics but also of modified KNN ceramics have been measured in this work as a function of composition, temperature and frequency. For hot-pressed pure KNN ceramics, no relaxations have been observed, highlighting the importance of the processing and in particular its reproducibility on the dielectric behaviour. In comparison, the conventionally sintered modified KNN ceramics and in particular the tantalum modified ceramics, don't show any relaxation at all. Dielectric spectroscopy can give valuable information about the relaxation mechanisms, but in the case of KNN based ceramics the measurements were non-reproducible due to electrical contact problems.

Humidity is also reported to affect the aging behaviour of the KNN ceramics. In this work, the evolution of the electromechanical properties of two compositions $((K_{0.47}Na_{0.47}Li_{0.06})NbO_3$ and $(K_{0.485}Na_{0.485}Li_{0.03})(Nb_{0.8}Ta_{0.2})O_3)$ is reported for different relative humidities, this stability with time being important for applications. The properties of tantalum modified ceramics revealed to be nearly time independent, and for both compositions, no effect of humidity was noticed.

5.1 Introduction

For a long time, the processing of potassium niobate based ceramics implied a washing step to remove the secondary phases, most of which are hygroscopic. Pure $KNbO_3$ and $(K_{0.5}Na_{0.5})NbO_3$ powders were obtained first by washing the powders with a hot solution of K_2CO_3 and then rinsed with distilled water [34, 42]. This procedure was replaced by a controlled solid state processing, which takes into account the evaporation of K_2O [35]. In this work by Flueckiger, the evaporation of K_2O was related to the humidity, since the temperature of oxidation of potassium carbonate to potassium oxide is lowered in the presence of water. To avoid as much as possible the presence of humidity, the powders should be prepared in a highly anhydrous atmosphere [32]. Furthermore, before the calcination step, no powder should be stored at temperatures below 200 °C [47, 89, 90]. A slight off-stoichiometry, which can be due to the presence of second phases, leads to the disintegration of the sintered samples [1, 90]. This again highlights the importance of a controlled processing of the ceramics.

In addition to the need of synthesising potassium niobate ceramics and crystals devoid of any second phase, the produced samples should as well show low dielectric losses. The first report on the difficulties inherent to the elaboration of potassium niobate single crystals with low losses, was published by Matthias *et al* [26]. The dielectric response of the crystals reported therein is shown in Figure 5.1.
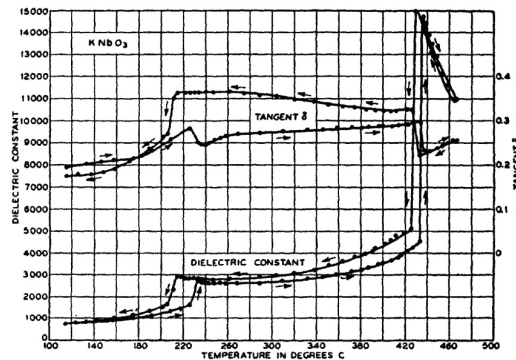

Figure 5.1: Dielectric permittivity and losses for $KNbO_3$ single crystals [26].

For potassium niobate ceramics, the temperature dependent measurements of the dielectric loss over a large frequency range are shown in Figure 5.2.
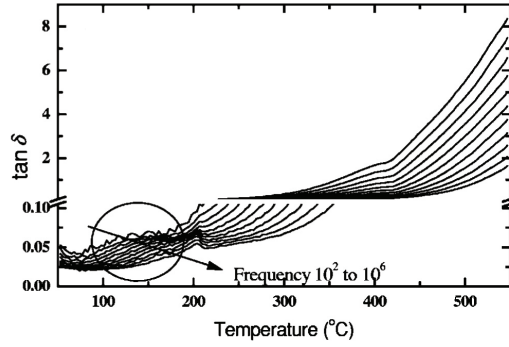
Figure 5.2: Dielectric losses for KNbO$_3$ ceramics as a function of temperature at various frequencies [91].

A dielectric relaxation peak can be seen for temperatures below 200 °C and the activation energy of this relaxation is in the same order of magnitude to those of likely relaxation mechanisms including the domain wall motion, hopping of free carriers (A or B site cation, oxygen vacancies) or interfacial polarisation. In the last part of that work, the authors concluded that the hopping of mobile charges and in particular of oxygen vacancies, was involved in the dielectric relaxation process [91]. Beside this low temperature relaxation, a low frequency (< 1 MHz) relaxation is observed for temperatures above 230 °C [90, 92]. Conductivity phenomena have been suggested to be the origin of this relaxation. However, the sensitivity of the materials to humidity cannot be totally excluded to be partially responsible for these phenomena, since hydroxides could easily have been formed [90].

In potassium niobate single crystals, high dielectric losses have also been reported at room temperature for low frequencies [93]. In this case, the porosity is assumed to be the reason; during the measurement the K$^+$ cations are supposed to diffuse on the surface around the pores due to the application of a field, necessary for the measurement.

For ultrasonic transducers, either high or low permittivities are needed to assure a low but measurable capacitance, in the case of rods (k$_{33}$ mode) and plates (k$_t$ mode), respectively. In both cases, low dielectric losses are required. For potassium sodium niobate ceramics, a combination of high densities and low dielectric losses is not trivial to obtain [42, 49]. By doping KNN ceramics, the densification process is improved and thus, leads to high densities, combined with low dielectric losses [46, 51]. As for potassium niobate ceramics, dielectric relaxations have been observed at temperatures around 170 to 200 °C [89, 47] in KNN ceramics. The conductivity due to the porosity or defects [89] and the hygroscopic sensitivity of potassium niobate [47] is believed to be the cause of these relaxations.

The aging behaviour of potassium sodium niobate ceramics is supposed to be strongly humidity dependent because their dielectric properties are sensitive to humidity [47]. The first aging measurements on potassium sodium niobates are shown in Figure 5.3.
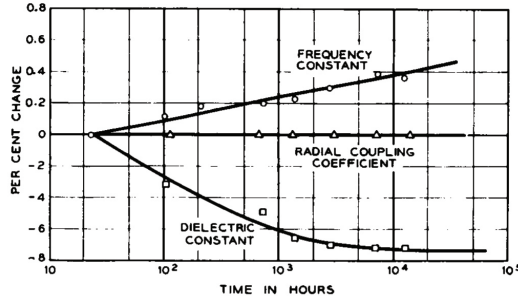
Figure 5.3: Aging of the dielectric constant, the radial coupling coefficient and the frequency constant of $(K_{0.5}Na_{0.5})NbO_3$ ceramics [42].

It can be observed that the radial coupling coefficient is constant with time, whereas the dielectric permittivity decreases with this parameter. The aging behaviour is supposed to depend on the nature of the raw powders (i.e. impurities) as well as the processing method. A preaging heat treatment is proposed as a solution to avoid the degradation of the properties in function of time [42], with a compromise of lower initial properties.

The time stability of conventionally sintered ceramics can be improved by hot pressing [45], but it is unclear whether the grain size reduction or the increased density (decrease of the porosity) of hot-pressed samples is the reason of the improved time-stability. The grain size can often be related to the domain wall mobility. Indeed, in the case of small grain sizes for instance, the domain walls are clamped due to high stresses [94].

Few reports show the influence of humidity on the aging behaviour. For example in the References [47, 90], the aging of KN and KNN samples kept in desiccators, i.e. with 15% relative humidity, has been measured and is shown in Figure 5.4.
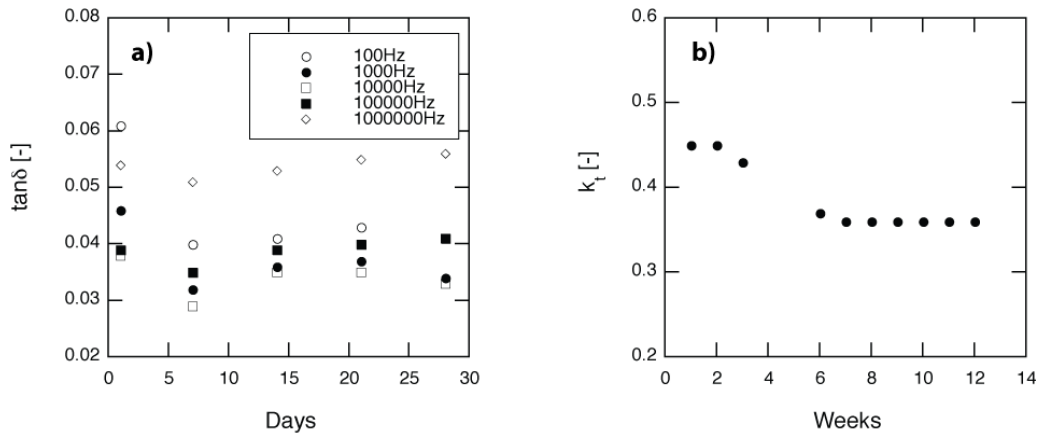

Figure 5.4: Aging of a) $\tan\delta$ of $KNbO_3$ [90] and b) the thickness coupling coefficient of $(K_{0.5}Na_{0.5})NbO_3$ ceramics [47] both stored in a desiccator.

Few reports on aging of the new KNN based ceramics have been published, for example by Saito *et al* [85] for dielectric losses and by Yang *et al* [95] for electromechanical properties of $(K_{0.44}Na_{0.52}Li_{0.04})(Nb_{0.96-x}Ta_xSb_{0.04})O_3$ ceramics. In the first report, the dielectric losses of tantalum modified ceramics remain stable with time (after 2500 days), which contrasts with the lithium modified ceramics whose dielectric losses increase with time. In tantalum modified KNN ceramics, the reduced diffusion of water in the samples

due to the high relative densities is given as the reason of this stability with time. In the second report, a small increase of the dielectric losses is observed and has been associated with the humidity sensitivity of the samples. Also a small reduction of the d_{33} and k_p coefficients has been measured, probably due to the domain wall relaxation with time. However, none of these two studies showed a relation between the humidity rate and the evolution of the properties with time.

The aim of the present chapter is to investigate the origins of the high dielectric losses in potassium niobate based materials. To determine the origin of these losses, dielectric measurements as a function of the temperature and frequency have been carried out. In particular, the introduction of a small atom like lithium, the conduction mechanisms are supposed to be modified. As the relaxation processes and the aging are both strongly dependent on the humidity, aging measurements have been performed in different atmospheres for different compositions.

5.2 Dielectric loss and conductivity

Compared to lead-based ceramics and in particular to PZT, the KNN ceramics have lower densities (4.52 g/cm^3) and higher acoustic wave velocities, which allows working with thicker samples. They are also interesting for high frequency applications due to their relatively high coupling coefficients and low dielectric permittivity. Indeed, thanks to these properties and especially to the reduced capacitance, an improved impedance matching can be obtained. Furthermore, it is primordial to understand the origin of the high dielectric losses before going to high frequency applications.

The dielectric response can give information on the polarisation mechanisms, which could be either of ionic and electronic nature (and called resonance processes) or due to space charge and dipolar polarisations (called relaxation processes). These mechanisms appear in different frequency ranges; at transition regions the dielectric losses and the dissipation of energy associated with these mechanisms increase (see Figure 5.5).
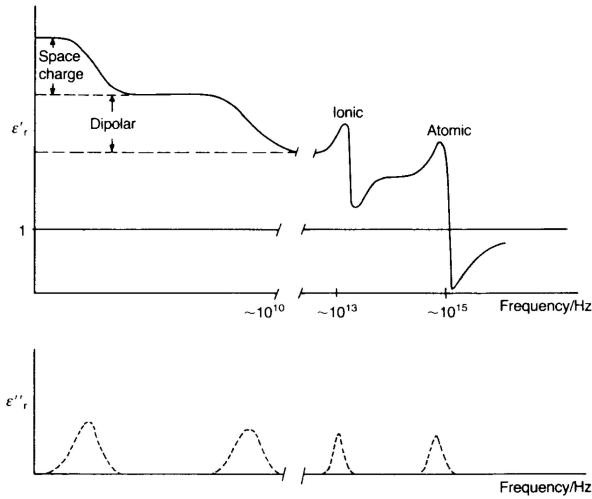
Figure 5.5: Variation of ε_r' and ε_r" with frequency. Space charge and dipolar polarisations are relaxation processes and are strongly temperature dependent; ionic and electronic polarisations are resonance processes and sensibly temperature independent. Over critical frequency ranges energy dissipation is a maximum as shown by peaks in ε_r"(ω) [10].

A classification of all types of dielectric responses found in solids is depicted in Figure 5.6 (adapted from work by Jonscher *et al.* [96]).
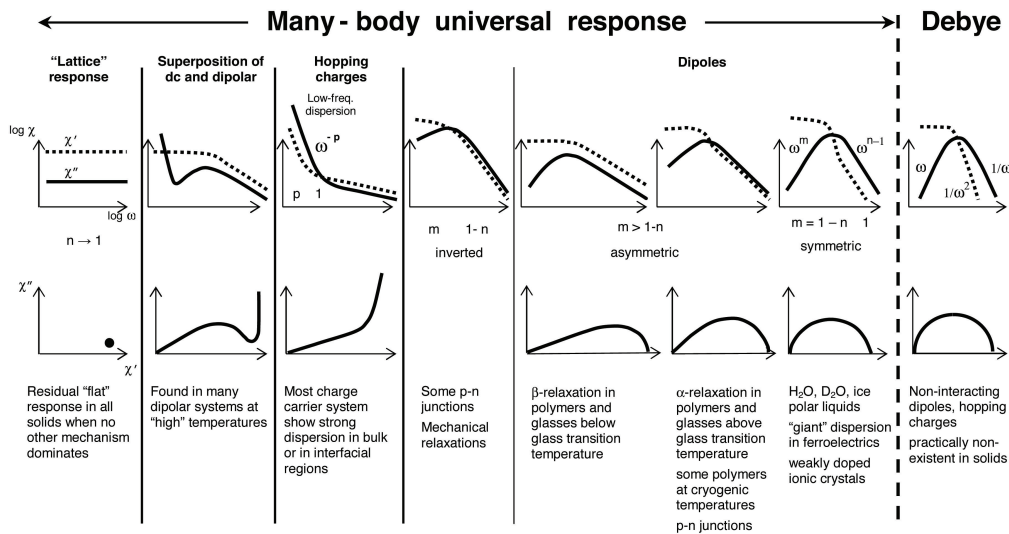
Figure 5.6: General classification of all types of dielectric responses found in solids. The upper row gives the diagrammatic representation of the logχ'(ω) (dotted line) and logχ"(ω) (solid line) against log ω, the lower row gives the corresponding complex susceptibility plots. Typical materials giving the various types of response are indicated. The extreme right gives the practically non-existent case of the Debye response, moving to the left the loss peaks appear increasingly broader for dipolar systems, further to the left the charge carrier responses corresponding to the strong low-frequency dispersion and to DC conductivity. On the extreme left is the limiting case of "flat" frequency- and temperature independent loss [96, 97].

Most of these mechanisms are also temperature dependent. As a consequence, the

dielectric response as a function of temperature and frequency gives information on the lossy mechanisms of the materials, using for example the analysis of the activation energies of the observed processes.

In a recent report, the activation energies of the likely mechanisms that lead to a low- frequency relaxation were carefully analysed [91]. The authors concluded that the principal origin of this relaxation process in $KNbO_3$ ceramics is the hopping of defect related dipoles (see Figure 5.6, the third response from the left), and in particular oxygen vacancies. For modified potassium sodium niobates, the dielectric response as a function of frequency and temperature can provide valuable information on the origin of the high dielectric losses observed at room temperature (see Section 4.7), as will be shown in this section.

The dielectric measurements as a function of the temperature were performed using an LCR meter (HP 4284A), with platinum tips for electrical contact. The samples were heated in a home made furnace with a heating rate of 2 °C/min, the temperature being controlled by a thermocouple placed next to the sample. The measurements were performed at different frequencies (ranging from 100 Hz to 1 MHz).

To measure the dielectric response of a ferroelectric material as a function of the frequency, and in particular to investigate the relaxation processes that can occur in the material (and which are related to defects) over many orders of magnitude, the dielectric spectroscopy method was used in this work and in particular the lock-in technique. The lock-in amplifier (SR 830) is used to create a sinusoidal signal on the sample and to measure the response of the sample. The charges measured on the samples are previously transformed into voltage by a charge amplifier (Kistler 5011) (see [97] for more details).

5.2.1   Potassium sodium niobate ceramics

The dielectric behaviour of several KNN samples (which have been synthesised in identical way) has been measured, because reproducibility is an important problem and its origins have not so far been reported. Some different dielectric behaviours of these KNN ceramics can be seen on Figure 5.7.
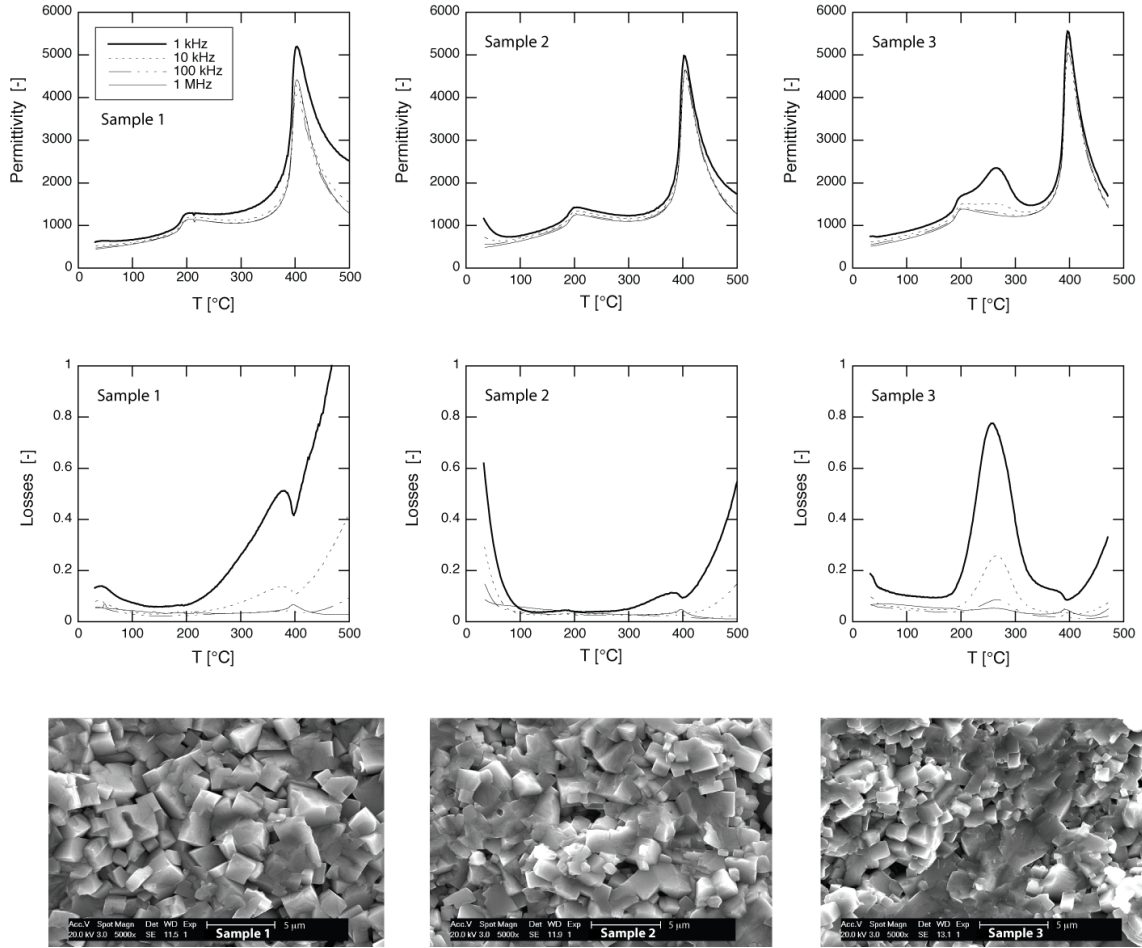
Figure 5.7: Dielectric permittivity and losses for 3 different KNN samples and corresponding SEM microstructures.

A relaxation is observed for the first sample around 300 to 400 °C and high losses appear at temperatures higher than 400 °C, the latter being observed for the 3 samples. The second sample also shows a low temperature relaxation and the third a relaxation in the intermediate temperature range (200 to 300 °C), both accompanied by high losses. The observed low temperature relaxation (between room temperature and 100 °C) can be suppressed by an annealing step at 150 °C for 30 minutes before the measurement. This relaxation could be due to a reaction with atmosphere (humidity problem), which can be related to non-stoichiometry and impurities, but the exact origins remain presently unknown. This low temperature relaxation is not a space charge effect related to grain boundaries as a similar behaviour has been observed in the case of single crystals, but it could be related to electrode-sample interface. As a consequence of this relaxation, the dielectric losses at room temperature are non reproducible. The intermediate relaxation (between 200 and 300 °C) has also been related to the humidity sensitivity of this family of ceramics or to niobium rich phases.

Nevertheless, the phase transitions temperatures, characterised by sharp discontinuities of the permittivity, are similar for all thes samples (200 °C for the orthorhombic to tetragonal phase transition and 400 °C for the Curie temperature). The values of the permittivity at these phase transitions (around 5000 for the Curie temperature and 1500 for the orthorhombic to tetragonal phase transition) are also reproducible from one sample

74

to the other, indicating the reproducibility of the intrinsic properties of the produced ceramics, but some charged defects, which are difficult to control can influence the dielectric properties. This is confirmed by the microstructures of the analysed samples shown also on Figure 5.7, as the grain size distribution is similar for all the samples and the densities are comparable (respectively 93.9, 93.9 and 92.8%). Sample 1 and 2 are even produced from the same powder batch.

As conclusion, the processing has a strong influence on dielectric properties. Indeed, for the first sample on Figure 5.7, no relaxation peak is observed, and the permittivity is in all the samples dependent of the frequency. Nevertheless, it is still difficult to control the properties in a reproducible way. As a consequence of these high dielectric losses, the poling of KNN samples is difficult.

On the other hand, in the case of hot-pressed samples, the dielectric permittivity is increased to 700, but the dielectric losses, which are reproducible from one sample to the other, are not strongly decreased (0.05). The dielectric behaviour of a hot-pressed KNN sample is shown in Figure 5.8.
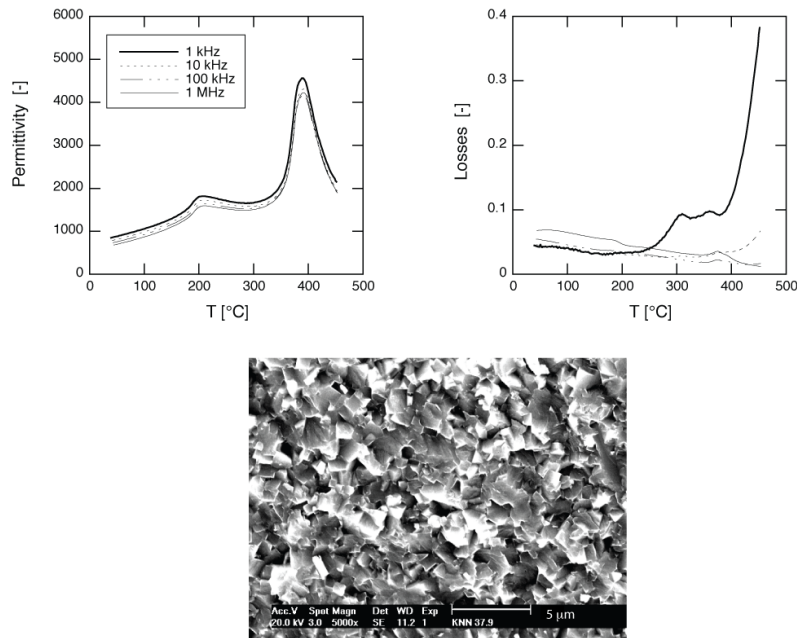
Figure 5.8: Dielectric permittivity and losses for a hot-pressed KNN sample.

The Curie temperature of the hot-pressed KNN ceramics is similar than for conventionally sintered ceramics, but the maximal value of the permittivity is lower (less than 5000) and the peak is broader. One possible explanation is the different microstructures of the hot-pressed ceramics compared to the conventionally sintered samples, indeed, the grain size is finer and the grain size distribution is narrower for hot-pressed samples as can be on Figure 5.8 compared to conventionally sintered samples on Figure 5.7.

Room temperature losses are reproducible and no strong dielectric dispersion is observed on the whole temperature range scanned, which is promising for applications. Unfortunately, hot pressing is not suitable for industrial use, due to its high cost and low throughput rate.

5.2.2 Modified potassium sodium niobate ceramics

For high frequency applications, low dielectric permittivity and losses are required. Thus, it is then desirable that the newly synthesised lithium and tantalum modified KNN ceramics satisfy these conditions. In that regard, room temperature dielectric permittivities and losses before polarisation are shown in Tables 5.1 and 5.2 for the lithium and the lithium with tantalum modified KNN ceramics, respectively.

Table 5.1: *Dielectric permittivities and losses at 1 kHz at room temperature for lithium modified KNN ceramics as a function of the lithium concentration.*

Li [%]	0	1	3	4	5	6	6.5	7
Permittivity [-]	400	405	425	440	500	680	680	950
Losses [-]	-	0.110	0.085	0.056	0.022	0.026	0.18	0.084

Table 5.2: *Dielectric permittivities and losses at 1 kHz at room temperature for lithium (3%) and tantalum modified KNN ceramics as a function of the tantalum concentration.*

Ta [%]	18	19	20	21	22
Permittivity [-]	750	780	920	928	970
Losses [-]	0.025	0.033	0.024	0.024	0.028

For pure KNN, no value of dielectric loss is indicated, because the reproducibility of the samples is poor. This is confirmed by the reported values, which are scattered between 0.02 and 0.07 depending on the source [42, 46, 47, 52, 57, 98, 99]. Compared to conventionally sintered samples, the hot-pressed samples have reproducible low dielectric losses and show better electromechanical properties after poling.

By increasing the lithium and tantalum concentrations, the dielectric permittivities increase. For high lithium concentrations, the permittivity reaches the values of the lithium and tantalum modified KNN ceramics, but the latter show lower dielectric losses.

Since the low-frequency measurements were non reproducible, it can only be suggested, that the high diffusivity of lithium causes high dielectric losses at room temperature and low frequency. Another explanation of the increased losses at about 6.5% lithium is the presence of a phase transition, but the permittivity is not maximal for such compositions. In a third and last hypothesis, some liquid phase between the grains could appear during the sintering. This phase could then lead to poor dielectric properties. This tentative explanation is supported by the fact that the sintering temperatures of lithium modified ceramics are close to the melting points.

Effect of temperature

Dielectric relaxations in pure KNN ceramics have been depicted in Figure 5.7. These relaxation processes have been related to humidity sensitivity of the samples. In that respect, it is interesting to show the dielectric behaviour as a function of temperature of the modified KNN ceramics. Prior to discussing the dielectric results, it is important to

point out the improvement in the densification with the introduction of lithium into KNN ceramics.

Typical temperature dependence of the dielectric constant and losses of unpoled lithium, lithium and tantalum modified KNN ceramics are shown in Figures 5.9 and 5.10.
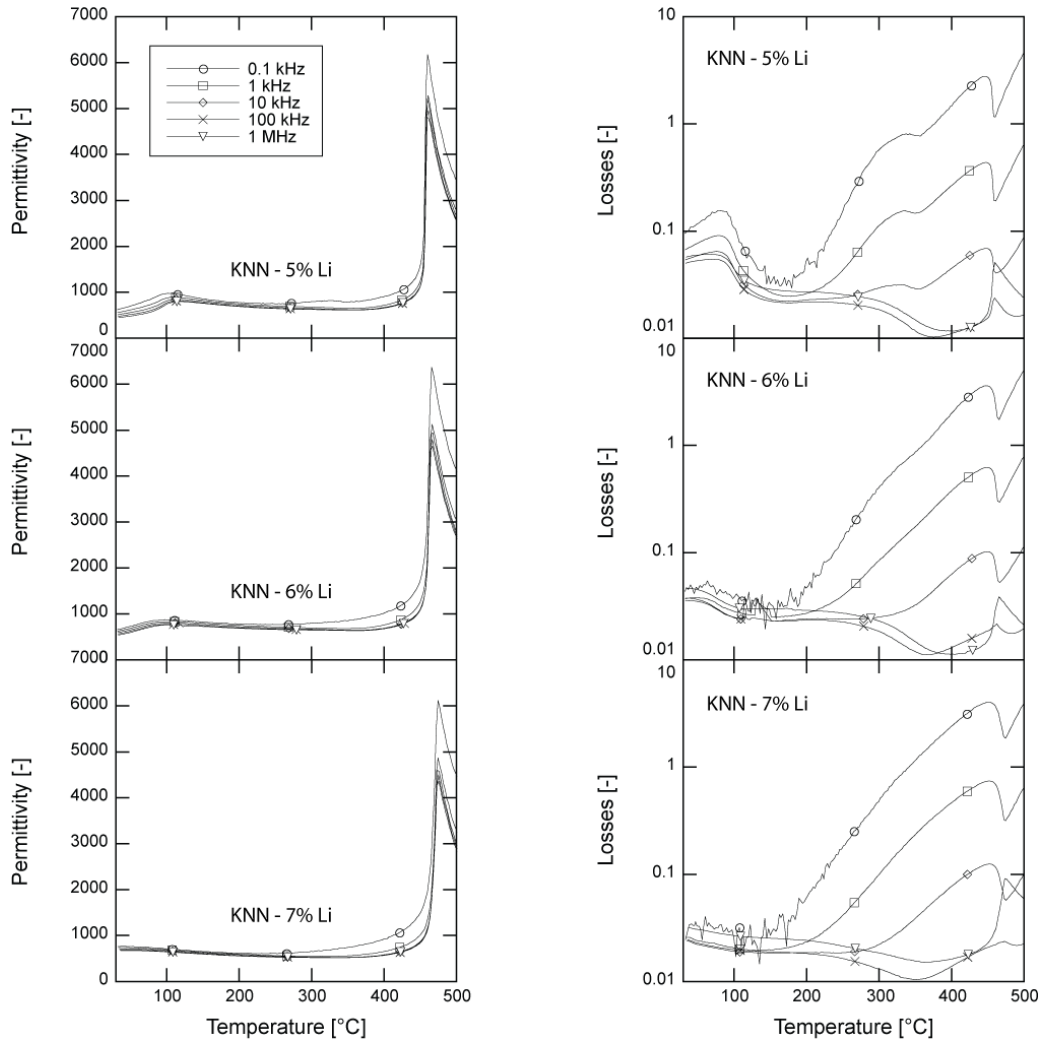

Figure 5.9: Dielectric permittivity and losses for modified KNN ceramics with 5, 6 and 7% lithium.

For pure KNN ceramics, the orthorhombic to tetragonal phase transition is at around 200 °C. It decreases with the amount of lithium and is found below room temperature for 7% lithium. The Curie temperature is shifted to higher temperatures as the lithium concentration increases (see also Figure 5.11), and thus, it can be concluded that an increasing lithium content stabilises the tetragonal structure.

With increasing the temperature, dielectric losses increase, especially at frequencies below 10 kHz. For these low frequencies, the high losses may be due to interface effects (Maxwell-Wagner phenomena), see p.74, which are thermally activated. At higher frequencies, this effect is not observed, as its activation time is higher than the frequency of the measurements. At the Curie temperature, the sharp peak in the dielectric permittivity is associated with low dielectric losses.

The high loss peak observed around 80 °C for 5% lithium, at 50 °C for 6% lithium and absent for 7 % lithium is related with the orthorhombic to tetragonal phase transition, as its temperature changes with the composition.
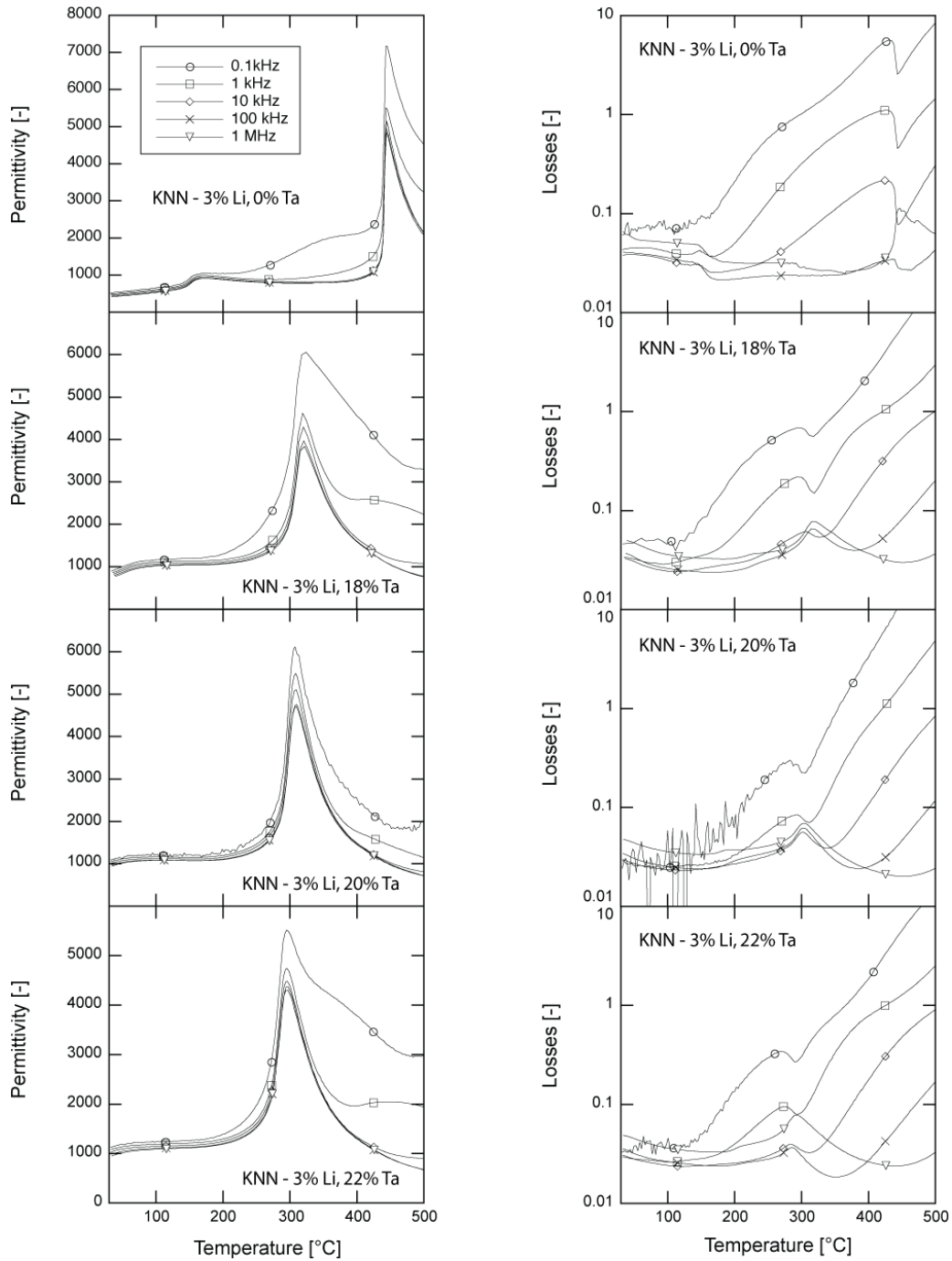
Figure 5.10: Dielectric permittivity and losses for modified KNN ceramics with 0, 18, 20 and 22% tantalum and with 3% lithium.

For lithium and tantalum modified ceramics, the orthorhombic to tetragonal phase transition is not as sharp as for the lithium modified ceramics. Moreover, the Curie temperature is shifted to lower temperatures with an increasing tantalum concentration. As for the other KNN based ceramics, a peak associated to high losses is observed at about

the Curie temperature, but no other dielectric peak is observed at lower temperatures. At room temperature, the permittivities of the lithium and tantalum modified ceramics are around 1000 and the losses around 2%.

In addition, dielectric measurements (at 1 kHz) of a wide set of compositions is shown in Figure 5.11. The compositions with concentrations higher than 7% lithium have not been synthesised in this work, the reason being that compounds with such high lithium contents have been reported to contain second phases of tungsten bronze structure ($K_3Li_2Nb_5O_{15}$) [57].
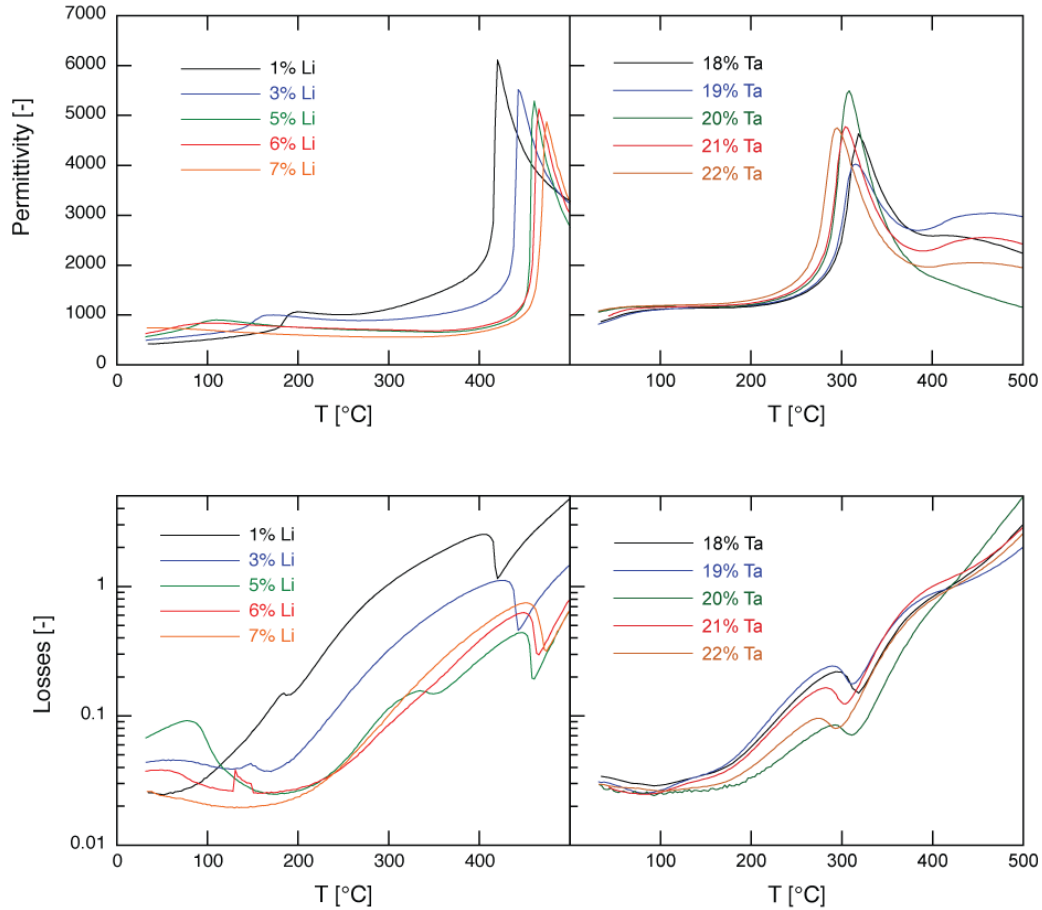
Figure 5.11: Dielectric permittivities and losses measured at 1 kHz for lithium and lithium with tantalum modified KNN ceramics.

As can be seen from the lattice parameters (Figure 4.41), as well as with the temperature dependent dielectric measurements, there is a phase transition from orthorhombic to tetragonal phase occurring at room temperature around 6 to 7% lithium and 20% tantalum for compositions with 3% lithium. This could lead to unstable properties around this temperature. In Chapter 6, the nature of the phase transition will be analysed and related to the stability of the electromechanical properties.

The tantalum and lithium modified ceramics have lower Curie temperatures at around 300 °C, compared to the 400-450 °C range in the case of the lithium modified ceramics. The tantalum modified ceramics seem more adequate for industrial applications, as they have lower dielectric losses at room temperature and similar values of permittivity. The only drawback is their lower Curie temperatures, but this should not affect their potential

for medical applications, since a thermal stability of only up to 140 °C is required for these purposes.

Dielectric losses at room temperature are significantly lower for tantalum modified ceramics. For these compositions, no relaxation peak is noticed up to the Curie temperature. For the lithium modified ceramics, a relaxation peak is seen close to room temperature for compositions with phase transitions near room temperature, but this peak shifts to higher temperatures with decreasing lithium concentration. For 5% lithium, this relaxation peak is the most significant. For this particular composition, another relaxation peak around 300 °C is shown in Figure 5.9. This peak has also been noticed in dielectric measurements on poled 7% lithium modified ceramics, as shown in Figure 5.12. The subsequently unpoled sample is also shown in this figure.
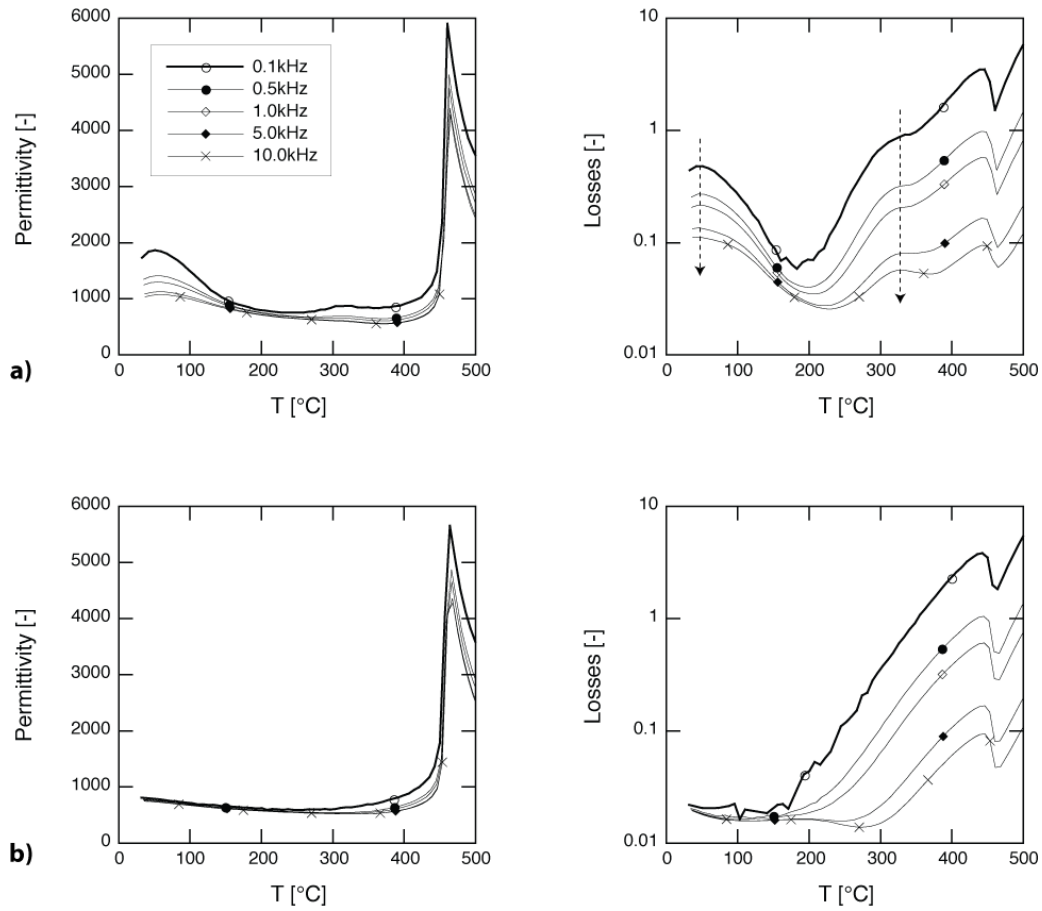
Figure 5.12: Dielectric permittivity and losses for a $(K_{0.465}Na_{0.465}Li_{0.07})NbO_3$ ceramic a) poled and b) depoled at 0.1, 0.5, 1, 5 and 10 kHz.

Two relaxation peaks can be observed in 7%-Li KNN ceramics, the first at low temperature (around 50 °C) and the second at higher temperatures (around 300 °C). These peaks are broad and independent on frequency, but their intensity is dependent on frequency. Similar peaks had been found for the 5% lithium modified ceramics (see Figure 5.9) and therefore it seems that these relaxations are not only related to the polarisation of the ceramics.

To understand the dielectric response of the modified ceramics, measurements at lower frequencies would enable us to gather valuable information on the underlying relaxation

mechanisms (Figure 5.6 below), since effects like charge hopping are important at these frequencies. As it has previously been suggested, lithium related defects or oxygen vacancies could be the origins of the high dielectric losses, and thus, dielectric measurements at low frequencies are essential to understand the conduction mechanisms of the KNN based ceramics. The results of these measurements will be presented in the next section.

Effect of frequency

In the literature, the dielectric behaviour of KNN ceramics as a function of the frequency has been reported [89, 91, 100] but only for frequencies above 100 Hz. Furthermore, in these reports the choice of the electrodes used was limited, since only gold or silver electrodes have been considered.

The permittivity and dielectric losses for $(K_{0.47}Na_{0.47}Li_{0.06})NbO_3$ ceramics for a frequency range from 1 kHz to 0.01 Hz are shown in Figure 5.13 for different types of electrodes. The reproducibility of the measurements is poor, which is highlighted by the fact that successive measurements show different results. The setup can't be responsible for this lack of reproducibility since measurements on other materials gave reproducible results.
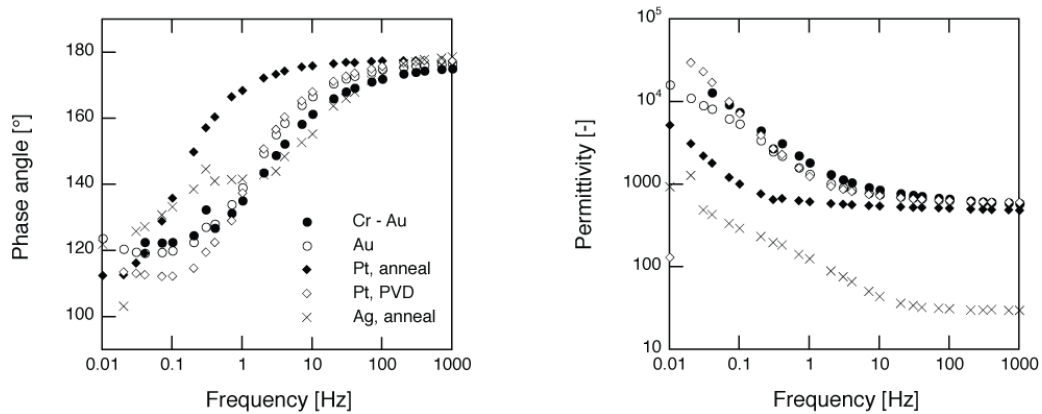
Figure 5.13: Dielectric permittivity and losses for $(K_{0.47}Na_{0.47}Li_{0.06})NbO_3$ ceramics with different types of electrodes.

At low frequencies, high losses have been observed, but the measurements are not reproducible for the same electrodes, and depend on the type of electrode. Platinum, gold, chrome-gold and silver electrodes have been deposited on the modified KNN ceramics. Platinum as well as silver electrodes require a sintering step at 800 °C for about 10 minutes. After such a thermal cycle, a reaction between the electrodes and the samples, especially samples with a high lithium content, could be observed and a representative example is shown in Figure 5.14.
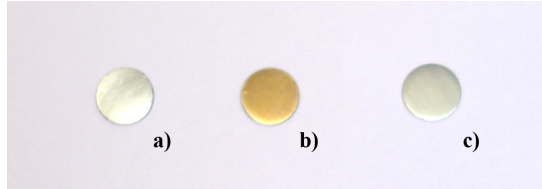
Figure 5.14: Pictures of $(K_{0.47}Na_{0.47}Li_{0.06})NbO_3$ ceramics with a) platinum and b) annealed platinum electrodes and c) $(K_{0.485}Na_{0.485}Li_{0.03})(Nb_{0.8}Ta_{0.2})O_3$ ceramics with annealed platinum electrodes.

By referring to the classification shown in Figure 5.6, the behaviour of the $(K_{0.47}Na_{0.47}Li_{0.06})NbO_3$ ceramics seems to be dominated, at least at low frequency, by hopping charges. This behaviour is characterised by an increase in both the permittivity and losses as the frequency decreases. The activation energies of hopping carriers is usually comprised between 0.6 and 1 eV [96] and a comparison with values found in literature in similar materials gives a hint on the nature of the implied charges. Unfortunately, this approach cannot be applied in our case (and thus the nature of the charge involved can't be deduced), because quantitative analyses are not possible due to the reproducibility problems. However, the behaviour seems to be qualitatively similar to the dielectric response of hard PZT ceramics at high temperatures, where the hopping of the charges is thermally activated [97].

5.3 Instability of materials with respect to humidity and time

The piezoelectric properties of the material often change with time and temperature. For potential applications, it is important to study the stability of the electromechanical properties of the used ceramics. The change of the properties with time is called aging and can be associated with the reduction of domain wall mobility or domain wall rearrangement. Understanding of aging as well as humidity effects on properties are essential for applications, as a good stability is required. An important point in the elaboration of new piezoelectric materials is the stabilisation of the domain wall structure after the polarisation step, which can lead to a decrease of the properties within a short time after polarisation.

In this work, the time dependent evolution of the electromechanical properties has been studied. The samples were stored in three chambers (desiccators) with different relative humidities, namely 15%, 44% and 90%. The humidities in the chambers have been stabilised using silica gel for the 15% environment and saturated solutions of potassium carbonate and sodium carbonate for the higher humidities.

The electromechanical properties were measured using the resonance method and for the piezoelectric coefficient d_{33}, a Berlincourt press was used. For measurements, the samples were removed from desiccators and then reinserted. The results are summarised in Figure 5.15 for the KNN-7% lithium ceramics and the KNN- 3% lithium with 20% tantalum ceramics. For the two compositions analysed, 3 samples have been kept in each chamber.
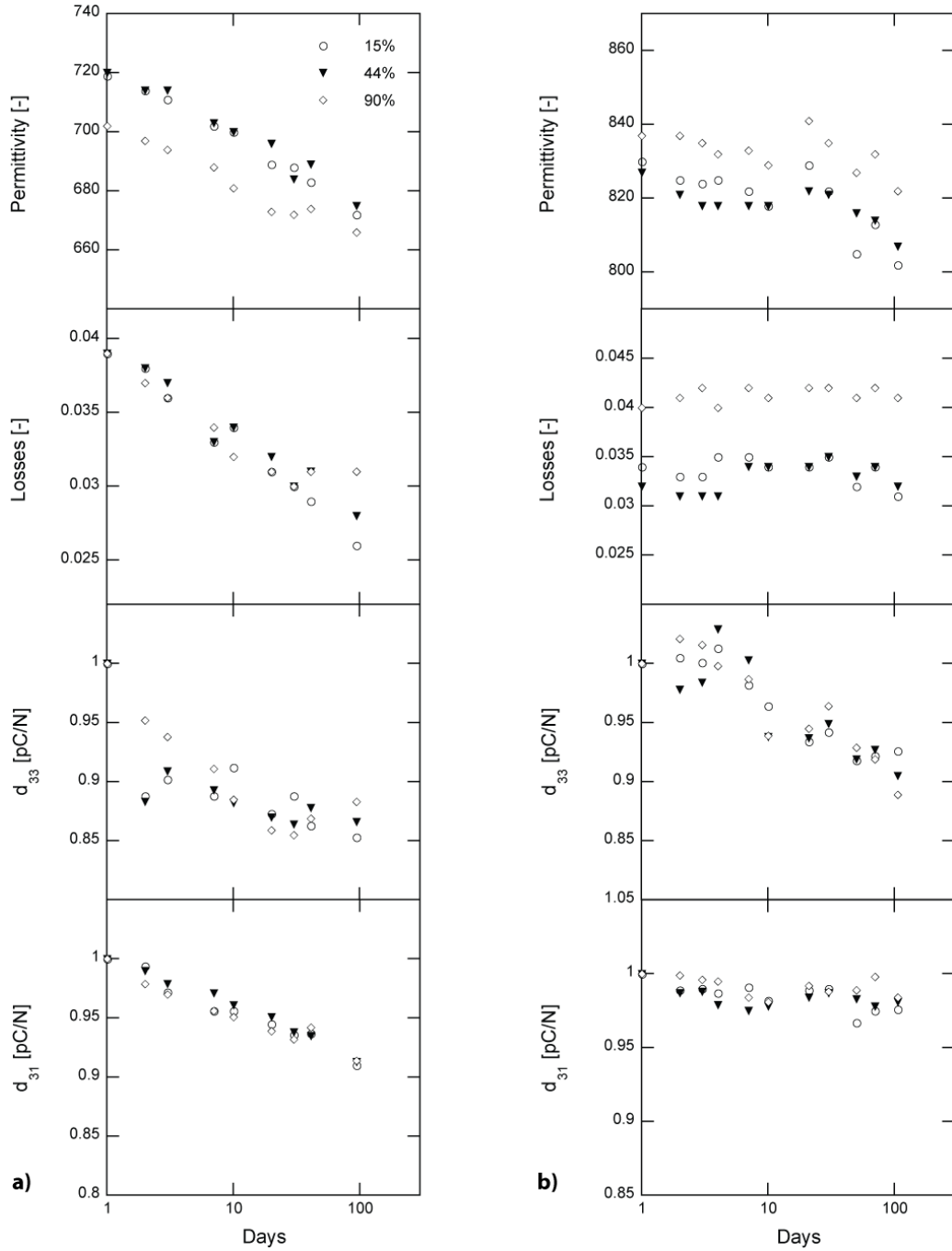
Figure 5.15: Time dependent evolution of the electromechanical properties, permittivity at 1 kHz, dielectric losses at 1 kHz, d_{31} and d_{33}, a) of 7% lithium and b) 3% lithium and 20% tantalum modified KNN ceramics, as a function of the relative humidity. For the 7% lithium modified KNN ceramics, the starting reference values of d_{33} and d_{31} are 167, 172, 168 pC/N and 59, 59, 58 pC/N, respectively, and this after 1 day and with increasing humidities. For the 3% lithium and 20% tantalum modified KNN ceramics, the values of d_{33} and d_{31} are 163, 168, 165 pC/N and 62, 65, 62 pC/N, respectively, and this after 1 day and with increasing humidities.

For both analysed compositions, the radial and thickness coupling coefficients of the two compositions are constant with time (no relaxation can be noticed after polarisation). This behaviour is in good agreement with previously published aging measurements on

KNN ceramics [42, 85, 95]. However, in more recent work, the radial coupling coefficient was shown to decrease with time by 20% [47].

All of the measured properties seemed to be insensitive to variation of the humidities, and this especially for the lithium and tantalum modified composition. This behaviour is synonymic of a good stability in any environment, which is an important factor with view to potential applications. This also indicates that no unreacted starting material can be found in the sintered samples.

The dielectric behaviour of the $(K_{0.485}Na_{0.485}Li_{0.03})(Nb_{0.8}Ta_{0.2})O_3$ ceramics is not altered with time, in contrast to the $(K_{0.475}Na_{0.475}Li_{0.07})NbO_3$ ceramics, where the dielectric permittivity and losses decrease with time. An increase of dielectric permittivity and losses is related to degradation of the properties due to domain wall relaxation. In the other case, the decrease of these properties can be compared to hard materials. In these materials, defect orientation can occur with time, thus reducing the dielectric properties. For pure KNN it has been shown by Birol *et al* [47], that the dielectric losses in KNN samples increase with time, as well as for lithium modified KNN ceramics [85].

The piezoelectric coefficients d_{31} and d_{33} measured by resonance and Berlincourt technique respectively, decrease with time. This behaviour is more pronounced for the $(K_{0.475}Na_{0.475}Li_{0.07})NbO_3$ composition, since a decrease of about 10% was measured for d_{31} after 100 days and this decrease reached even 15% for d_{33} in the same time span. The time dependent aging behaviour of the piezoelectric coefficients is logarithmic and given by Equation 5.1:

$$d = 1 - \alpha \cdot \log(t) \tag{5.1}$$

with $0.04 < \alpha < 0.06$

However, in the case of the d_{31} for the lithium and tantalum modified ceramics, the aging is even slower ($\alpha < 0.01$).

This logarithmic aging of electromechanical properties has also been reported for barium titanate ceramics [101] and is illustrated in Figure 5.16.
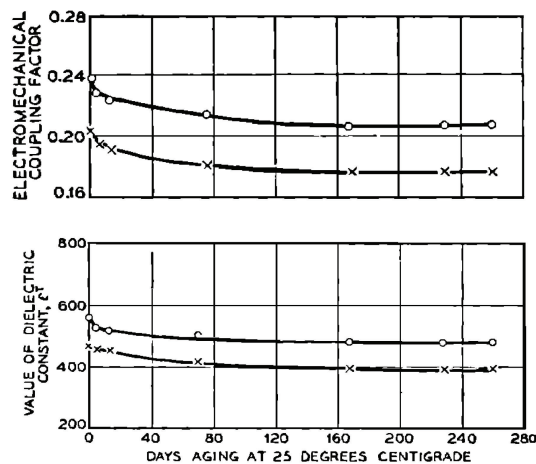

Figure 5.16: Aging behaviour in BaTiO$_3$ ceramics and in particular of the coupling factor (top) and dielectric constant (bottom) [101].

Aging in these barium titanate ceramics is more important than in the KNN modified ceramics, shown in Figure 5.15. For example, the permittivity after 100 days decreased of about 13% for $BaTiO_3$, while the diminution was below 7% for the two modified KNN ceramics. This difference is also seen for the radial coupling coefficients.

In general, the aging behaviour is associated with a decrease of the remanent polarisation. Many models for the aging of $BaTiO_3$ ceramics have been proposed in the literature and are based on the relaxation of domain walls, which tends to decrease the internal stresses. In particular, models based on the thermal activation of domain walls, 180° domain clamping, domain wall vibration and stress relaxation caused by 90° domain nucleation have been proposed. Some other models take into account the diffusion of defects to the domain walls, or to their ordering inside of the grains.

Nevertheless, not all the piezoelectric materials show a logarithmic dependency of aging like the PZT for example [102]. In that respect, one interesting feature is the aging properties of PZT ceramics with varying composition. In Figure 5.17, the aging behaviour of $Pb_{0.92}Mg_{0.04}Sr_{0.025}Ba_{0.015}(Zr,Ti)O_3$ + 0.5 wt.% CeO_2 + 0.225 wt.% MnO_2 ceramics is shown for a wide range of compositions. It is to note that the aging rate near MPB compositions is the fastest.
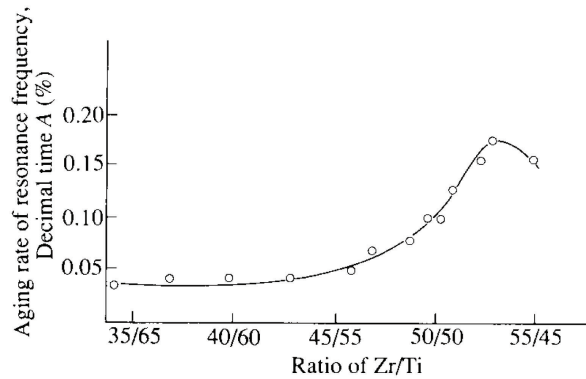
Figure 5.17: Aging per decade of the resonance frequency versus the ratio Zr/Ti in the ceramic $Pb_{0.92}Mg_{0.04}Sr_{0.025}Ba_{0.015}(Zr,Ti)O_3$ + 0.5 wt.% CeO_2 + 0.225 wt.% MnO_2 [102].

As seen in Figure 5.17, the aging of the PZT is maximum around the MPB, due to the ease of the polarisation rotation and thus the domain wall motion. As at room temperature, our two ceramics $(K_{0.475}Na_{0.475}Li_{0.07})NbO_3$ and $(K_{0.485}Na_{0.485}Li_{0.03})(Nb_{0.8}Ta_{0.2})O_3$ are located near the orthorhombic to tetragonal phase transition, the aging should be the maximum.

5.4   Conclusions

Phase transitions were observed by temperature dependent dielectric measurements. For lithium modified ceramics, the Curie temperature increases with lithium concentration and the temperature of the orthorhombic to tetragonal phase transition decreases. The tetragonal phase can thus be considered to be stabilised by the addition of lithium. In the case of lithium and tantalum modified ceramics, the Curie temperature is lowered to about 300 °C.

The dielectric measurements as a function of the temperature confirm the non reproducibility of pure KNN ceramics, as low and high temperature relaxations appear for some samples. In the case of modified KNN ceramics, low and high temperature relaxations can also be observed, but these relaxations appear only for lithium modified compositions. The low temperature relaxation is thought to be due to a phase transition, and in particular to domain wall structures taking place at this transition. The origin of the high temperature relaxation could not be assessed.

The room temperature losses of the tantalum modified ceramics are lower than for pure or lithium modified ceramics, which makes them interesting for ultrasonic transducers. The dielectric spectroscopy measurements were not reproducible due to electrical contact problems. The introduction of lithium into KNN ceramics made it impossible to densify platinum or silver electrodes at high temperatures without the occurrence of a reaction between the electrodes and the samples. Nevertheless, the dielectric response is dominated at low frequencies by a process that manifests itself like the hopping of charge carriers.

As a conclusion from the dielectric measurements as a function of temperature and frequency, the modified KNN ceramics are a complex system with many contributions to the polarisation, comprising for example hopping of charged carriers or space charge effects. To understand the role of each mecanisms further impedance spectroscopy measurements should be performed. The Cole-Cole plots of such measurements could for example give information of grain boundary effects.

The produced ceramics were not moisture sensitive. Indeed, time dependent measurements of samples immersed in different humidities didn't show much influence of the humidity on the electromechanical properties. After 100 days, the piezoelectric coefficients have not decreased by more than 15% of the initial values and the coupling coefficients remain almost unaltered. The time stability of the lithium and tantalum modified ceramics is remarkable. The dielectric loss and permittivity are almost constant with time and the piezoelectric properties suffer only a minimal decrease. Tantalum is thus supposed to stabilise the domain wall structure by inhibiting their displacement, leading to a decrease in the properties variation as a function of the time. Compared to barium titanate ceramics, the properties of modified KNN ceramics are more stable with time.

Chapter 6

Thermal stability: MPB vs thermally induced phase transitions

The aging behaviour of the ceramics discussed in the previous chapter is important for applications. Temperature stability is another important factor, in particular for medical ultrasonic transducers, since the probes need to be heated for sterilisation and during transducer preparation. This factor is not to be neglected for all the applications, as small temperature fluctuations can influence the electromechanical properties. This effect becomes stronger for materials near a phase transition, like the modified KNN ceramics. In this context, a difference of thermal stability is expected for materials near a compositionally or thermally induced phase transition.

Around compositionally or temperature induced phase transitions, the electromechanical properties are increased due to a flattening of the Gibbs free energy and resulting dielectric softening. For phase transitions involving a change in the direction of the spontaneous polarisation, the polarisation rotation is facilitated, which leads to an enhancement of the piezoelectric properties.

The aim of this chapter is to determine the nature of the phase transitions in lithium and lithium with tantalum modified KNN ceramics, using temperature and composition dependent dielectric and piezoelectric measurements. Dielectric measurements reveal a mixture of thermally and compositionally induced phase transitions, as the tetragonal to orthorhombic phase transition temperature varies with composition. The evolution of the electromechanical properties, which reach a maximum at the transition temperature, confirms the results from dielectric measurements. These results could not be confirmed by hysteresis loop measurements, as the coercive field and the remanent polarisation don't show clear maxima at the phase transition. Finally and considering the importance of thermal stability for applications, successive cycling should not affect the properties of the ceramics. This stability has been measured by different techniques.

6.1 Introduction

Nowadays the best electromechanical properties are found in systems showing a phase transition and, more importantly, lying in close proximity to this phase transition [1]. In the literature, distinction of temperature, composition or electrically induced phase transitions is considered. Barium titanate is used as a model for the first type of phase transition and PZT compositions near the MPB for the second, as the phase transition is nearly independent of the temperature.

The enhancement of the electromechanical properties in the vicinity of phase transitions has been related to polarisation rotation or elongation [6, 103]. In PZT, a monoclinic structure at the MPB has been discovered [5, 7], which reinforces this idea, as the number of equivalent polarisation directions is 24 in this structure. Associated with this monoclinic phase are the different polarisation rotation mechanisms which have been proposed and are summarised in Figure 6.1 [104].
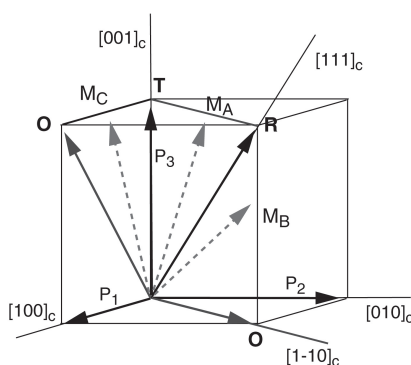
Figure 6.1: Polarisation in the cubic coordinate system and monoclinic polarisation path. M_A and M_B describe polarisation rotation paths for a rhombohedral crystal, while M_C describes a polarisation rotation path in a tetragonal crystal [104, 105].

In single crystals, it has been reported that the piezoelectric response for several ferroelectric perovskites is not maximal along the direction of spontaneous polarisation [4, 30, 106]. For tetragonal $BaTiO_3$, which presents temperature induced phase transitions, this is the case only for a small temperature range near the temperature of the orthorhombic to tetragonal phase transition [107].

To understand the origin of the enhanced piezoelectric response near the phase transitions, the contributions to this effect should be analysed. The piezoelectric response in ferroelectric materials can be divided into two parts, an intrinsic contribution related to the piezoelectric properties of a single ferroelectric domain, also called lattice contribution, and an extrinsic contribution, related to the domain-wall and phases interfaces displacement [108]. The lattice contribution can be calculated for example by using the Landau-Ginzburg-Devonshire (LGD) phenomenological thermodynamic theory. This theory can give an explanation of the anisotropy of the piezoelectric response and in particular why in many ferroelectric perovskites the piezoelectric response is not maximal along the direction of spontaneous polarisation. For example, the anisotropy of the longitudinal piezoelectric coefficient for $BaTiO_3$ is shown for two particular temperatures in Figure 6.2 [107]. In this case, the orthorhombic to tetragonal phase transition is at 278 K.
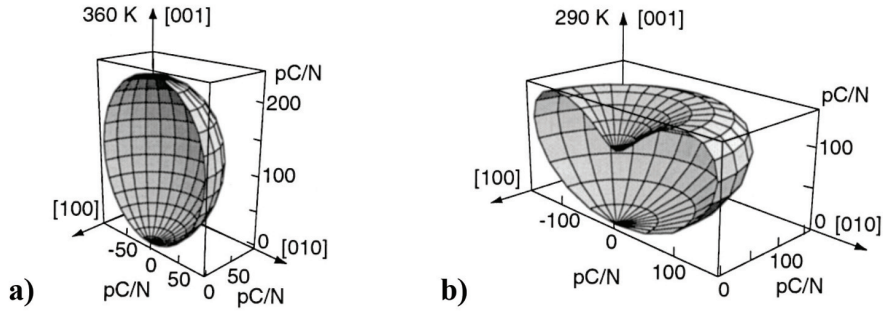
88

Figure 6.2: 3D representation of the longitudinal piezoelectric coefficient d_{33} of $BaTiO_3$ at a) 360 and b) 290 K [107].

In $BaTiO_3$, the enhancement of the shear piezoelectric coefficients near the tetragonal to orthorhombic and the orthorhombic to rhombohedral phase transitions is related to the dielectric softening perpendicular to the polar axis. In Figure 6.3 [109], the evolutions of the longitudinal and shear piezoelectric coefficients and the relative susceptibilities are shown.
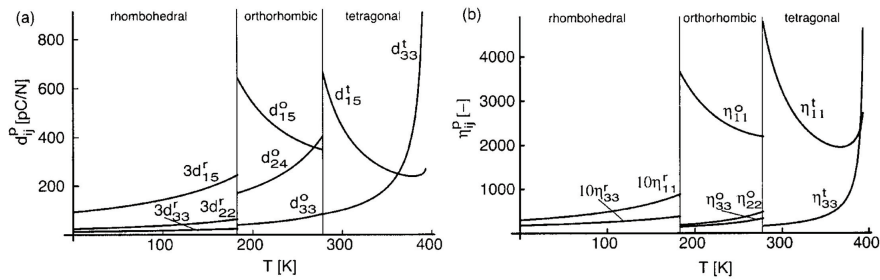

Figure 6.3: Temperature dependence of a) the longitudinal and shear piezoelectric coefficients and b) the relative susceptibilities for $BaTiO_3$ in all three ferroelectric phases [109].

Around these phase transitions the shear coefficient increases, which can be associated to a dielectric softening [110] perpendicular to the polar axis. When the ratio d_{15}/d_{33} exceeds a certain value, the direction of maximal d_{33} does not coincide with the spontaneous polarisation direction. Budimir *et al* [109] showed that the presence of a sequence of phase transitions as a function of the temperature (typically in barium titanate) imply variations of the directions of the maximal longitudinal piezoelectric coefficient.

Similar results for phase transitions as function of the composition have been found [104]. Figure 6.4 shows the dependence on orientation of d_{33} for two different compositions of PZT in the rhombohedral domain.
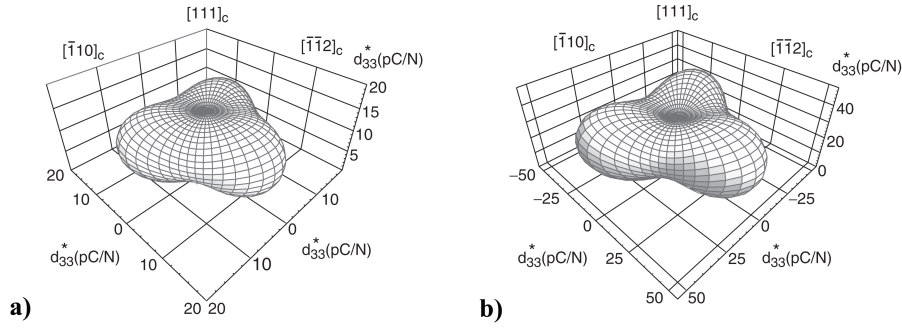
Figure 6.4: 3D representation of the longitudinal piezoelectric coefficient d_{33} of $Pb(Ti_xZr_{1-x})O_3$ for a) 90/10 and b) 60/40 [104].

This anisotropy of d_{33} is stronger for compositions closer to the MPB. To understand the origin of this anisotropy, the Gibbs free energy has been calculated using LGD theory. A illustrated in Figure 6.5, the Gibbs free energy profile is flattening off near the MPB for rhombohedral PZT.
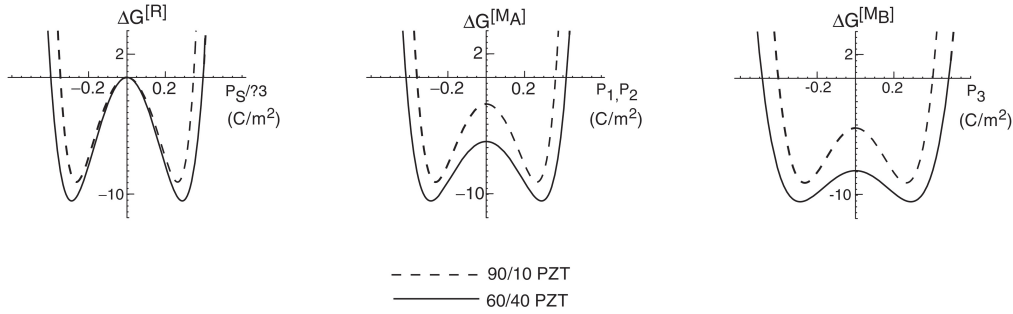

Figure 6.5: Cross-sections of the Gibbs free energy for 90/10 and 60/40 $Pb(Ti_xZr_{1-x})O_3$ along the a) [R], b) [M_A] and c)[M_B] path [104].

The situation in the tetragonal domain of PZT is different as the ratio d_{15}/d_{33} is not high enough and so the direction of maximal d_{33} coincides with the polar axis. Nevertheless, a flattening of the Gibbs free energy is observed approaching the MPB [104].

For barium titanate, approaching the tetragonal to orthorhombic phase transition temperature, the Gibbs free energy profile flattens [104] (Figure 6.6), similarly to the case of a compositionally induced phase transition. At higher temperatures, the behaviour of $BaTiO_3$ is close to that of tetragonal PZT, i.e. d_{33} is maximal along the polar axis.
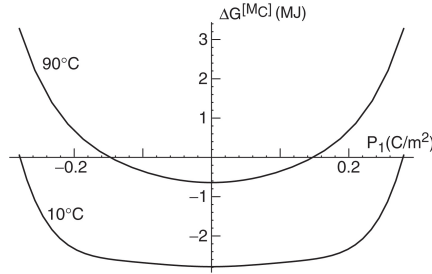
Figure 6.6: Gibbs free energy profile for tetragonal $BaTiO_3$ at 10 and 90 °C [104].

The LGD theory has also been applied to study the ferroelectric hysteresis loop around the MPB in perovskites and it has been determined that the coercive field decreases in the vicinity of the MPB [111], which is confirmed experimentally for Nb-PZT (see Figure 6.7 [112]). In this case, a clear increase of the remanent polarisation can be noted in combination with the decrease of the coercive field. This behaviour can be associated with the facilitated polarisation rotation near the MPB.
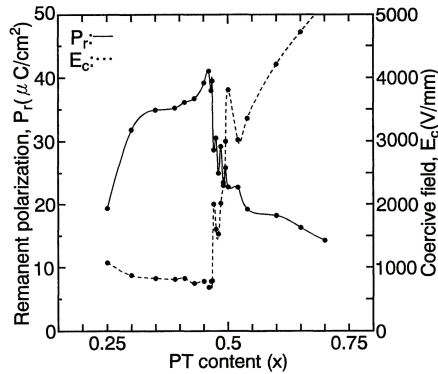
Figure 6.7: Compositional dependence of the remanent polarisation and the coercive field for niobium doped PZT [112].

Similarly to the observed behaviour of the coercive field and remanent polarisation in PZT as a function of the composition, in potassium niobate and barium titanate single crystals [113, 114, 115] an increase of the coercive field and spontaneous polarisation around the orthorhombic to tetragonal phase transitions has been measured as a function of the temperature, as shown in Figure 6.8.
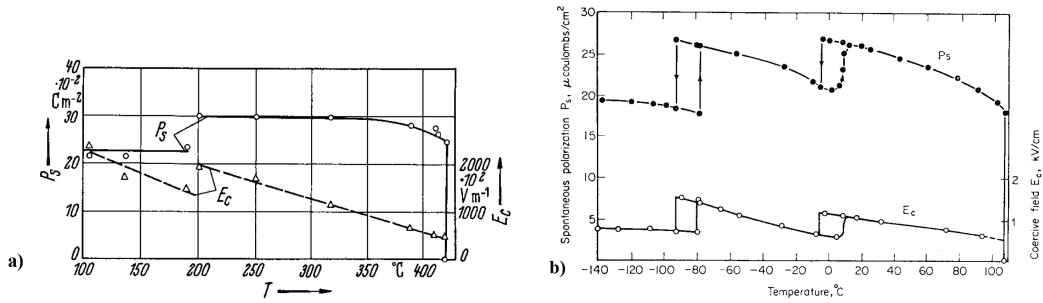
Figure 6.8: Spontaneous polarisation P_s and coercive field E_c as a function of temperature for a) $KNbO_3$ single crystals, with measurements in parallel to the pseudocubic [100] direction [113] and b) for $BaTiO_3$ single crystals, with measurements in parallel to tetragonal [100] direction [114, 115].

From these observations we can conclude that the measurements of ferroelectric hysteresis loops (in particular the remanent polarisation and coercive field as a function of temperature and composition) can be a tool to determine the nature of the phase transition, e.g. thermally or compositionally induced.

The lithium and tantalum modified ceramics reported by Saito *et al* [55] show enhanced piezoelectric properties at room temperature principally in the vicinity of the orthorhombic to tetragonal phase transition. However, the authors did not investigate on the nature of this phase transition, i.e. determined whether it was thermally or compositionally induced. To study this transition in our modified KNN ceramics, compositions based on previous works have been synthesised [55, 57]. The synthesised ceramics can be classified into two families; the first is lithium modified KNN ceramics with compositions around 6% lithium and the second is lithium (3%) and tantalum (20%) modified KNN ceramics. Many compositions in the vicinity of the phase transition have been synthesised, for example with 3% lithium, 18, 19, 20, 21 and 22% tantalum concentrations (see Table 4.1).

For these new compositions, it is important from a technological point of view to determine the origin of the observed phase transition. Considering compositions near a vertical MPB (Figure 6.9a), the properties as a function of temperature will only be influenced by thermal effects and not by crossing the phase transition point. Therefore they show more stable properties in function of the temperature than in samples with compositions close to a non vertical MPB and thermally induced phase transition (Figure 6.9b).
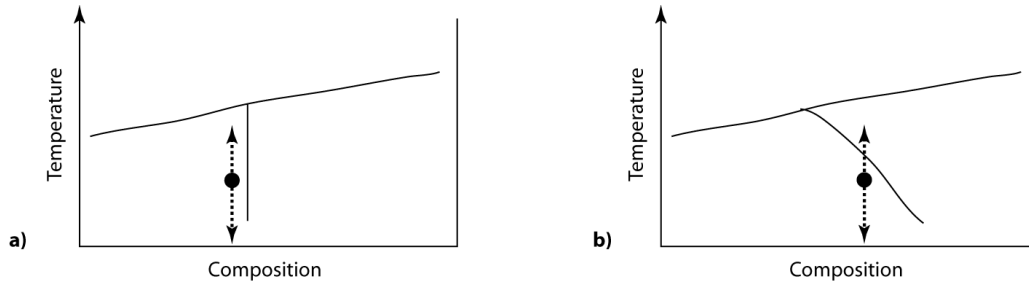
Figure 6.9: Schematic phase diagram showing a a) compositionally or b) thermally induced phase transition.

The piezoelectricity in ceramics is due to the existence of a macroscopic polarisation induced by a strong external electric field. However, the poled ceramics often lose their piezoelectric properties at a temperature below the Curie temperature due to thermal instability of the poled state. This thermal depoling of ferroelectrics determines the temperature limit for potential applications. To consider the replacement of the lead-based materials in some medical transducers, the piezoelectric properties should be maintained after a thermal cycle up to 140 °C, as a sterilisation process at such temperature is performed before each use. Repeated thermal cycling can lead to partial depoling, which then affects the piezoelectric properties.

The aims of this chapter are to investigate, firstly the nature of the phase transition of the modified KNN ceramics near room temperature, and secondly the thermal stability of the electromechanical properties. In the first part, dielectric, ferroelectric (hysteresis loops) and piezoelectric properties as a function of composition and temperature have been measured. In the second part, the electromechanical properties have been measured for repeated cycles up to 140 °C, in order to observe the depolarisation of the samples.

6.2   Dielectric characterisation

For applications, the thermal stability is an important point, which means that a high Curie temperature is required. Barium titanate, which is a good lead-free alternative, has quite a low Curie temperature (120 °C [104]), and a transition temperature from orthorhombic to tetragonal near room temperature (5 °C). Due to these characteristics, its properties are not stable at room temperature. Compared to barium titanate, potassium sodium niobate has a high Curie temperature (around 400 °C) and an orthorhombic to tetragonal phase transition around 200 °C, but these phase transitions are shifted by the introduction of lithium and tantalum.

The measurement of the dielectric constant and losses as a function of temperature is an important way of characterising the phase transitions that occur in ferroelectric materials [1]. At the Curie temperature and at ferroelectric-ferroelectric phase transitions between rhombohedral, orthorhombic and tetragonal phases, sharp discontinuities in permittivity are observed.

The dielectric behaviour of modified ceramics as a function of temperature is illustrated in Figures 6.10 and 6.11 for lithium and lithium with tantalum modified KNN ceramics, respectively.
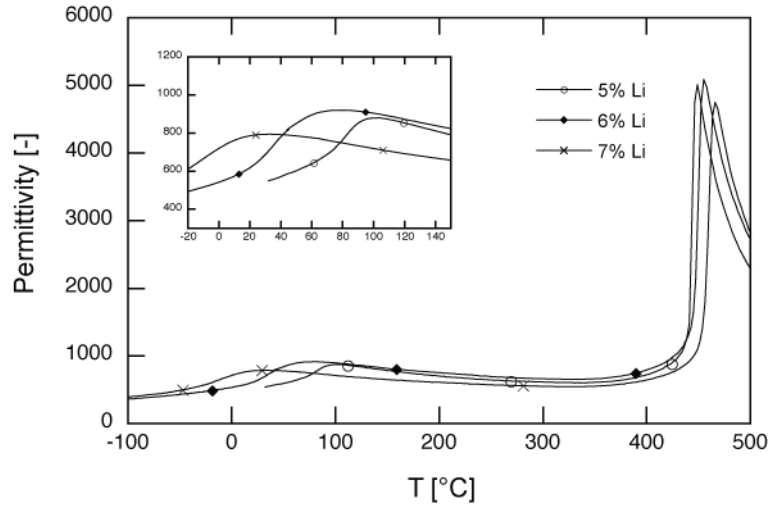
Figure 6.10: Dielectric permittivity as a function of temperature at 1 kHz for 5, 6 and 7% lithium modified KNN ceramics. The inset shows the orthorhombic to tetragonal phase transition.
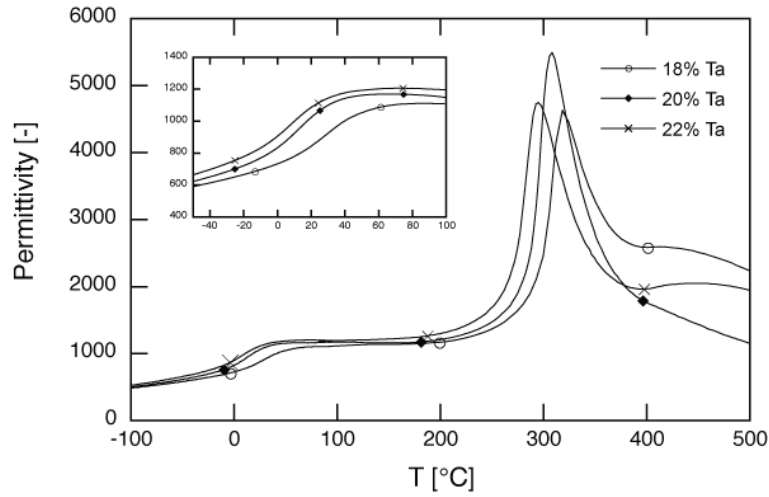

Figure 6.11: Dielectric permittivity as a function of temperature at 1 kHz for 18, 20 and 22% tantalum modified KNN ceramics with 3% lithium. The inset shows the orthorhombic to tetragonal phase transition.

Basing on the Curie temperatures, lithium modified ceramics are more suitable for applications than the lithium and tantalum modified KNN ceramics, but they also show higher dielectric losses. For the orthorhombic to tetragonal phase transition, the peak is broader, making a precise measurement of the transition temperatures difficult. This behaviour is even more accentuated in the case of lithium and tantalum modified ceramics. The phase transition temperature can be determined by calculating the derivative of the permittivity when plotted as a function of the temperature. This confirms the proximity of the orthorhombic to tetragonal phase transition to room temperature for the KNN compositions with 6% lithium (75 °C) on one side and with 3% lithium and 20% tantalum (65 °C) on the other side.

These phase transition temperatures are comparable to those recently obtained by Matsubara *et al* [83]. This phase diagram of lithium modified KNN ceramics is shown

94

in Figure 4.39. 0.38% mole KCT has been used to improve the densification of those samples, but this also modifies the properties of the final ceramics, as for pure potassium sodium niobate ceramics the Curie temperature is slightly shifted to lower temperatures (395 °C) than for other reports on KNN ceramics (400-410 °C [44, 47]).

The line separating the tetragonal and orthorhombic structure is temperature dependent, which is confirmed by dielectric, piezoelectric and Raman measurements carried out by N. Klein and shown in Figure 6.12.
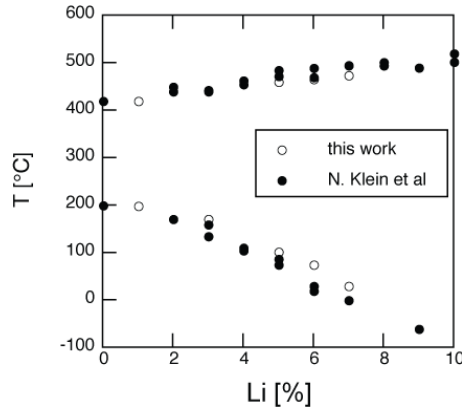
Figure 6.12: Phase diagram of lithium modified KNN ceramics [116].

From the dielectric measurements as a function of temperature, it can be deduced that the orthorhombic to tetragonal phase transition in KNN modified ceramics is temperature dependent. In terms of temperature variation, this phase transformation behaves like a polymorphic transitions in $BaTiO_3$. In terms of MPB, the phase line between orthorhombic and tetragonal phases in the temperature-composition phase diagram represents a strongly curved MPB.

6.3 Ferroelectric Hysteresis Loops

The samples should be as thin as possible (typically 0.3 mm) to avoid break-down during the hysteresis loop measurements. Gold electrodes without a chrome layer have been deposited on both surfaces. In this work, no breakdown occurred in the silicon oil for fields over 80 kV/cm but the effect of high field on the properties is not significant, and therefore, the maximal field 50 kV/cm has been chosen for the polarisation step, as discussed in Section 3.2.3. For KNN, the hysteresis loop of a cycled sample is schematised on Figure 6.13.
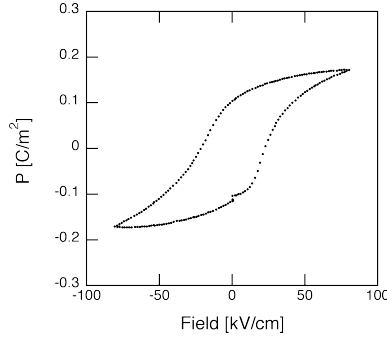
Figure 6.13: Polarisation loop for KNN.

The coercive field and the remanent polarisation for pure KNN are 22 kV/cm and 10 μm/cm^2, respectively, which represents a low remanent polarisation combined with a high coercive field. As the reproducibility of the KNN ceramics is very poor, the loop characteristics can vary significantly from sample to sample. The hysteresis loops strongly depend on the processing of the ceramics (homogeneities, porosity, defects). This diversity can also be observed by the broad range of literature values of the remanent polarisation and the coercive field for pure KNN ceramics, e.g. by Yang *et al* ($P_r = 32$ μm/cm^2, $E_c = 13$ kV/cm) [98], Matsubara *et al* ($P_r = 22$ μm/cm^2, $E_c = 11$ kV/cm) [83] and Birol *et al* ($P_r = 20$ μm/cm^2, $E_c = 20$ kV/cm) [47].

To characterise the hysteresis relaxation after 1, 5, 10 and 20 successive cycles, the hysteresis loops as a function of the composition for lithium and lithium with tantalum modified KNN ceramics have been measured and are shown in Figures 6.14 and 6.15.
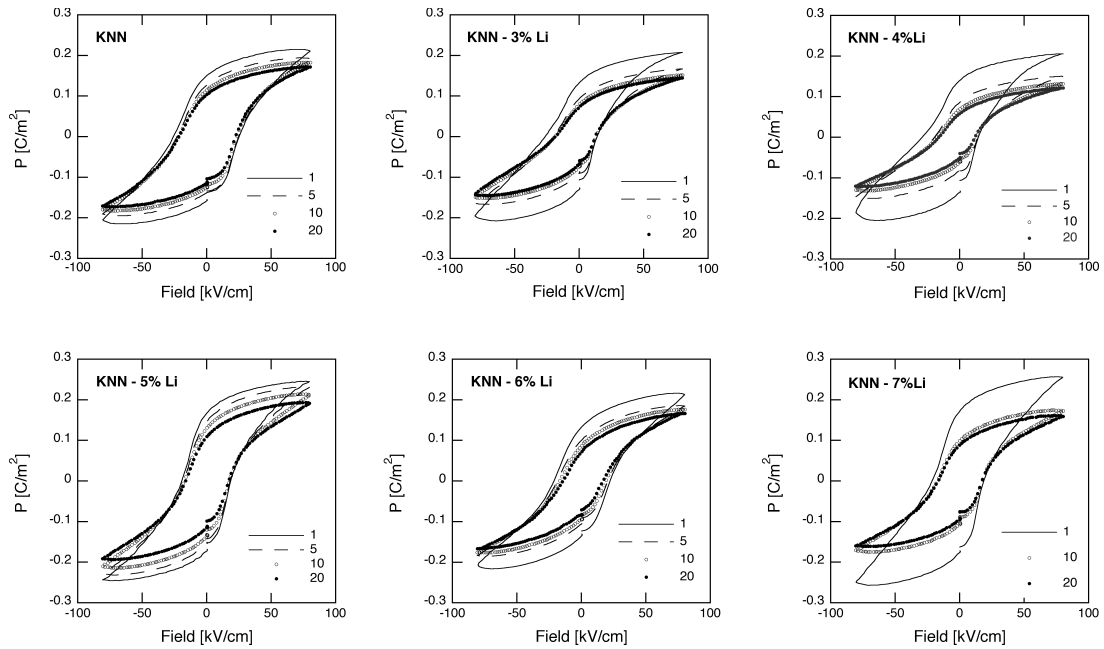

Figure 6.14: Polarisation loops for KNN modified with lithium, for 0, 3, 4, 5, 6 and 7% lithium, for 1, 5, 10 and 20 cycles, at 50 Hz.
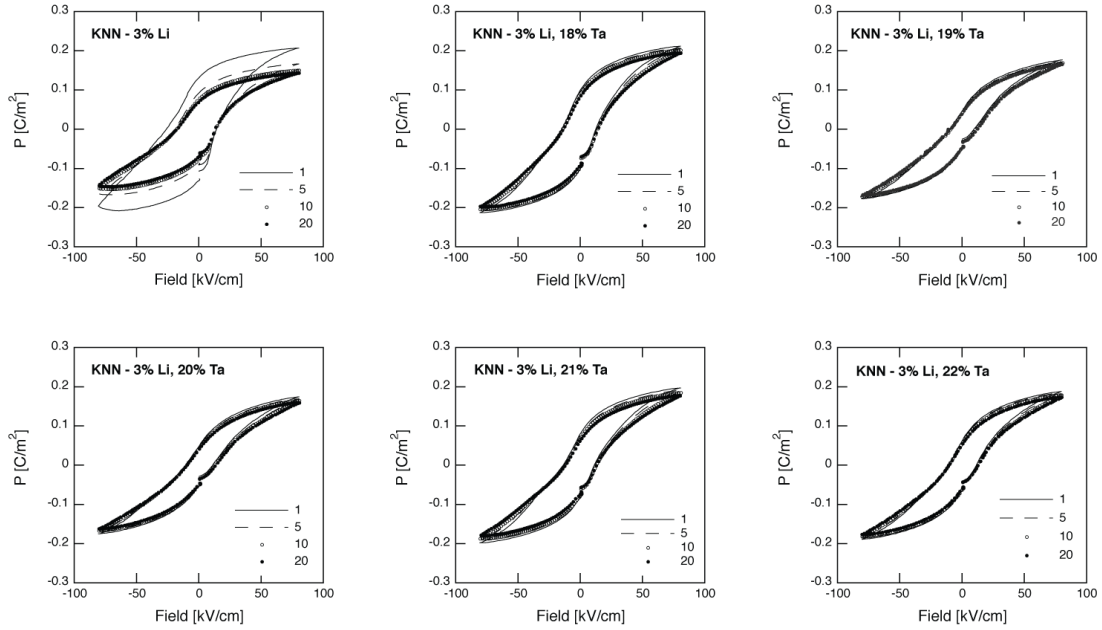
Figure 6.15: Polarisation loops for KNN modified with lithium (3%) and tantalum (0, 18, 19, 20, 21 and 22%), for 1, 5, 10 and 20 cycles, at 50 Hz.

The hysteresis loops in Figure 6.15 are slightly pinched, which is a typical feature of hard materials [97] and which is not observed in the case of lithium modified ceramics, pointing out the "hardening" effect of tantalum. Nevertheless, a similar behaviour for niobium has also been observed in pure KNN.

With an increasing number of cycles, the tantalum modified ceramics show a more stable response than the pure and lithium modified KNN ceramics for which a drop of the remanent polarisation is observed already after few cycles. After 20 cycles, the decrease of the remanent polarisation is higher than 30% for pure and lithium modified KNN ceramics and below 20% for the lithium and tantalum modified ceramics. This decrease of the remanent polarisation with an increasing number of cycles (fatigue behaviour) can be observed in many ferroelectric materials, like for PZT-5A bulk ceramics, where the remanent polarisation can decrease by about 30%, after 10^8 cycles [97, 117], Figure 6.16.
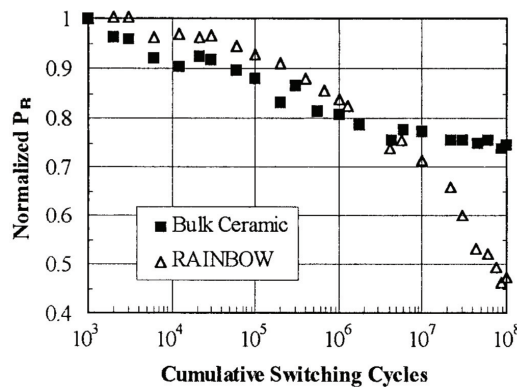

Figure 6.16: Normalised remanent polarisation of the commercially available PZT-5A bulk ceramics as a function of switching cycles [117].

97

The domain wall mobility is decreased during cycling either because of the movements of the domain walls towards defects (and their resulting pinning) or because of the orientation of coupled defects creating internal fields. These mechanisms are susceptible to be responsible of the decrease in the remanent polarisation [97]. They can be used to interpret the different fatigue behaviour of the lithium and lithium with tantalum modified KNN ceramics, as the tantalum could stabilise the domain wall structure, like was is observed for hard PZT for example. The fatigue behaviour of the remanent polarisation is reflected in the electromechanical properties, which also decrease during cycling [118].

The polarisability increases slightly in the proximity of the phase transitions, for lithium contents about 6-7% and for 20% tantalum (with 3% lithium) as shown in Figure 6.17. It is noteworthy mentioning that the coercive field also increases around the phase transition, like for $0.948(K_{0.5}Na_{0.5})NbO_3$-$0.052LiSbO_3$ ceramics [60]. In the case of compositionally induced phase transitions, the remanent polarisation shows a maximum at the composition close to the transition and the coercive field is at a minimum (see Figure 6.7), which is not observed in the two families of modified KNN ceramics.
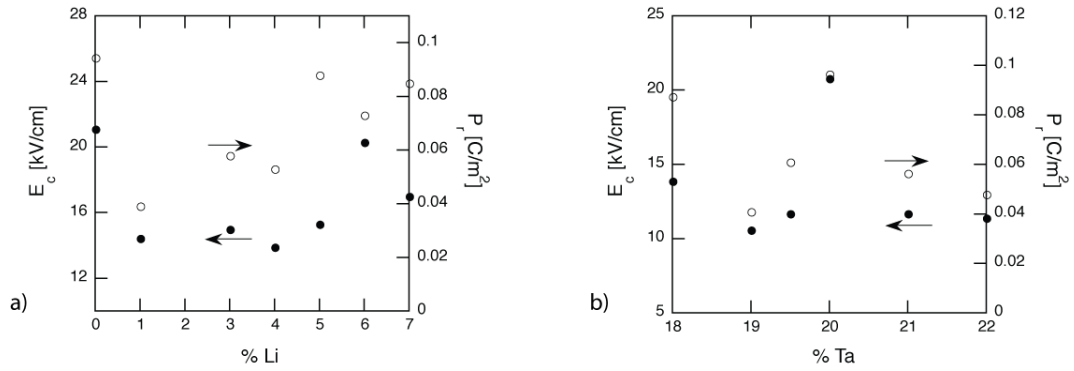

Figure 6.17: Coercive field and remanent polarisation as a function of a) the lithium and b) the tantalum content (with fixed 3% lithium concentration) for modified KNN ceramics.

The parameters of the polarisation loops as a function of temperature for $(K_{0.47}Na_{0.47}Li_{0.06})NbO_3$ and $(K_{0.485}Na_{0.485}Li_{0.03})(Nb_{0.80}Ta_{0.20})O_3$ ceramics are shown in Figure 6.18.
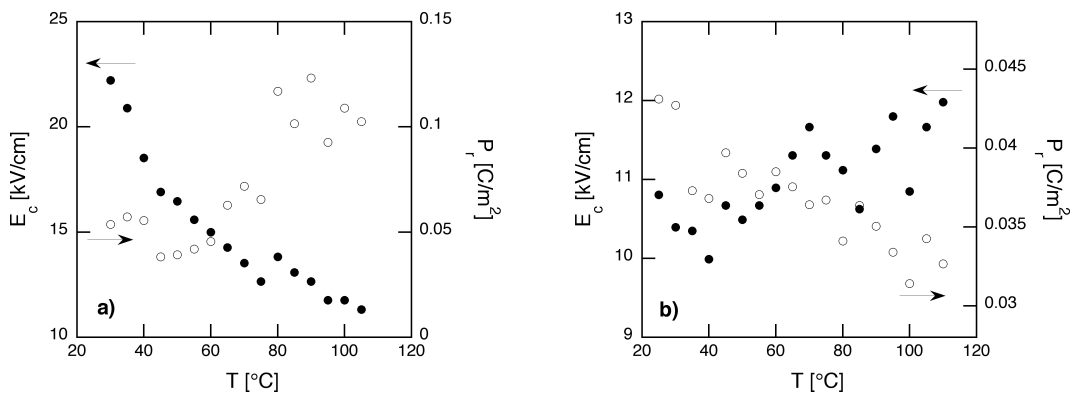

Figure 6.18: Coercive field and remanent polarisation as a function of the temperature for a) $(K_{0.47}Na_{0.47}Li_{0.06})NbO_3$ and b) $(K_{0.485}Na_{0.485}Li_{0.03})(Nb_{0.80}Ta_{0.20})O_3$ ceramics.

On one hand, in lithium modified ceramics, the remanent polarisation increases with temperature, but a maximum at the phase transition temperature is not clearly observed and the coercive field decreases with temperature. The 6% Li KNN ceramic behaves like $BaTiO_3$ (see Figure 6.8) and which is significatif of thermally induced phase transitions.

On the other hand, in tantalum modified ceramics the remanent polarisation decreases and the coercive field increases with the temperature. This behaviour, which is not typical differs from the behaviour of $BaTiO_3$ and PZT ceramics, can be explained as follows: first, for materials with temperature driven phase transitions like $BaTiO_3$ or $KNbO_3$, the remanent polarisation and the coercive field are maximal at the temperature of the phase transition. This has been observed in the case of $(K_{0.47}Na_{0.47}Li_{0.06})NbO_3$ (Figure 6.18) and $0.948(K_{0.5}Na_{0.5})NbO_3$ - 0.052 $LiSbO_3$ ceramics (Figure 6.19 [60]).
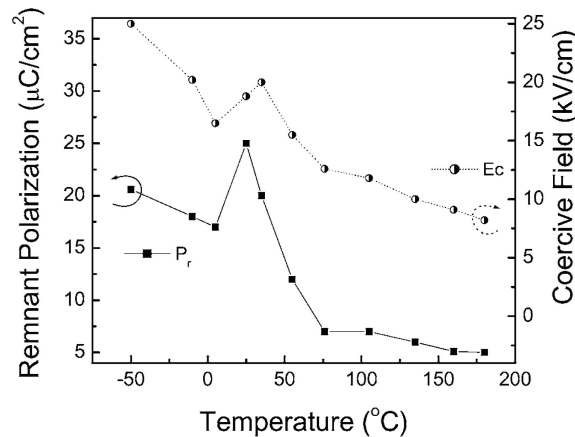

Figure 6.19: Coercive field and remanent polarisation as a function of the temperature for $0.948(K_{0.5}Na_{0.5})NbO_3$ - 0.052 $LiSbO_3$ ceramics [60].

Second, for materials with compositionally driven phase transitions, the coercive field is supposed to be minimum and the remanent polarisation maximal around the MPB.

The response of the modified KNN ceramics in function of the temperature is influenced by many mecanisms possibly including the hopping of charged carriers or conduction as it has been observed for the temperature dependent dielectric measurements. The interpretation of the hysteresis loops behaviour as a function of the temperature might then be difficult, especially as the hysteresis loops have been measured at low frequency (50 Hz).

In conclusion, the remanent polarisation and coercive field calculated from P-E hysteresis loops have on one hand allowed to confirm the temperature dependence of the phase transition in the case of lithium modified ceramics (shown in the previous section using dielectric measurements) and on the other hand, not allowed to confirm the nature of the phase transition in the lithium and tantalum modified ceramics. It should nevertheless be considered that numerous mecanisms contribute to the polarisation as a function of the temperature and that the temperature dependent hysteresis loops should be used only as complementary to dielectric and piezoelectric measurements.

6.4 Stability of piezoelectric properties

In this work, converse, resonance and direct piezoelectric measurements have been performed as a function both of the composition and the temperature. These piezoelectric measurements can give important information on the thermal stability of the ceramics. The domain configuration changes upon crossing the orthorhombic to tetragonal phase transition. This may lead to partial depoling of the samples, which is of considerable practical importance. For medical applications, for example, the probes containing piezoelectric transducers sometimes need to be sterilised at temperatures close to 140 °C. Comparable temperatures may be encountered during the probe fabrication as well. Ideally, for transducers operating at room temperature, the initial room temperature properties should be recovered after repeated sterilisation cycles.

6.4.1 Converse measurements (high field)

The first study on thermal behaviour has been reported by Saito *et al.* [55] for (K,Na,Li)(Nb,Ta,Sb)O$_3$ ceramics and is shown in Figure 6.20. The increase of the piezoelectric coefficient near the phase transition was investigated and according to the authors, texturing such compositions stabilises the strain over the measured temperature interval, which is important for actuators, for example.
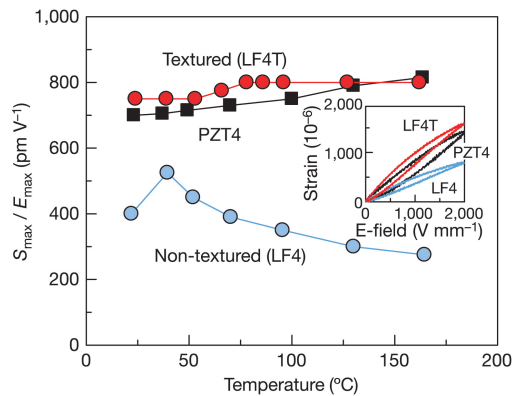

Figure 6.20: Temperature dependences of electric-field induced longitudinal strain for the textured and non textured LF4 ceramics, compared to PZT4 [55].

In this work, the temperature dependence of the converse piezoelectric coefficient d$_{33}$ has been measured and is shown in Figure 6.21. The piezoelectric coefficient d$_{33}$ was measured every 5 °C after the temperature had stabilised.
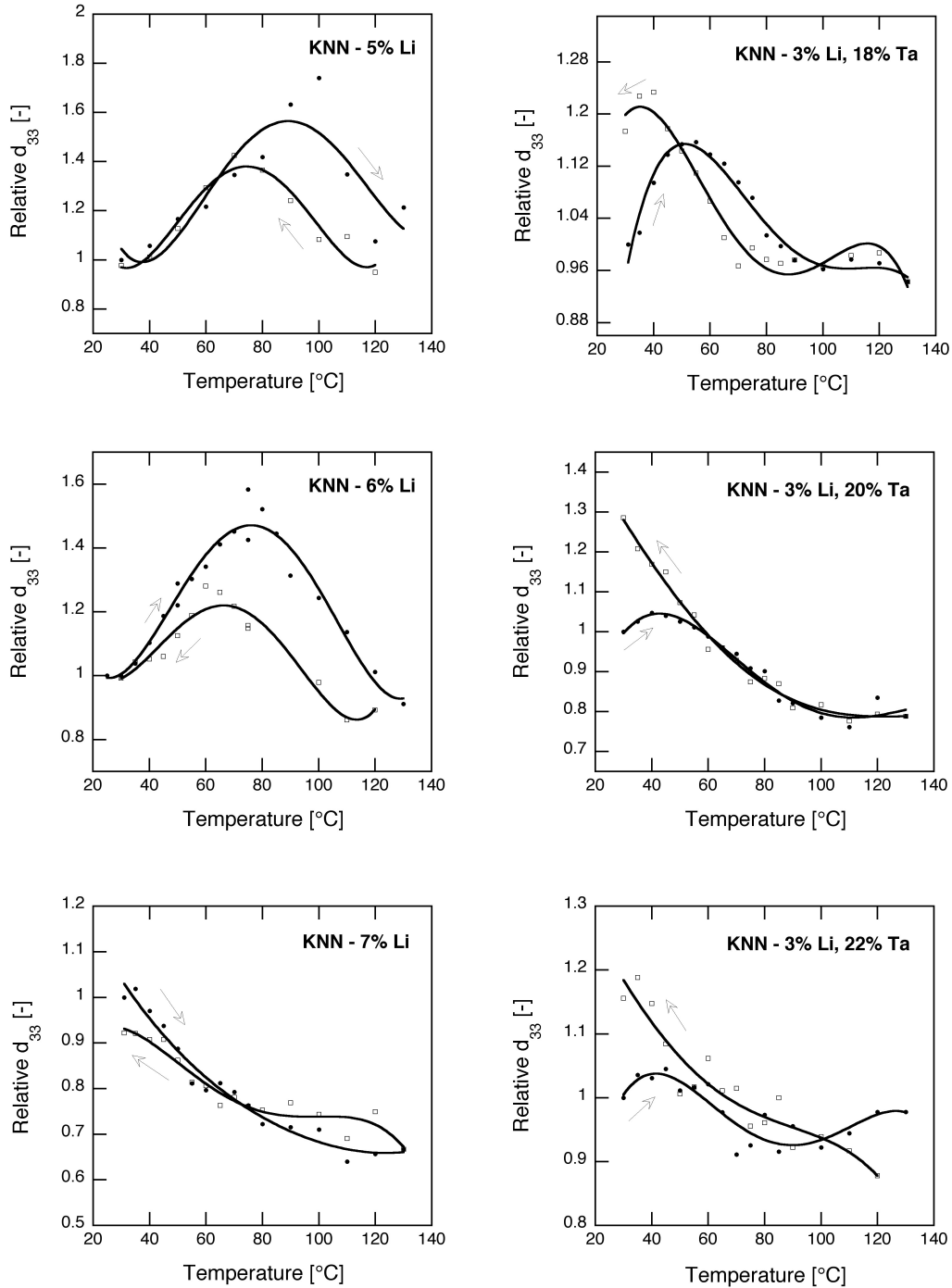
Figure 6.21: Relative d_{33} coefficients as a function of the temperature for lithium, lithium and tantalum modified KNN ceramics, measured at 1 kV from strain-field hysteresis. The initial values of d_{33} are for the lithium modified KNN ceramics, 206 (5% lithium), 175 (6% lithium), 222 pm/V (7% lithium) and for the lithium and tantalum modified ceramics 210 (18% tantalum), 273 (20% tantalum), 209 pm/V (22% tantalum).

As a high electric field is applied during the thermal cycling (about 10 kV/cm), no depoling is observed. For compositions showing a higher d_{33} coefficient after the measurement, the samples were probably further poled during the measurement, thus showing that the poling conditions could be improved. The piezoelectric coefficients are maximal

at the phase transition, and there is a shift of about 20 °C between the heating and cooling cycles, which is characteristic for first order phase transitions.

6.4.2 Resonance measurements

Compared to converse measurements, the resonance technique is a low field measurement, meaning that no repoling during the measurement is possible. If depolarisation occurs with repeated thermal cycling, resonance technique is more suited to detect it.

For the thermal stability analysis, different compositions were analysed, depending on the temperature at which the tetragonal to orthorhombic transitions occurs. Two types of materials were tested, one showing a phase transition in the temperature range of 25 to 140 °C (5% and 6% lithium), and the other being either orthorhombic (3% lithium) or tetragonal (7% lithium) within this temperature range. Similar measurements were performed with lithium and tantalum modified samples, with a fixed lithium concentration (3%).
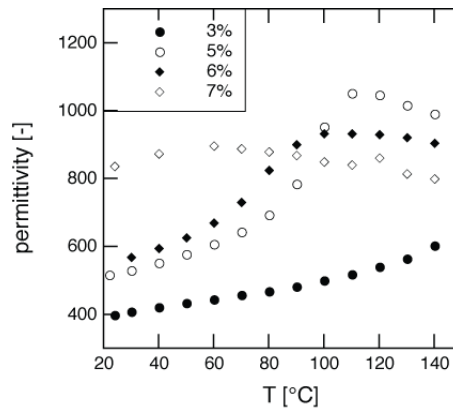

Figure 6.22: Permittivity as a function of the temperature for lithium modified ceramics with 3, 5, 6 and 7% lithium.

The temperature dependence of the permittivity (shown in Figure 6.22) confirms the presence of a phase transition in the temperature region between 25 and 140 °C for compositions with 5 and 6% lithium. The composition containing 3% lithium has a phase transition temperature from the orthorhombic to the tetragonal structure higher than 140 °C. In the case of 7% lithium ceramics, the orthorhombic to tetragonal phase transition temperature is below room temperature. The apparent peak in permittivity visible for this composition between 40 and 60 °C (see Figure 6.22) is present only in poled samples (see also Figure 5.12) and powder diffraction indicates the tetragonal structure at room temperature (Figure 4.38). Thus the ceramics with 3% and 7% lithium do not change crystal structure and remain, respectively, orthorhombic and tetragonal over the examined temperature interval.

The temperature dependences of the electromechanical properties of ceramics of composition $(K_{0.47}Na_{0.47}Li_{0.06})NbO_3$ are shown in Figure 6.23 for two successive cycles.
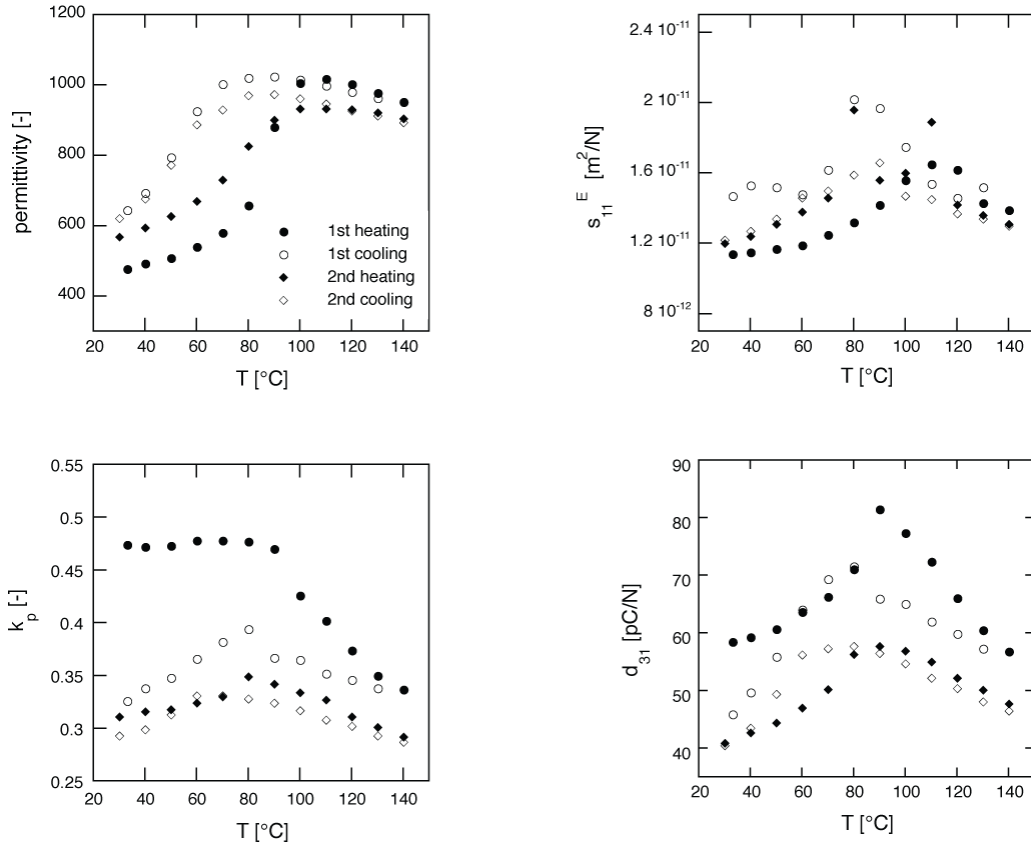
Figure 6.23: The permittivity, elastic compliance $s_{11}{}^E$, coupling coefficient k_p and piezoelectric coefficient d_{31} of 6% lithium modified KNN ceramics as a function of the temperature, for 2 successive cycles up to 140 °C.

Thermal hysteresis of the dielectric permittivity of about 20-30 °C during the heating and cooling cycles is indicative of the first order phase transition between the orthorhombic and tetragonal phases, and confirms the shift observed during the converse measurements. All the other electromechanical properties measured show a maximum at the temperature of the phase transition. For this particular composition, a decrease of about 30% of the piezoelectric coefficient d_{31} and the radial coupling coefficient k_p can be noticed after the first cycle. Considering the properties after the first and the second heating and cooling cycle, no additional significant decrease in properties is observed.
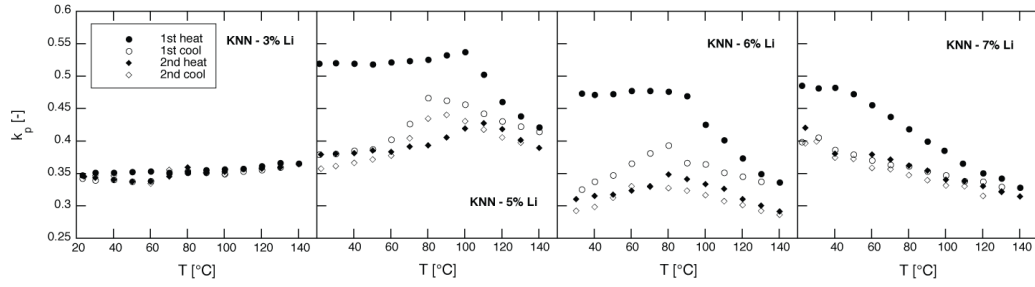
Figure 6.24: Radial coupling coefficients as a function of the temperature for lithium modified KNN ceramics, with 3, 5, 6 and 7% lithium.

The variation of the radial coupling coefficients as a function of temperature is shown in Figure 6.24 for all the lithium modified ceramics. The depoling (decease in k_p between 20 and 30%) during the first heating cycle is stronger for the two compositions, 5% and 6% lithium, going through a phase transition in the temperature range of the measurement, which can be due to the domain wall rearrangement when going through a phase transition. The same behaviour is also seen in the case of the piezoelectric coefficient d_{31}. In the case of the ceramic with 3% lithium, the thermal cycling does not affect the radial coupling coefficient, as well as the other properties obtained for this composition. In the tetragonal ceramic (7% lithium), only a small depoling (a decrease of about 10% of the piezoelectric properties) is observed. After the second heating and cooling cycle, when the properties are stabilised, this composition exhibits the best properties amongst all of the examined lithium modified ceramics with d_{31} = -69 pC/N and k_p = 0.41.

From a technological point of view, the thickness coupling coefficient is more important than the radial coupling coefficient. For 6% lithium modified ceramics, the cycling of k_t is shown in Figure 6.25.
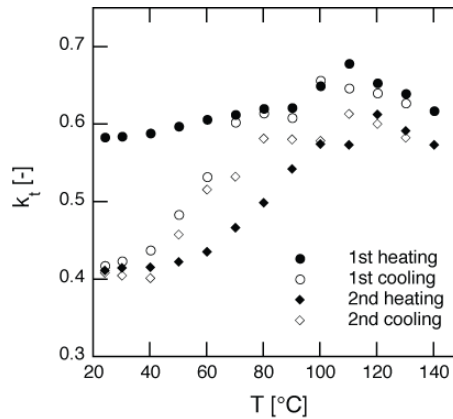

Figure 6.25: Thickness coupling coefficient as a function of the temperature for 6% lithium modified KNN ceramics.

Nevertheless, for other compositions, the k_t coefficient was difficult to determine precisely due to broad minima in the impedance spectrum, as shown in Reference [119].

From an application point of view, the most stable properties are found for lithium and tantalum modified ceramics, as the degradation in the properties after a temperature

104

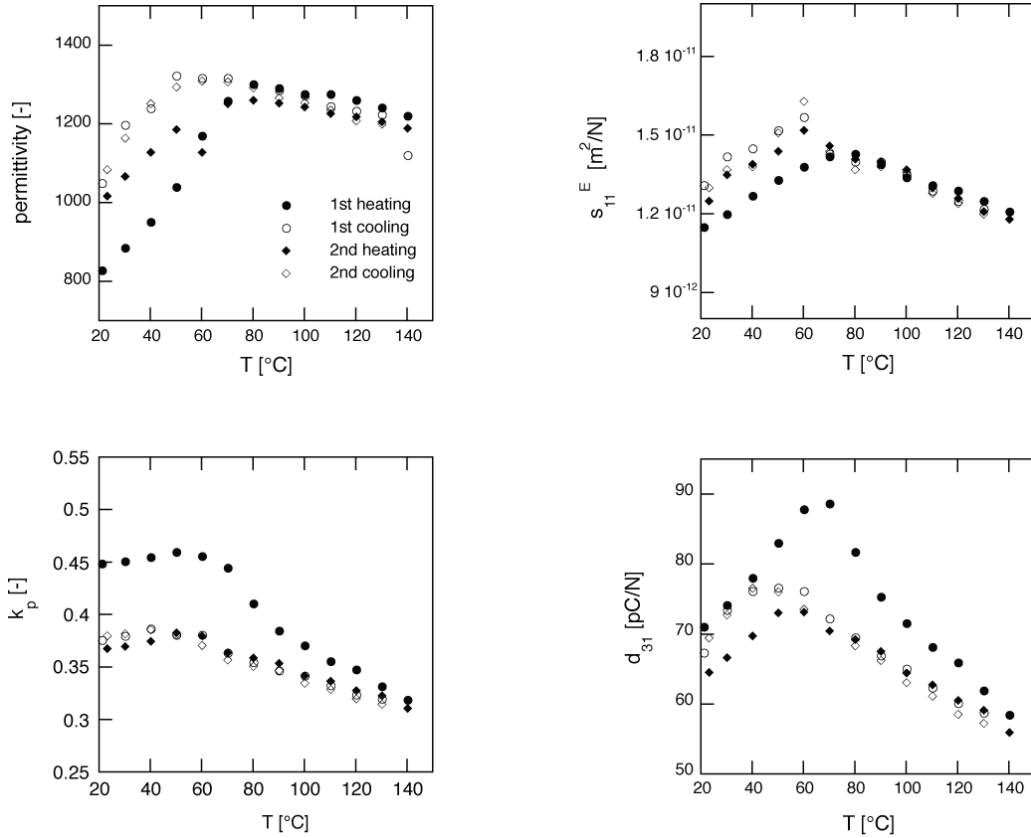cycle is the smallest, as can be seen in Figure 6.26 for 20% tantalum and 3% lithium modified ceramics.

Figure 6.26: The permittivity, elastic compliance $s_{11}{}^E$, coupling coefficient k_p and piezoelectric coefficient d_{31} of 3% lithium and 20% tantalum modified KNN ceramics as a function of the temperature, for 2 successives cycles up to 140 °C.

The radial coupling coefficient is decreased by about 16% (from 0.45 to 0.38) and the piezoelectric coefficient d_{31} only by 5% (from 71 to 67 pC/N) for 20% tantalum and 3% lithium modified ceramics. The final and stabilised properties of this composition are comparable to the stabilised electromechanical properties of 7% lithium modified KNN ceramics (k_p = 0.41 and d_{31} = -69 pC/N). A similar behaviour during thermal cycling has been reported on LiSbO$_3$ modified KNN ceramics [60].

The poling conditions (50 °C, 50 kV/cm) used were the best found for these ceramics. However, as the poling temperature lies in the temperature range of the measurements, there is a concern that depoling may be related to a relatively low poling temperature. Another poling has been performed on a 7% lithium modified KNN ceramic, at 150 °C, with a field of 30 kV/cm applied for 15 minutes, with field cooling.
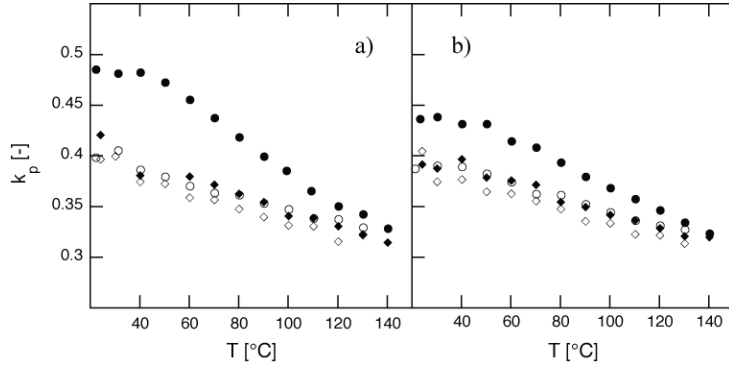
Figure 6.27: Radial coupling coefficient of KNN - 7% poled under 2 different poling conditions, a) at 50 °C with 50 kV/cm for 15 minutes and b) at 150 °C with 30 kV/cm for 15 minutes and field cooling.

The electromechanical properties after the high temperature poling (d_{31} = -70 pC/N and k_p = 0.44) are not as good as the properties after low temperature poling (d_{31} = -76 pC/N and k_p = 0.49), as can be seen in the case of the radial coupling coefficient in Figure 6.27. After cycling the two samples up to 140 °C, the properties seem to stabilise at similar values. At least for this composition the poling conditions do not seem to affect the thermal stability of the electromechanical properties.

The evolution of the relative piezoelectric coefficient d_{31} as a function of the temperature for the compositions located near the phase transition is shown in Figure 6.28.
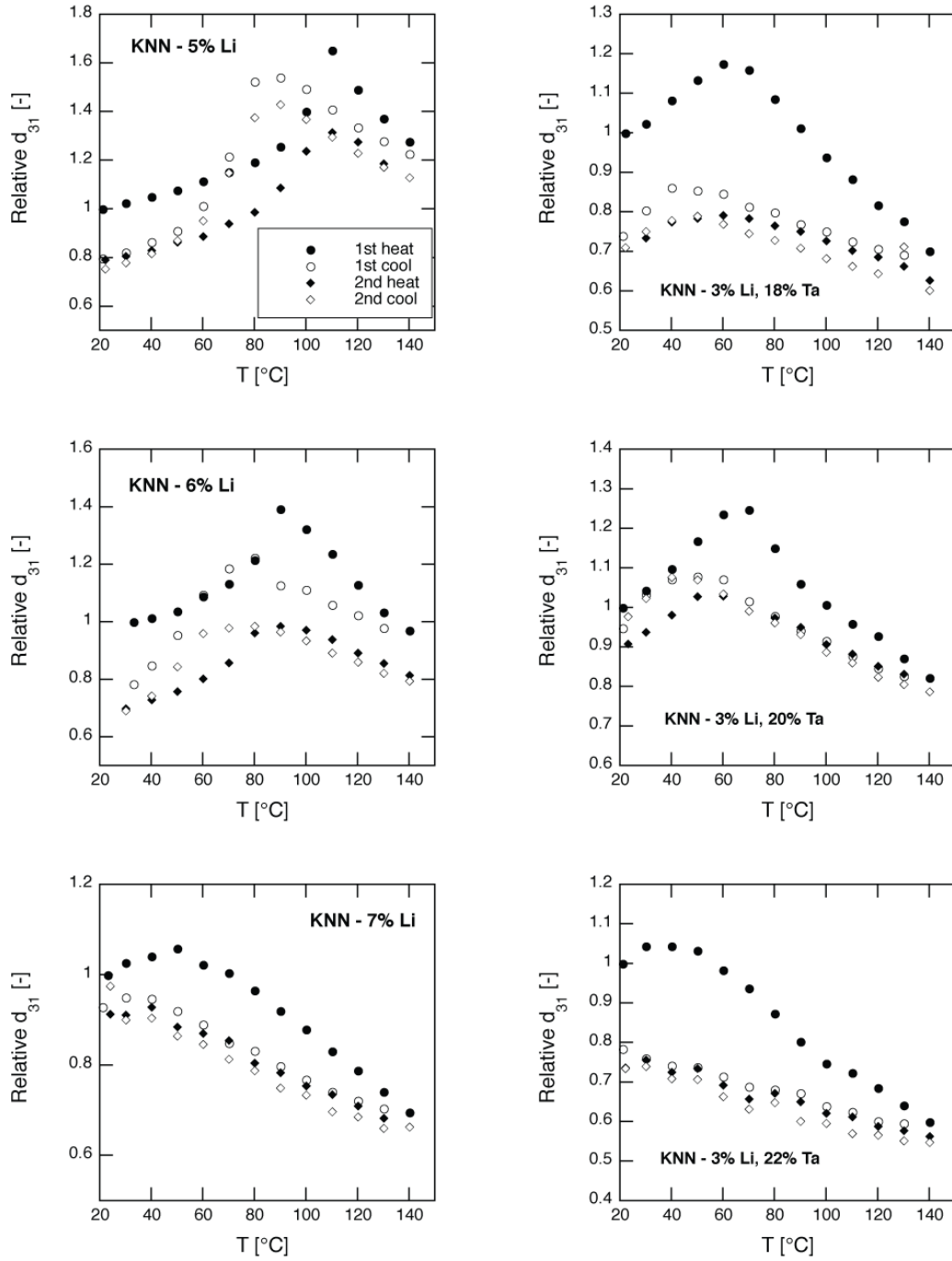
Figure 6.28: Relative d_{31} as a function of temperature for different compositions. The initial values of d_{31} are for the lithium modified KNN ceramics, 59 (5% lithium), 59 (6% lithium), 76 pC/N (7% lithium) and for the lithium and tantalum modified ceramics 54 (18% tantalum), 71 (20% tantalum), 55 pC/N (22% tantalum).

The depolarisation varies from one composition to the other and ranges from almost no depoling (20% Ta and 3% Li) to about 30% (6% Li). The highest stabilised value of d_{31} is similar for 7% Li (69 pC/N) and 20% Ta with 3% Li KNN ceramics (70 pC/N). This behaviour is the same as for the radial coupling coefficient shown above.

In conclusion, the electromechanical properties of the new developed ceramics decrease after the first thermal cycling, but stabilise after the second. The best thermal stability

is observed for the composition near the phase transition (20% Ta and 3% Li). However, the final properties are close to the properties of 7% Li modified KNN ceramics.

To determine precisely the temperature of the orthorhombic to tetragonal phase transition, measurements of the electromechanical properties should be measured using smaller temperature intervals.

6.4.3   Direct measurements

The thermal stability of the piezoelectric coefficient d_{33} can be determined by direct measurements, in a similar way as for resonance measurements, the fundamental difference being the presence of a compressive stress during direct measurements depoling the samples.

For measurements performed as a function of the temperature with a maximal dynamic stress of 0.8 MPa, the evolution of the relative piezoelectric coefficient d_{33} is shown in Figure 6.29 for two successive cycles up to 140 °C, in a similar way as for resonance measurements.
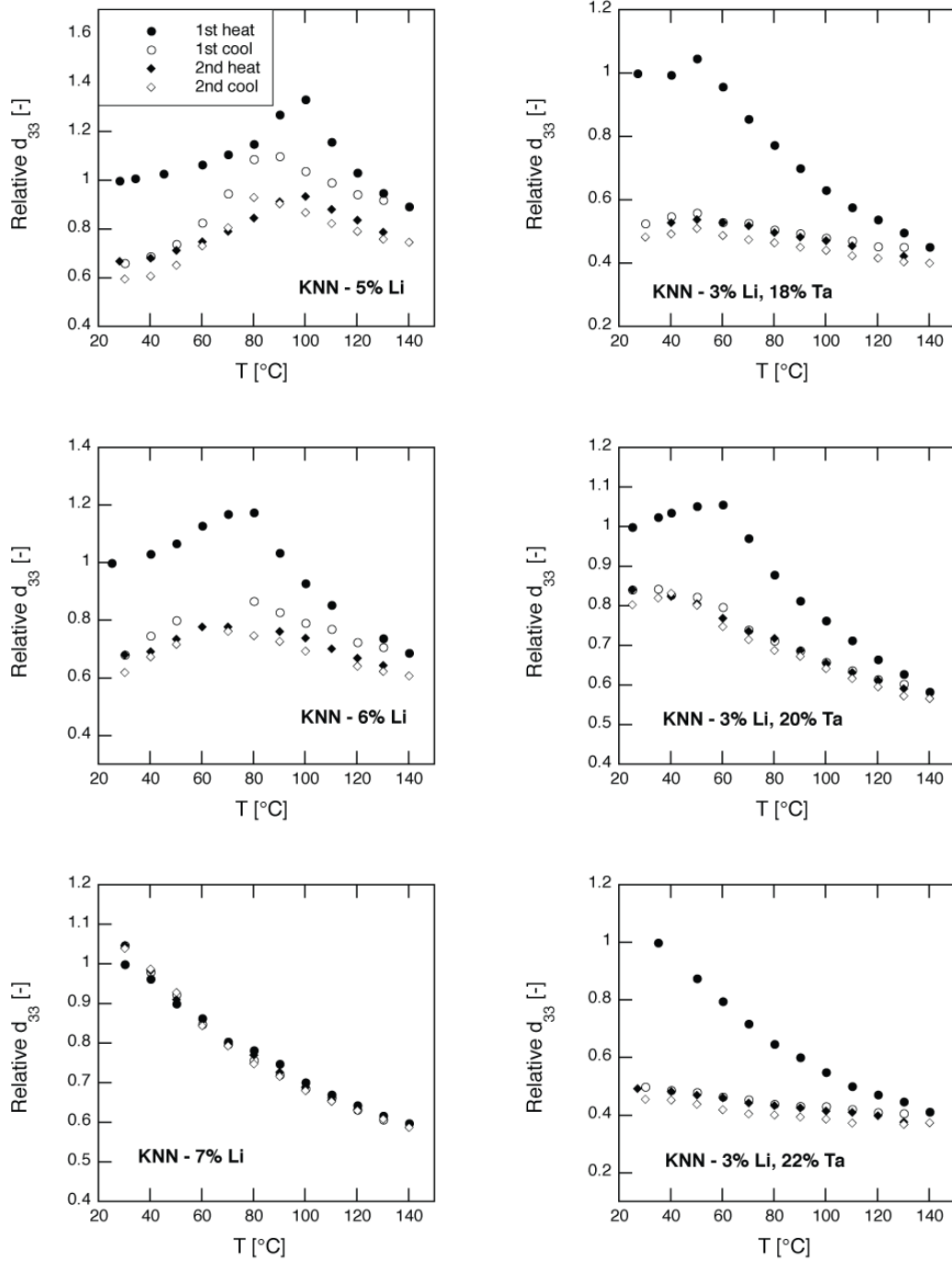
Figure 6.29: Relative d_{33} as a function of the temperature for the lithium and lithium with tantalum modified KNN ceramics, measured at 100 Hz, 0.8 MPa dynamic stress and for a static stress of 4 MPa. The initial values of d_{33} are for the lithium modified KNN ceramics, 135 (5% lithium), 137 (6% lithium), 141 pC/N (7% lithium) and for the lithium and tantalum modified ceramics 137 (18% tantalum), 206 (20% tantalum), 114 pC/N (22% tantalum).

A marked depolarisation can be observed for almost every composition except for $(K_{0.465}Na_{0.465}Li_{0.07})NbO_3$, and it can reach 50% of the initial value. The depolarisation can be caused by the thermal cycling but also by the application of a dynamic or static stress.

By comparing the depolarisation of d_{33} obtained by direct measurements and of d_{31} determined by resonance measurements, the causes of this depolarisation can be determined. The depolarisations calculated from resonance and direct piezoelectric measurements are summarised in Table 6.1

Table 6.1: Depolarisation (in %) of the modified KNN ceramics after the first thermal cycle up to 140 °C, for the resonance (d_{31}) and direct (d_{33}) piezoelectric measurements.

Compositions	Loss of d_{31} (resonance)	Loss of d_{33} (direct)
3% Li, 0% Ta	4	7
5% Li, 0% Ta	21	34
6% Li, 0% Ta	22	32
7% Li, 0% Ta	7	0
3% Li, 18% Ta	26	48
3% Li, 20% Ta	5	16
3% Li, 22% Ta	22	50

The decrease of d_{33} is always superior to the one of d_{31}, because in d_{33} measurements the sample is additionally depoled by the static prestress. This stress reduces the domain wall motion and therefore the piezoelectric coefficient. The two modified KNN ceramic families show different behaviours. For the lithium modified KNN ceramics, the depolarisation is the highest for the composition that undergo a phase transition during the measurement. The depolarisation of the samples, which are not going through this transition, arises only from thermal effects. The lithium and tantalum modified KNN ceramics show the opposite behaviour, since the thermal stability is the best for the 3% lithium and 20% tantalum composition. This behaviour is difficult to explain, as PZT ceramics with compositions near the MPB display the worst thermal stability [74]. Finally, the ceramics with 7% lithium show the best thermal stability of all the analysed ceramics.

In Figure 6.30 are compared the measurements as a function of the temperature for d_{31} obtained by resonance and d_{33} obtained by direct measurements during the first thermal cycle. The maxima of the d_{31} coefficient are 10 °C higher than those of d_{33}, which is also the case in PZT [1] and which explains the difference in the phase transition temperatures found in literature [55, 57].
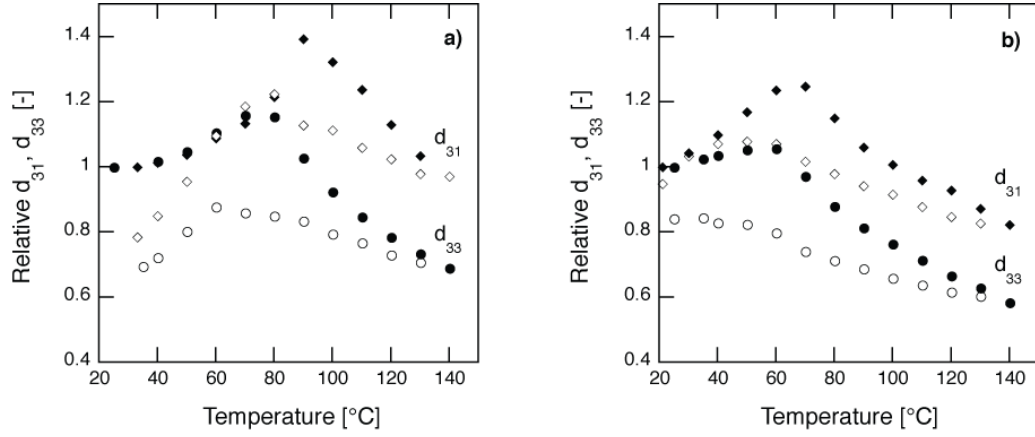
Figure 6.30: Relative d_{31} and d_{33} as a function of the temperature for a) $(K_{0.47}Na_{0.47}Li_{0.06})NbO_3$ and b) $(K_{0.485}Na_{0.485}Li_{0.03})(Nb_{0.80}Ta_{0.20})O_3$ ceramics for one cycle up to $140\,^\circ C$.

Table 6.2 presents a summary of the orthorhombic to tetragonal phase transition temperatures obtained by dielectric and piezoelectric measurements. The measurement errors are $\pm$ 5-10 °C, like the temperature steps in the different measurements.

Table 6.2: Orthorhombic to tetragonal phase transition temperatures obtained by dielectric measurements, converse, resonance and direct piezoelectric measurements, for lithium and lithium with tantalum modified ceramics. The determination method is shown in brackets.

Compositions	Dielectric $[d\varepsilon/dT = 0]$	Resonance $[\max(d_{31})]$	Converse $[\max(d_{33})]$	Direct $[\max(d_{33})]$
5% Li, 0% Ta	102	110	100	100
6% Li, 0% Ta	75	90	75	80
7% Li, 0% Ta	30	50	< 25	< 25
3% Li, 18% Ta	86	60	55	50
3% Li, 20% Ta	65	60	40	60
3% Li, 22% Ta	73	40	40	< 25

For lithium modified KNN ceramics, these phase transition temperatures are slightly higher than the temperatures found in Figure 4.38 and 6.12. The shift of the transition temperature from measurements of d_{31} or d_{33} is clearly visible in Table 6.2.
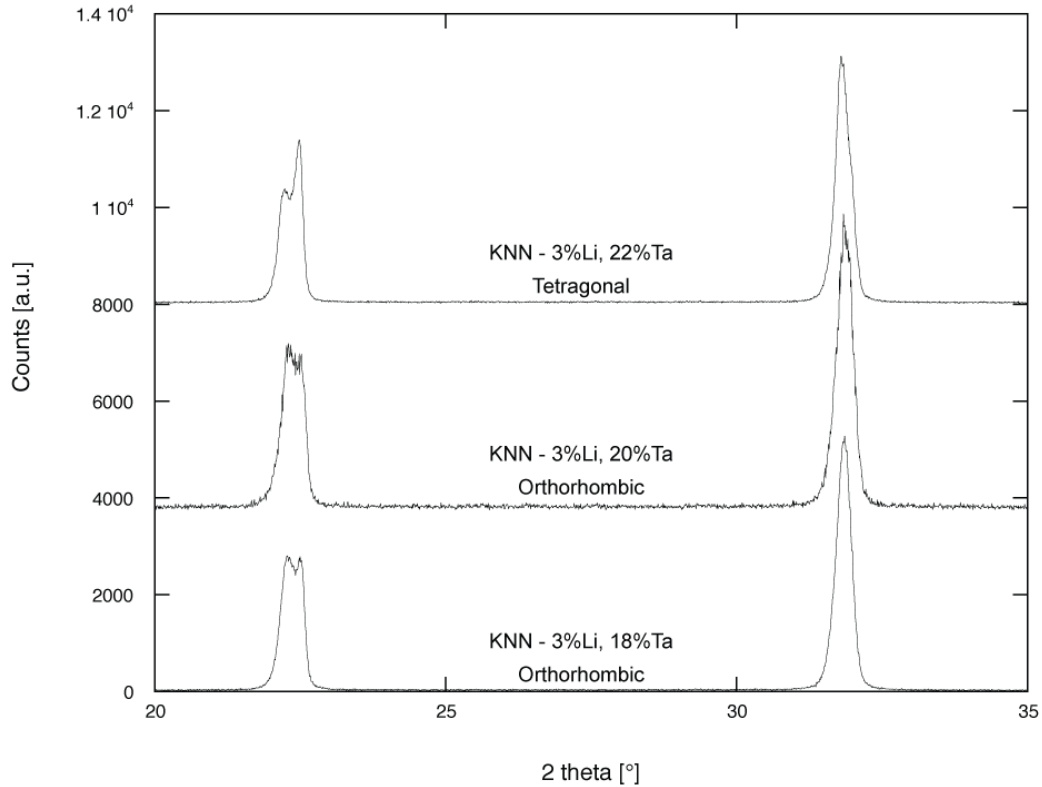
Figure 6.31: Diffraction pattern of lithium and tantalum modified KNN ceramics with 3% lithium, 18, 20 and 22% tantalum.

For the lithium and tantalum modified ceramics, the phase transition temperature obtained by dielectric measurements don't decrease continuously with the tantalum concentration, but at room temperature, XRD measurements clearly indicate this phase transition (see Figure 6.31), as for tantalum concentrations below 20% the structure is orthorhombic and above 20% it is tetragonal. The phase transition temperature nevertheless is not as sensitive on the tantalum concentration as it is the case for lithium modified KNN ceramics.

6.5 Conclusions

For the two families of modified KNN ceramics, dielectric and piezoelectric measurements were carried out as a function of temperature to determine the phase transition temperatures from orthorhombic to tetragonal phase. The evolution of the phase transition temperatures as a function of composition shows that the orthorhombic to tetragonal phase line in the temperature-composition phase diagram is strongly curved, unlike in PZT. The phase transition temperatures obtained in this work are higher than those reported in a phase diagram of lithium modified KNN ceramics (see Figure 6.12 [83]). Furthermore, a clear dependence of the phase transition on temperature is observed. In the case of hysteresis loop measurements, the nature of the phase transition could be confirmed only for lithium modified ceramics. In the case of lithium and tantalum modified ceramics, no clear maxima could be detected in the remanent polarisation as a function of the temperature and composition. The temperature seems to be the most contributing

factor in the decrease of the electromechanical properties during thermal cycling comparing to the effect of composition. Indeed, the decreases are more marked for ceramics undergoing phase transitions than those for which no phase transition occurs.

The thermal stability of the ceramics was analysed from piezoelectric measurements as a function of the temperature. During converse measurements, no depoling was noticed, since the high field repoles the samples during measurement. In low field measurements for the lithium modified ceramics (7% lithium), the tetragonal ceramics show the best electromechanical properties before and after stabilisation and have the lowest depoling. The depolarisation is the highest for compositions going through a phase transition (5-6% Li). In the case of lithium and tantalum modified ceramics, the best stability is reached by the composition near the phase transition (20% Ta and 3% Li). The properties of these two compositions (7% Li-KNN and 3% Li, 20% Ta-KNN) are similar after 2 cycles. The depolarisation is higher for d_{33} than for d_{31} as the applied stress is combined to the thermal effect.

Chapter 7

Domain wall contributions to the piezoelectric properties: phase transitions effects

The direct piezoelectric response is relevant for applications and in particular for sensors, because the materials in these devices are subjected to high stresses. For soft PZT, a hysteretic charge-stress response, as well as a non linear behaviour of the piezoelectric coefficient as a function of stress is observed [120]. The pinning of domain walls is the principal mechanism responsible for this behaviour. A phenomenological model based on the Rayleigh law for magnetic materials is used to characterise the piezoelectric response and to differentiate its reversible and irreversible contributions.

As shown in Chapter 6, the KNN based ceramics with increased electromechanical properties operate in the vicinity of a thermally induced phase transition. As the domain wall configurations are different in the tetragonal and orthorhombic structures, their contributions will be affected during the transition.

The direct measurements have been performed by varying the applied dynamic and static stresses and also as function of the frequency and temperature in order to establish the effect of a structural change on the domain wall contribution.

7.1 Introduction

It has been mentioned in the previous chapter that the piezoelectric response can be divided into intrinsic and extrinsic contributions. The extrinsic contribution mainly originates from the displacement of non-180° domain walls and phase interfaces [108, 121, 122]. The result of an irreversible component of the movement of domain walls is a nonlinear and hysteretic piezoelectric response [123, 124]. Since ferroelectric ceramics are widely used to make transducers, actuators or sensors, the characterisation of the nonlinear behaviour of piezoelectric ceramics is very important, especially for high-precision applications. It is then essential to understand the origin of the nonlinear properties in ferroelectric ceramics in order to optimise the performance of the ceramic devices.

Typical behaviours of piezoelectric ceramics, as a function of the applied dynamic field and the frequency are shown in Figure 7.1.
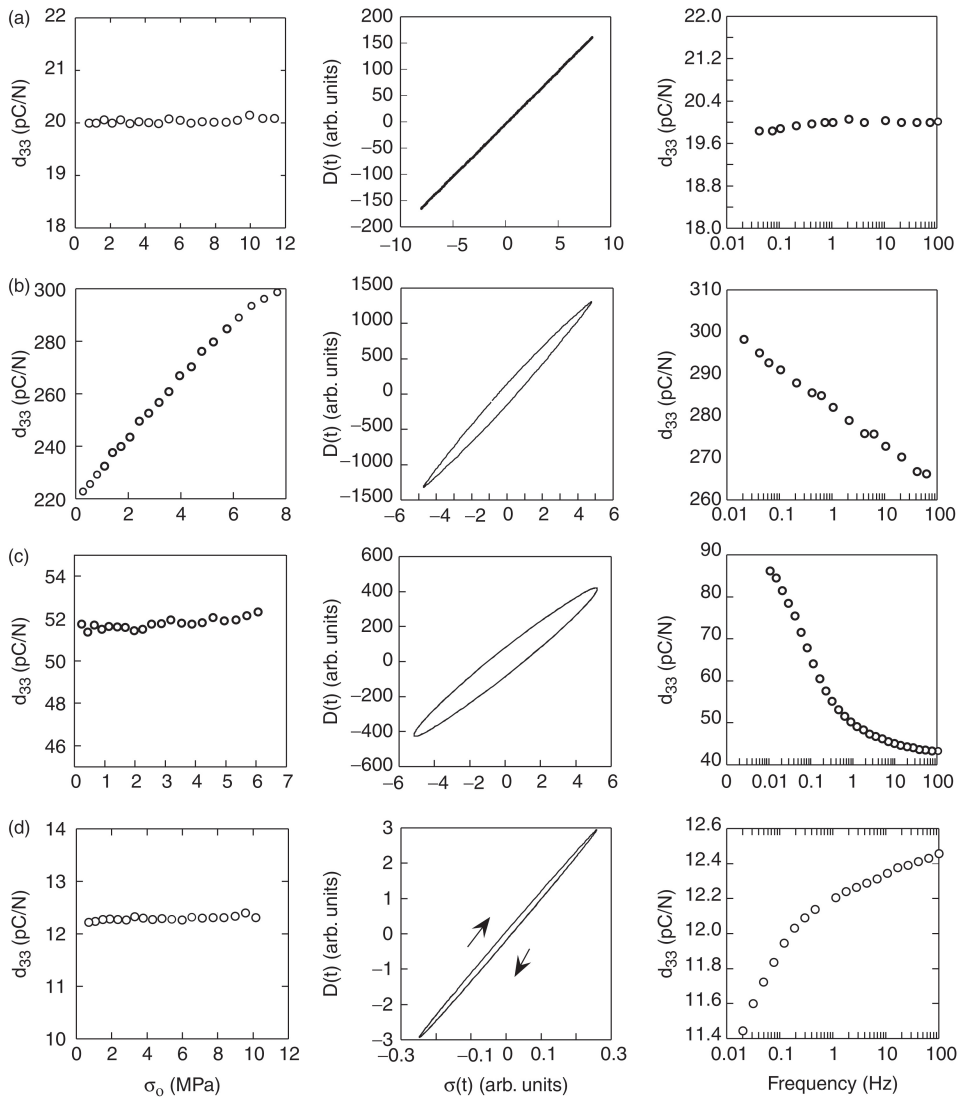

Figure 7.1: Dynamic stress dependence, hysteresis and frequency dispersion associated with the direct piezoelectric effect in a) $SrBi_4Ti_4O_{15}$ b) Nb-doped PZT, c) $(Pb,Sm)TiO_3$ and d) Mn-doped $SrBi_4Ti_4O_{15}$ [104].

The typical behaviour of donor-doped PZT ceramics, which are the most widely used piezoelectric ceramics, is shown in Figure 7.1 b). The piezoelectric response of Nb-PZT exhibits strong nonlinearity, charge pressure hysteresis and a logarithmic dispersion as a function of frequency. The dependence as a function of field of this response is a consequence of the pinning of domain wall on randomly distributed pinning centres and is responsible for the weak-field hysteresis.

Many models assuming the domain wall motion to be the main contribution to the weak field piezoelectric behaviour have been proposed [120, 125, 126]. The domain wall motion is complex and depends on many factors like the defects, microstructure and composition. Nevertheless, it has experimentally been observed for different materials that the piezoelectric response can be described by modified Rayleigh equations [120, 127, 128].

The Rayleigh law for direct piezoelectric effect is expressed by:

$$d = d_0 + \alpha \sigma_0 \qquad (7.1)$$

$$D(\sigma) = (d_0 + \alpha \sigma_0)\sigma \pm \frac{\alpha}{2}(\sigma_0^2 - \sigma^2) \qquad (7.2)$$

where d_0 is the static piezoelectric coefficient and represents the reversible component of the piezoelectric coefficient, σ_0 is the maximal dynamic stress amplitude, D is the charge density and α is the Rayleigh coefficient, which is the measure of the nonlinearity.

The reversible contribution is equivalent to the zero-field piezoelectric coefficient d_0 and its fraction is given by $(d_0)/(d_0 + \alpha \sigma_0)$ [120]. The irreversible and nonlinear contribution fraction is $(\alpha \sigma_0)/(d_0 + \alpha \sigma_0)$. Therefore, d_0 is the linear part of the response and it takes into account the intrinsic response and the reversible field independent extrinsic response (for example, the reversible displacement of domain wall effects), while $\alpha \sigma_0$ comprises the irreversible displacement of domain walls. These parameters α and d_0 are determined experimentally.

In Figure 7.2 is illustrated the movement of the domain walls in a medium containing randomly distributed pinning centres, with a large distribution of energy barriers. The irreversible movement of a domain wall is characterised by a jump from one energy minimum to the other due to a large enough field to overcome the energy barrier, whereas the small displacements around each minimum is reversible. As the domain wall moves from one minimum to the other under an applied field, the pinning and unpinning of this wall leads to a hysteretic behaviour.
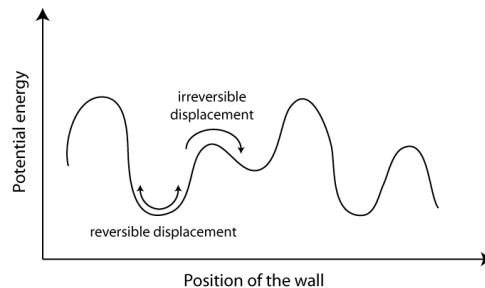

Figure 7.2: Potential energy of the domain wall in a medium which contains randomly distributed defects [120].

The linear stress dependences of the longitudinal piezoelectric coefficients of some materials are shown in Figure 7.3. For BaTiO$_3$ (at 1 Hz, 1.8 MPa stress amplitude and 1 MPa bias stress) and PZT ceramics with composition near the MPB (at 1 Hz, 6.8 MPa stress amplitude and 20 MPa bias stress), this irreversible contribution reaches 35 and 20% of the total response respectively [129], but strongly depends on the measurement conditions.
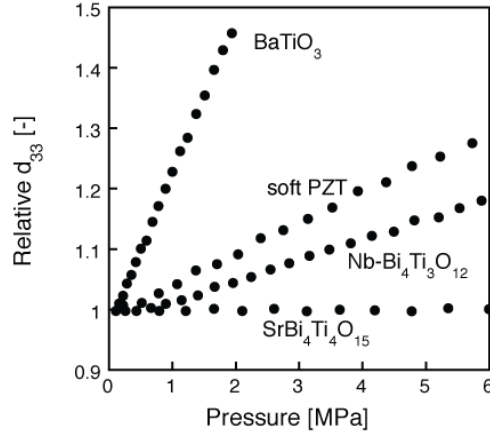

Figure 7.3: The direct d_{33} piezoelectric coefficient as a function of the AC pressure amplitude for different ferroelectric ceramics. The DC pressure applied was the half of the maximum amplitude of the dynamic stress, which is different for the various materials [130].

Concerning the analysis of anisotropy of the longitudinal coefficient described in the previous chapter, it is noteworthy adding that the direct piezoelectric coefficient is maximal at the compositionally or thermally induced phase transition, as shown in Figure 7.4.
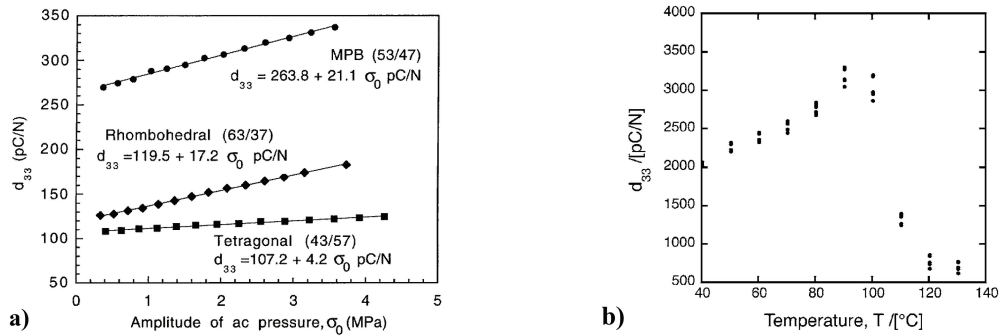

Figure 7.4: a) The direct piezoelectric coefficient d_{33} as a function of the AC pressure amplitude for PZT (doped with 4%Nb) ceramics with different crystallographic structures. The bias pressure is 15 MPa [129]. b) d_{33} as a function of temperature for $[001]_c$-poled PZN-8PT single crystal measured upon heating at 1, 7, 10 and 50 Hz for a bias pressure of 2 MPa and a dynamic stress of 0.5 MPa [128].

This thermal dependence is important for applications, since, as shown in the previous chapter, the piezoelectric properties of KNN based ceramics are affected by thermal cycling. The irreversible and reversible contributions can then be determined as a function of the temperature around the phase transition, as shown for PZN-8PT in Figure 7.5

[128]. In this particular case, the irreversible contribution can reach more than 50% of the total response above the temperature of the phase transition.
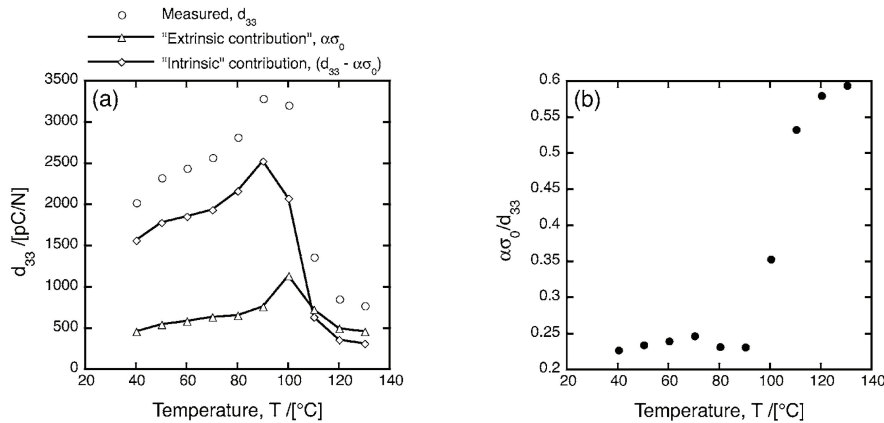

Figure 7.5: a) Intrinsic and extrinsic contributions to d_{33} assuming Rayleigh behaviour in the direct response of $[001]_c$-poled PZN-8PT at 1 Hz and b) proportion of the extrinsic contribution to the total measured response [128].

Another factor influencing the piezoelectric response of ferroelectric ceramics is the processing. In that respect, a good example is the effect of the grain size on the stress dependence of d_{33} for barium titanate, as shown in Figure 7.6 [94, 129].
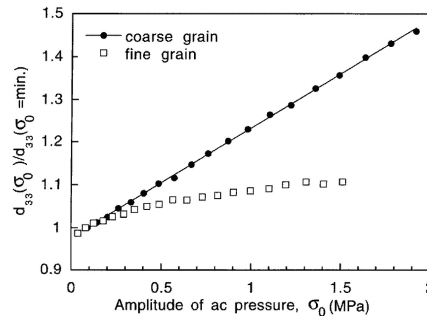

Figure 7.6: The relative direct piezoelectric coefficient d_{33} as a function of AC pressure amplitude for coarse- and fine-grained $BaTiO_3$ ceramics at 1 Hz. The bias pressure is 1MPa [129].

Complementary to the nonlinear behaviour of d_{33} as a function of stress, materials where the properties are controlled by pinning of domain walls on the randomly distributed defects, show a logarithmic dependence as a function of the frequency. This behaviour is illustrated on Figure 7.1 b) for soft PZT. The logarithmic dependence of the piezoelectric coefficient in these cases can be expressed by [131]:

$$d(\omega) = F_0 - Fln(\omega) \tag{7.3}$$

To describe the frequency dispersion and the nonlinearity in dielectric and piezoelectric responses, a power-law model has been proposed [132].

The aim of this chapter is to determine the contributions to the piezoelectric response of the modified KNN ceramics and in particular the evolution as a function of temperature.

119

This evolution is analysed especially for the ceramics going through a phase transition during the thermal cycles. The effects of high static stresses as well as the frequency will be briefly discussed.

7.2 Dynamic measurements

A typical evolution of the piezoelectric coefficient as a function of the applied dynamic static stress for different frequencies for $(K_{0.47}Na_{0.47}Li_{0.06})NbO_3$ and $(K_{0.485}Na_{0.485}Li_{0.03})(Nb_{0.80}Ta_{0.20})O_3$ ceramics is shown in Figure 7.7. The maximal value of the amplitude of the applied dynamic stress is 5 MPa with a static stress of 15 MPa, for different frequencies (100, 10 and 1 Hz). An increase of the piezoelectric coefficient of about 30% is observed for both compositions and the behaviour is slightly non-linear at high driving fields.
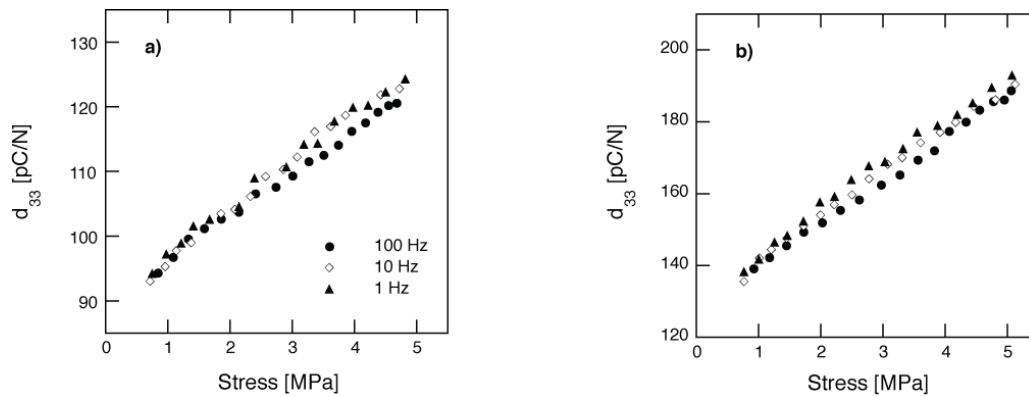

Figure 7.7: d_{33} as a function of the applied dynamic stress for a) $(K_{0.47}Na_{0.47}Li_{0.06})NbO_3$ and b) $(K_{0.485}Na_{0.485}Li_{0.03})(Nb_{0.80}Ta_{0.20})O_3$ ceramics with a static stress of 15 MPa, at 100, 10 and 1 Hz.

The evolution of the corresponding charge-stress hysteresis of $(K_{0.47}Na_{0.47}Li_{0.06})NbO_3$ and $(K_{0.485}Na_{0.485}Li_{0.03})(Nb_{0.80}Ta_{0.20})O_3$ ceramics are shown in Figure 7.8. It is to remark that the hysteresis have no rounded tips, which is typical of conductivity in the materials.
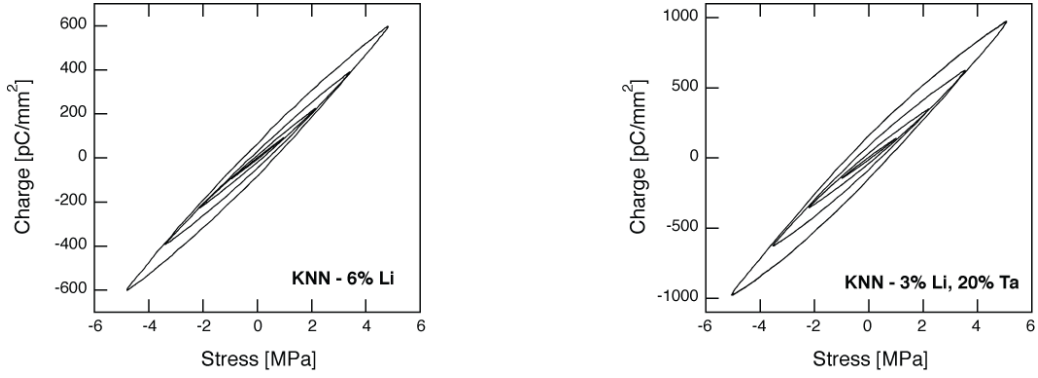
Figure 7.8: Charge-stress hysteresis for a) $(K_{0.47}Na_{0.47}Li_{0.0b})NbO_3$ and b) $(K_{0.485}Na_{0.485}Li_{0.03})(Nb_{0.80}Ta_{0.20})O_3$ ceramics with a static stress of 15 MPa, at 1 Hz.

In this figure, the time dependent charge density is given in function of the dynamic stress which is a zero centred function. For mathematical purposes, the charge density is also zero-centred.

The ceramics of different compositions have different grain sizes, as shown in Figure 4.36 and in particular the lithium and tantalum modified ceramics have smaller grain sizes than the lithium modified ceramics. For barium titanate, the grain size influences the domain wall motion, which in turn affects the irreversible contribution of the piezoelectric response. For small grain sizes, the irreversible movement of the domain wall is more difficult due to internal stresses, which lowers the irreversible contribution [104]. For the modified KNN ceramics at room temperature, the dependence of d_{33} as a function of dynamic stress is shown in Figure 7.9 for compositions with 5, 6 and 7% lithium on one side and with 18, 20 and 22% tantalum (with 3% lithium) on the other side.
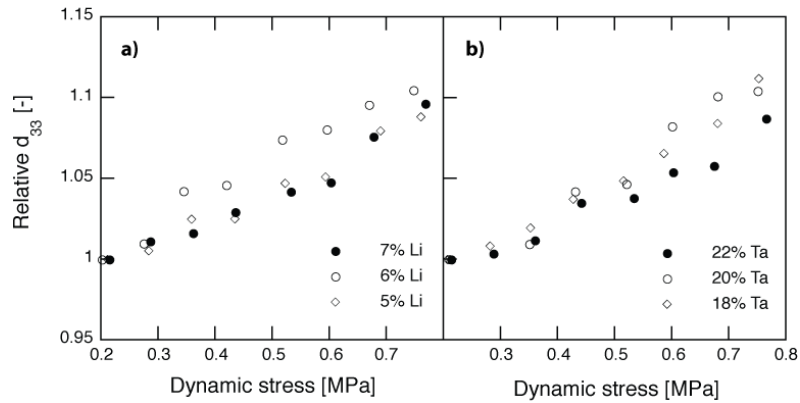

Figure 7.9: Relative d_{33} as a function of applied dynamic stress for a) 5,6 and 7% lithium and b) 18, 20 and 22% tantalum with 3% lithium modified KNN ceramics with a static stress of 4 MPa, at 100 Hz. The initial values (at 0.2 MPa) of d_{33} are for the lithium modified KNN ceramics, 124 (5% lithium), 124 (6% lithium), 129 pC/N (7% lithium) and for the lithium and tantalum modified ceramics 123 (18% tantalum), 187 (20% tantalum), 108 pC/N (22% tantalum).

As the irreversible contributions of the lithium, lithium and tantalum modified KNN ceramics are similar, the effect of the grain size can be neglected.

The linear behaviour at low dynamic stress can be related to the Rayleigh equation (Equation 7.1) and the reversible and irreversible contributions can be calculated from the experimental data presented in Chapter 6. Figure 7.10 shows the d_{33} dependence of the dynamic stress at different temperatures for the $(K_{0.47}Na_{0.47}Li_{0.06})NbO_3$ and $(K_{0.485}Na_{0.485}Li_{0.03})(Nb_{0.80}Ta_{0.20})O_3$ ceramics. The d_{33} as a function of stress was measured up to 140 °C, as for resonance and converse measurements.
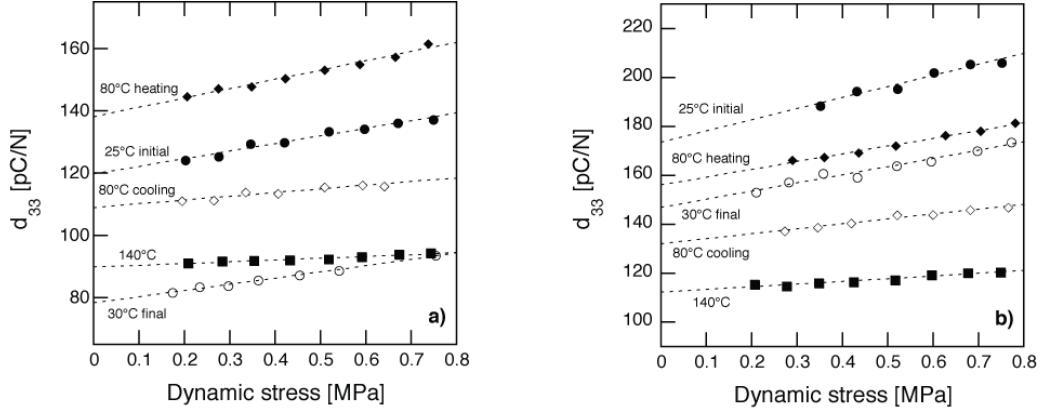

Figure 7.10: d_{33} as a function of the dynamic stress for a) $(K_{0.47}Na_{0.47}Li_{0.06})NbO_3$ and b) $(K_{0.485}Na_{0.485}Li_{0.03})(Nb_{0.80}Ta_{0.20})O_3$ ceramics at 100 Hz and for a static stress of 4 MPa, for different temperatures, assuming a Rayleigh behaviour.

The piezoelectric responses of tetragonal and orthorhombic ceramics present a Rayleigh type behaviour, characterised by a linear behaviour of the piezoelectric coefficient as a function of the dynamic stress and by a hysteretic behaviour. This behaviour has not been reported previously in orthorhombic materials. An example of hysteresis is shown in Figure 7.11 for $(K_{0.485}Na_{0.485}Li_{0.03})(Nb_{0.80}Ta_{0.20})O_3$ ceramics as a function of the temperature.
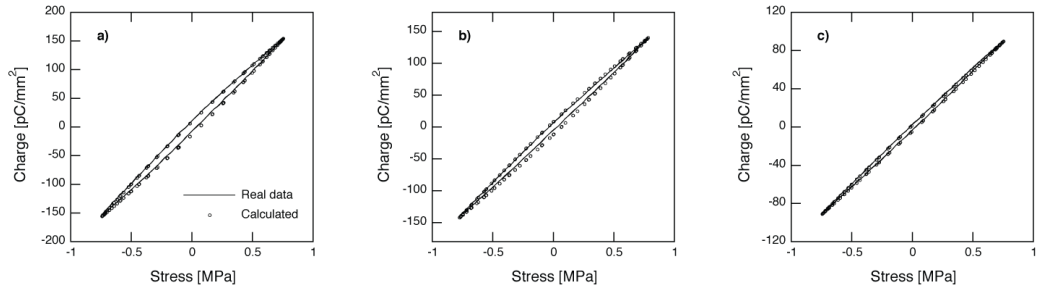
Figure 7.11: Charge-stress hysteresis of $(K_{0.485}Na_{0.485}Li_{0.03})(Nb_{0.80}Ta_{0.20})O_3$ ceramics with curve fitting using Equation 7.2, at a) 25 °C b) 80 °C and c) 140 °C, at 100 Hz and for a static stress of 4 MPa.

In these direct measurements, the domain walls move under the applied stress and this movement increases with the stress, thus increasing the charge-stress hysteresis. The stress applied can depole the samples during the measurement differing from converse measurements, for which a repolarisation takes place during the measurement. The strain-field hysteresis obtained from converse measurements show a small hysteresis characteristic of

122

hard materials whereas from direct measurements, the charge-stress hysteresis are larger (typical of soft materials). The hard behaviour of the modified KNN ceramics has previously been observed in Section 6.3 (pinched P-E hysteresis loops). In conclusion, depending on the type of measurement, these ceramics can show either a soft or hard behaviour, which has also been reported by Shrout *et al* [60].

7.2.1   Extrinsic and intrinsic contributions

The irreversible contributions for lithium modified ceramics calculated from the Rayleigh equation $((\alpha\sigma_0)/(d_0 + \alpha\sigma_0))$ as a function of temperature are shown in Figure 7.12.

Figure 7.12: Irreversible contribution $(\alpha\sigma_0)/(d_0 + \alpha\sigma_0)$ during heating and cooling for lithium modified KNN ceramics.

From this figure it can be deduced that the irreversible contributions are maximal at the phase transition and are higher in the orthorhombic phase. The domain wall contribution is expected to be higher on the orthorhombic side, compared to the tetragonal structure. This is due to the different domain configurations in the two structures (see Figure 3.2). Indeed, in the orthorhombic structure, the number of possible domains contributing to the total piezoelectric response is higher than for the tetragonal structure. In the orthorhombic structure, 90° and 180° domain walls can be found as in the tetragonal structure, but also 60° and 120° domain walls. Similarly to the behaviour observed in tetragonal and rhombohedral phase, the strain associated the distortions due to the domain wall movement in the two structures could explain the facilitated domain wall rotation in the orthorhombic phase compared to the tetragonal.

At room temperature, the irreversible contribution of the lithium modified ceramics is around 20%, like in the case of PZT-Nb [120]. For comparison this contribution is higher for rhombohedral PZT (30%) [133] and barium titanate (35%) [127]. In the case of tantalum modified ceramics with the composition $(K_{0.485}Na_{0.485}Li_{0.03})(Nb_{0.80}Ta_{0.20})O_3$, the irreversible contribution is slightly higher than in the lithium modified ceramics, as can be seen in Figure 7.13, but it never exceeds 30% of the total piezoelectric response under the field amplitudes examined.

Figure 7.13: Irreversible contribution $(\alpha\sigma_0)/(d_0 + \alpha\sigma_0)$ during heating and cooling for $(K_{0.485}Na_{0.485}Li_{0.03})(Nb_{0.80}Ta_{0.20})O_3$ ceramics.
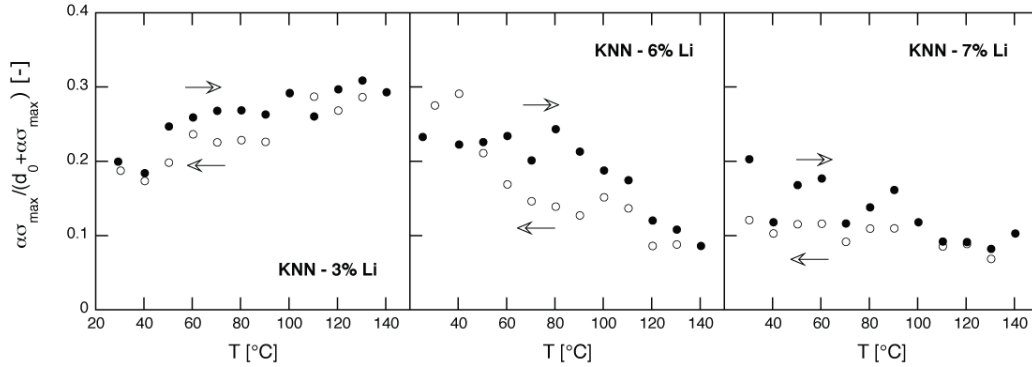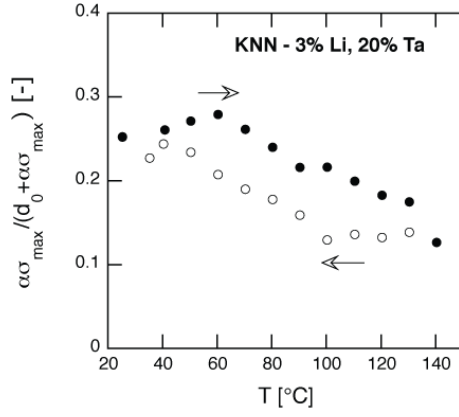
The irreversible contribution at different temperatures as a function of the lithium concentration is shown in Figure 7.14.
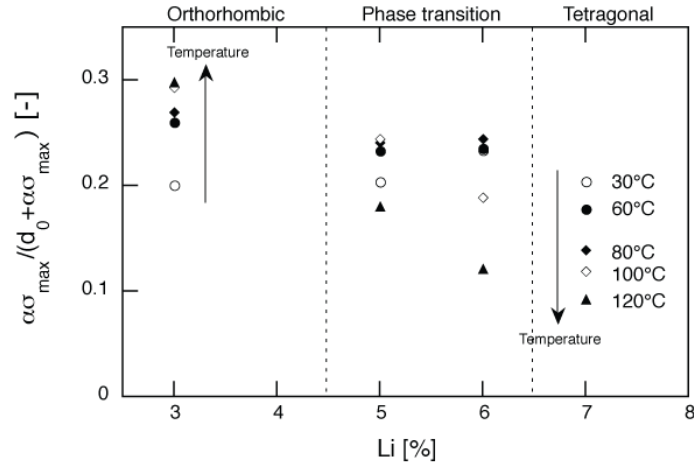

Figure 7.14: Irreversible contribution $(\alpha\sigma_0)/(d_0+\alpha\sigma_0)$ as a function of the lithium concentration at 30, 60, 80, 100 and 120 °C.

For orthorhombic ceramics, e.g. 3% lithium modified KNN, the irreversible extrinsic contribution increases with temperature, this behaviour being opposite for tetragonal ceramics (7% lithium modified KNN). For compositions going through a phase transition, the irreversible contribution is maximal at the phase transition. The behaviour of the ceramics not crossing a phase transition is nevertheless influenced by a transition situated at higher and lower temperatures for orthorhombic and tetragonal cases respectively.

The charge-stress hysteresis are explained in function of domain wall motion. Their surface increases with facility of domain wall motion, which can be due to thermal or phase transitional effects. Indeed, when approaching the phase transition, the energy barrier from orthorhombic to tetragonal is reduced, and as a consequence the domain wall structure is unstable, thus the domain walls can move easier. The thermal effects on the hysteresis loops depend on the material, for example the Curie temperature, or the proximity of a phase transition.
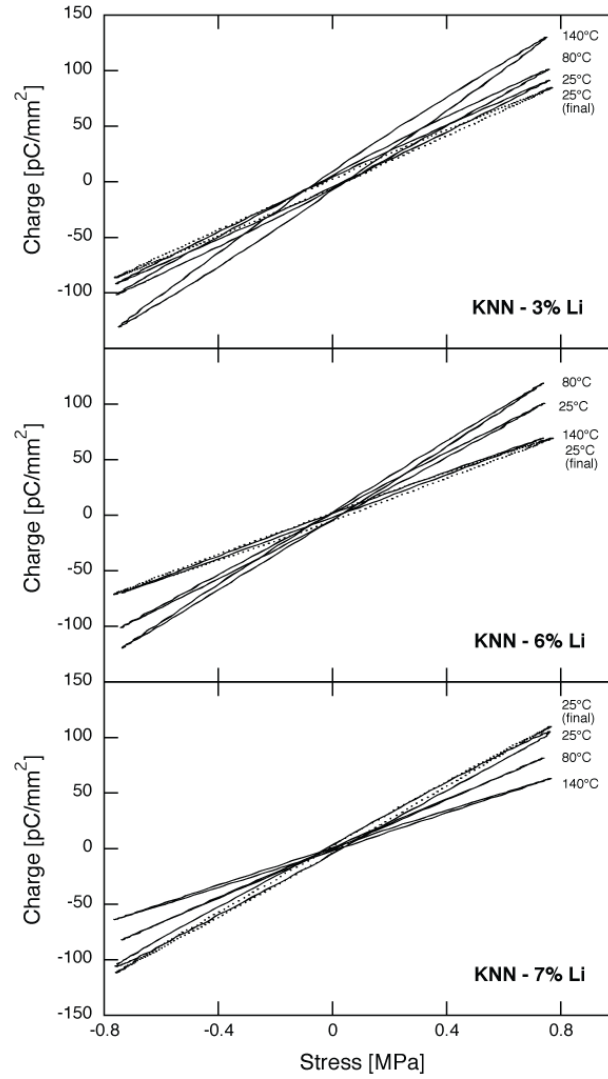
124

Figure 7.15: Evolution of the charge-stress hysteresis for 3,6 and 7% lithium modified ceramics, at 25 °C, 80 °C, 140 °C and 25 °C after the thermal cycle up to 140 °C, at 100 Hz.

During the evolution of the hystereses with temperature and in the case of the lithium modified ceramics (Figure 7.15), the charge becomes maximum at the phase transition and the surface of the hysteresis maximum, showing the phase transitional effects. Indeed, in 6% lithium modified ceramics, the hysteresis loop at high temperature (140 °C) is comparable to the room temperature loop. For 7% lithium modified ceramics and with increasing the temperature, i.e. moving away from the orthorhombic to tetragonal phase transition, the hysteresis loop becomes smaller. This is an indication of the small thermal effects and the more stable domain wall configuration in the tetragonal structure. This is due to the difficulty in the tetragonal structure to change the orientation of the spontaneous polarisation of a domain to an equivalent polarisation direction, for example from [001] to [010], as compared to the orthorhombic structure, from [101] to [011] (Figure 3.3).

7.2.2 Frequency dependence

The frequency dependence of the piezoelectric coefficient at low dynamic stresses is shown in Figures 7.16 and 7.17 for lithium, lithium and tantalum modified KNN ceramics, respectively.
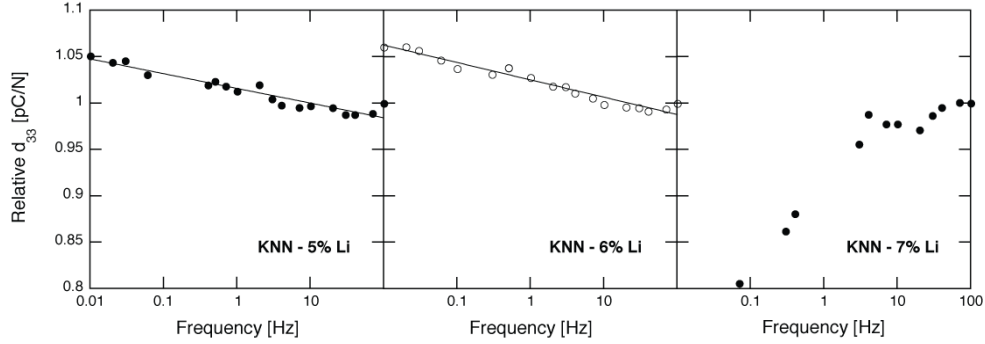

Figure 7.16: *Relative piezoelectric coefficients d_{33} as a function of the frequency for lithium (5, 6 and 7%) modified KNN ceramics, for an applied dynamic stress of 1 MPa and a static stress of 3 MPa. The initial values (at 100 Hz) of d_{33} are 130 (5%), 140 (6%), 140 pC/N (7%).*
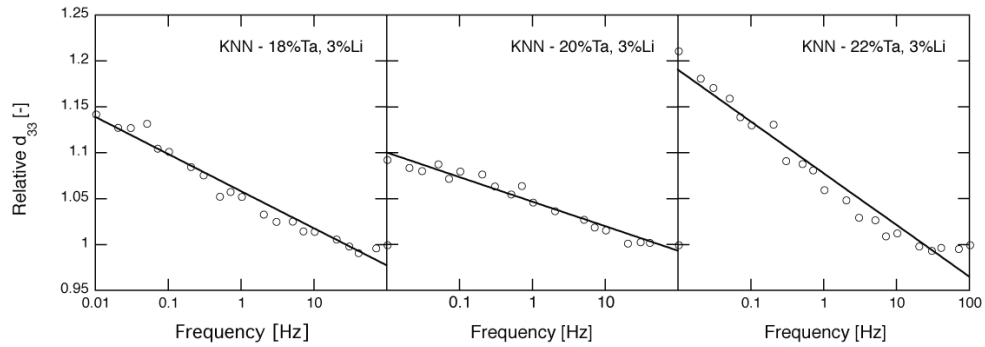
Figure 7.17: *Piezoelectric coefficients d_{33} as a function of the frequency for tantalum (18, 20 and 22%) with lithium (3%) modified KNN ceramics, for an applied dynamic stress of 1 MPa and a static stress of 3 MPa. The initial values (at 100 Hz) of d_{33} are 140 (18%), 195 (20%), 116 pC/N (22%).*

The increase of d_{33} as a function of the frequency is logarithmic except for the 7% lithium modified KNN ceramics. This logarithmic behaviour is characteristic of domain-wall pinning on random distributed defects [131] and is comparable to what is observed for soft PZT (Figure 7.1 b).

For 7% lithium modified KNN ceramics the piezoelectric coefficient d_{33} drops strongly at low frequencies. This behaviour at low frequencies has also been reported in $Bi_4Ti_3O_{12}$ ceramics (see Figure 7.18).

Figure 7.18: Piezoelectric coefficients d_{33} and $\tan\delta$ of a single phase $Bi_4Ti_3O_{12}$ ceramic with highly anisotropic grains. On the right-hand side, the charge-stress hysteresis loops are shown at selected frequencies, with clockwise hysteresis at 0.07 Hz and counterclockwise at 70 Hz [134].

In this highly anisotropic material in function of the frequency, the rotation of the hysteresis is inverted, indicating the presence of at least two dispersion processes, one dominant at low frequencies and the other at higher frequencies. This inversion of rotation direction is nevertheless not observed in the 7% lithium modified KNN ceramics, which is not due to measurements, as close and pointed loops have been recorded. As no other material has been reported to show such a behaviour, a more detailed analysis of the 7% lithium modified KNN ceramics should be performed at low frequencies.

7.2.3 Static stress effect

The effect of static stress for lithium, lithium and tantalum modified KNN ceramics is shown in Figure 7.19, for the compositions near the phase transition. The static stress first increases up to 20 MPa and then decreases down to the initial value of 2.5 MPa. A net decrease of the piezoelectric coefficient can be observed with an increasing static stress, as observed in the case of PZT [129] and by decreasing the stress, the initial values could not be recovered for most of the compositions.
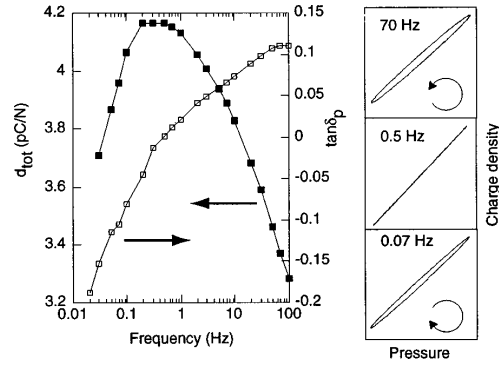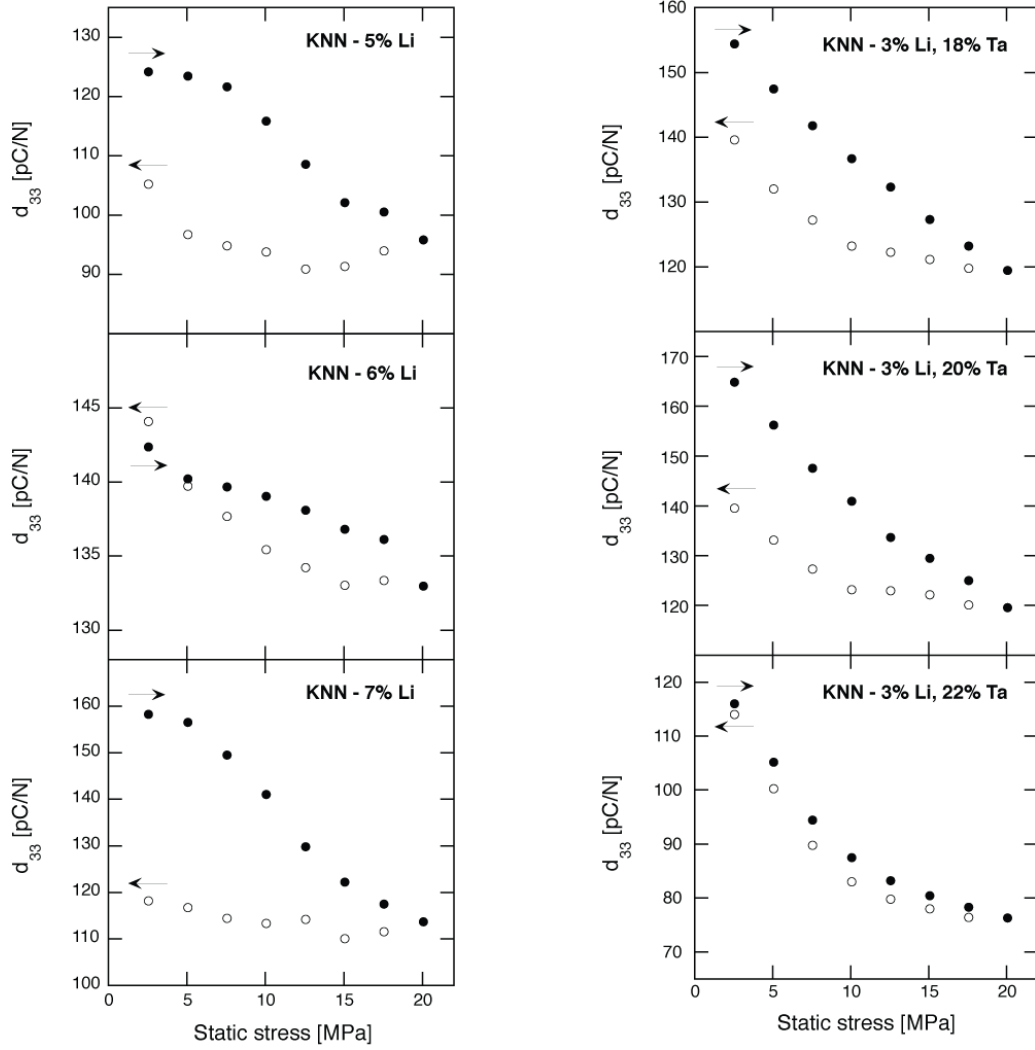
Figure 7.19: Piezoelectric coefficient d_{33} as a function of the static stress for lithium (5, 6 and 7%) and tantalum (18, 20 and 22%) with lithium (3%) modified KNN ceramics, which are around the MPB for an applied dynamic stress of 1 MPa and at 100 Hz. Static stress is first increased and then decreased. The initial values (at 2.5 MPa static stress) of d_{33} are for the lithium modified KNN ceramics, 124 (5% lithium), 142 (6% lithium), 158 pC/N (7% lithium) and for the lithium and tantalum modified ceramics 154 (18% tantalum), 170 (20% tantalum), 116 pC/N (22% tantalum).

This difference between the initial and the final piezoelectric coefficients is associated with a depolarisation for most of the compositions studied. This depolarisation is more pronounced for lithium modified KNN ceramics and is not recovering with time as reported for PMN-PT [77]. However, further cycling does not lead to further depolarisation, since the domain wall structure is stabilised. At high stresses, the domain walls are clamped, which can be observed in the hysteresis in Figure 7.20.

Figure 7.20: Charge-stress hysteresis at 2.5 and 20 MPa static stress, 100Hz and 1 MPa dynamic stress for a) $(K_{0.47}Na_{0.47}Li_{0.0b})NbO_3$ and b) $(K_{0.485}Na_{0.485}Li_{0.03})(Nb_{0.80}Ta_{0.20})O_3$ ceramics.

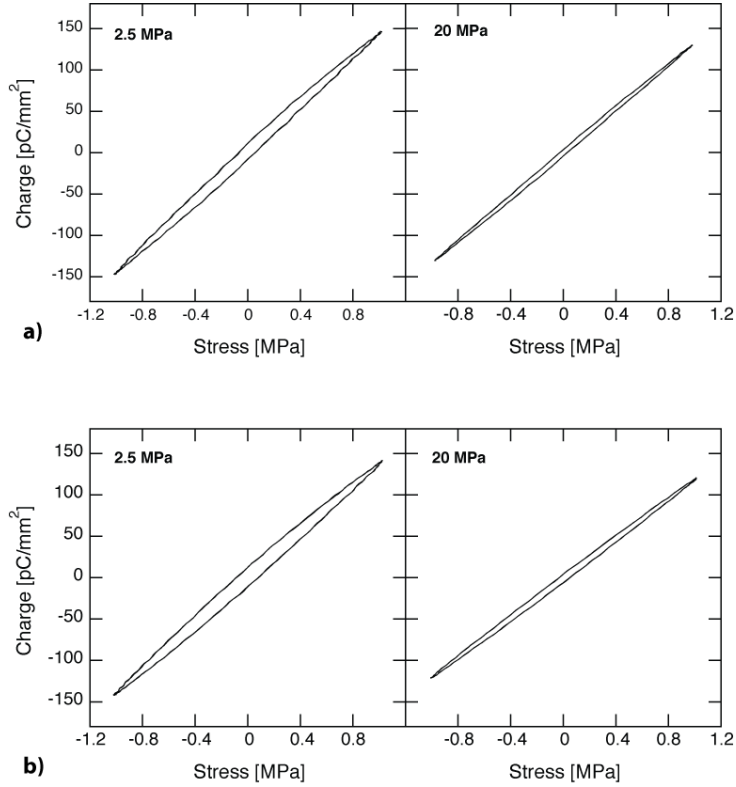The behaviour of better stability of lithium and tantalum modified KNN ceramics as a function of high static stress, along with their afore mentioned thermal and time stabilities, is clearly another improvement compared to other ceramics.

7.3   Conclusions

A Rayleigh-type behaviour was observed for the tetragonal and orthorhombic modified KNN ceramics and the Rayleigh coefficients were determined experimentally. The hysteretic behaviour of the charge as a function of dynamic stress was well fitted by this Rayleigh equation. The irreversible contribution of the piezoelectric effect could be deduced from the Rayleigh law and described as a function of composition and temperature.

At room temperature, the irreversible contribution of the modified KNN ceramics varies between 15 and 25% of the total response, which is slightly lower than for $BaTiO_3$ (35% for 3 MPa total charge and 25% for 6 MPa total charge) under similar experimental conditions, but significantly smaller than morphotropic PZT (40% for 10 MPa total charge).

For various compositions of PZT, the extrinsic contributions are maximal for near-MPB compositions, which is not the case for the modified KNN ceramics. Nevertheless, a maximum of the irreversible contribution at the temperature of the phase transition is observed and the irreversible contribution is higher in the orthorhombic structure. The increase of the irreversible contributions at temperatures of the phase transition can be related to the depolarisation observed in Chapter 6 and the nature of the phase transition

(thermally induced).

The frequency dependence of the modified KNN ceramics is similar to donor-doped PZT and is logarithmic. A different behaviour has been observed in the case of the 7% Li ceramics. The increase of d_{33} with the frequency remains unexplained as no other material has been reported to show a comparable behaviour.

In direct measurements, the modified KNN ceramics behave like soft materials (large charge-stress hysteresis), unlike in converse measurements. The modified KNN ceramics then behave as soft or hard materials depending on the measurement type.

Chapter 8

Conclusions and perspectives

Initially the aim of the thesis was the development of pure potassium sodium niobate ceramics and their complete characterisation including converse and especially direct measurements to understand the piezoelectric response. With the discovery of the new lead-free ceramics based on these KNN ceramics, the priorities moved to the characterisation of these new ceramics, which also arose new questions, principally about the study of the observed phase transition. The main results of this thesis work are the following:

- The processing, incorporating a second calcination and attrition milling instead of ball milling, led to high quality ceramics. The relative densities for modified KNN ceramics prepared during this work are higher than 94% and are obtained in a reproducible way. One essential point in the processing part is the importance of the initial powders, their purity and powder characteristics as for example particle size distribution and mean particle size. This is the principal limitation encountered in this work, since the initial powders revealed to be impossible to grind to submicron sizes, which causes secondary phases in the micron size observed with scanning electron microscope.

- It has long been believed that the potassium sodium based ceramics were moisture sensitive. In particular, most of the initial powders for the synthesis of potassium niobate based ceramics are hygroscopic. However, measurements as a function of time for three different humidities have shown that it is not the case for the lithium and tantalum modified KNN ceramics. The small decrease of the properties observed as a function of time is not related to the humidities. An important point for applications is that the electromechanical properties do not decrease with time, especially for the 3% lithium and 20% tantalum modified ceramics.

- Dielectric spectroscopy measurements were not reproducible due to electrical contact problems, but the qualitative trends are similar for all types of electrodes tested. At low frequencies, the dielectric response is characteristic of hopping charges conduction. As no quantitative measurements could be done, the nature of these charges is unknown, but possible carriers are oxygen vacancies or lithium atoms. To improve the electrical contact, a conductive layer as $SrRuO_3$ between the samples and the electrode could be tested.

- A fundamental question arises from the increase of the piezoelectric properties around the phase transition. Is this increase similar to what has been observed

for PZT, i.e. dependent on the composition or is it also thermally activated? The ferroelectric properties (hysteresis loops), have not been able to answer this question for the lithium and tantalum modified ceramics, as no significant increase of these properties has been noticed, either as a function of the temperature, or as a function of the composition. The phase transitions have been characterised by dielectric and piezoelectric measurements as a function of the composition and temperature, showing a marked temperature dependence, which is consistent with the presence of a thermally induced phase transition. In order to improve further the thermal stability of the properties of the ceramics, the phase transition should be shifted to higher or lower temperatures, for example by chemical modifications.

- High piezoelectric properties of near phase transition compositions have been obtained, with a maximal value of 310 pm/V for the 3% lithium and 20% tantalum modified ceramics. For tetragonal ceramics, the strain versus electric field response is nearly anhysteretic, which is comparable to hard PZT for example, but for the moment no chemical modifications lead to tunable properties from "hard" to "soft" as in PZT. The new KNN modified ceramics can either show a soft or hard behaviour depending on the measurements.

- The thermal stability is important from an application point of view, especially for the medical transducers. To prove the depolarisation of the samples, the electromechanical properties have been measured by the resonance technique. Successive cycling showed depoling for all the compositions, the amount depending on the composition. Nevertheless, after the second cycling, the properties stabilised. The best thermal stability was also shown by the lithium and tantalum modified KNN ceramics. For medical transducers, the thermal stability should be improved, as the reusable probes need to be sterilised.

- The piezoelectric response has been analysed using a house-made press. The dynamic and static stresses, as well as the frequency and temperature of measurement have been modified. The extrinsic and intrinsic contributions have been calculated from the Rayleigh equations. The irreversible extrinsic contributions never exceeded 30% under the driving fields used and are highest near the phase transition.

In the last three years, a tremendous effort focused firstly on the design of new lead-free ceramics compositions, which was essentially triggered by the discovery of the modified KNN ceramics by Saito and co-workers. Secondly, the optimisation of the processing of the new compositions was attempted despite of the difficulties met for potassium niobate based ceramics. Finally, a thorough determination of the properties of the new materials was carried out. Due to this development, the lead-free ceramics are nowadays not only promising materials for medical applications, but also for any kind of applications, as their piezoelectric properties are close to those of lead-based ceramics.

Bibliography

[1] B. Jaffe, W. R. Cook, and H. Jaffe. *Piezoelectric Ceramics*. Academic Press, New York, 1971.

[2] B. Jaffe, R.S. Roth, and S. Marzullo. Piezoelectric Properties of Lead Zirconate-Lead Titanate Solid-Solution Ceramics. *J. Appl. Phys.*, 25(6):809–810, 1954.

[3] E. Ringgaard and T. Wurlitzer. Lead-free piezoeceramics based on alkali niobates. *J. Europ. Ceram. Soc.*, 25(12):2701–2706, 2005.

[4] S.-E. Park and T. R. Shrout. Ultrahigh strain and piezoelectric behavior in relaxor based ferroelectric single crystals. *J. Appl. Phys.*, 4(15):1804–1811, 1997.

[5] B. Noheda, D. E. Cox, G. Shirane, J. A. Gonzalo, L. E. Cross, and S.-E. Park. A monoclinic ferroelectric phase in the $Pb(Zr_{1-x}Ti_x)O_3$ solid solution. *Appl. Phys. Lett.*, 74(14):2059–2061, 1999.

[6] R. Guo, L. E. Cross, S.-E. Park, B. Noheda, D. E. Cox, and G. Shirane. Origin of the high piezoelectric response in $PbZr_{1-x}Ti_xO_3$. *Phys. Rev. Lett.*, 84(23):5423–5426, 2000.

[7] B. Noheda, D.E. Cox, G. Shirane, R. Guo, B. Jones, and L.E. Cross. Stability of the monoclinic phase in the ferroelectric perovskite $PbZr_{1-x}Ti_xO3$. *Phys. Rev. B: Condens. Matter*, 63(1):014103, 2001.

[8] S.-E. Park and T. R. Shrout. Relaxor based ferroelectric single crystals for electro-mechanical actuators. *Mat. Res. Innovat.*, 1(1):20–25, 1997.

[9] S.-E. Park and T. R. Shrout. Characteristics of Relaxor-Based Piezoelectric Single Crystals for Ultrasonic Transducers. *IEEE Transactions on Ultrasonics, Ferroelectrics, and Frequency Control*, 44(5):1140–1147, 1997.

[10] A. J. Moulson and J. M. Herbert. *Electroceramics*. Chapman and Hall, 1997.

[11] *www.ferroperm-piezo.com*.

[12] *http://www.faqs.org/health/Sick-V3/Lead-Poisoning.html*.

[13] D. Damjanovic. Materials for high temperature piezoelectric transducers. *Curr. Opin. Solid State Mater. Sci.*, 3(5):469–473, 1998.

[14] H.S. Shulman, M. Testorf, D. Damjanovic, and N. Setter. Microstructure, Electrical Conductivity, and Piezoelectric Properties of Bismuth Titanate. *J. Am. Ceram. Soc.*, 79(12):3124–3128, 1996.

[15] T. Takeuchi, T. Tani, and Y. Saito. Piezoelectric Properties of Bismuth Layer-Structured Ferroelectric Ceramics with a Preferred Orientation Processed by the Reactive Templated Grain Growth Method. *Jpn. J. Appl. Phys. Part 1*, 38(9B):5553–5556, 1999.

[16] H. Takahashi, Y. Numamoto, J. Tani, and K. Matsuta. Lead-Free Barium Titanate Ceramics with Large Piezoelectric Constant Fabricated by Microwave Sintering. *Jpn. J. Appl. Phys. Part 1*, 45(1):L30–L32, 2006.

[17] *http://www.nature.com/news/2000/000413/full/000413-7.html*.

[18] G. A. Smolensky, V. A. Isupov, and A. I. Agranovskaya. *Soviet Physics. Solid State*, 1961.

[19] Y. Hiruma, R. Aoyagi, H. Nagata, and T. Takenaka. Ferroelectric and Piezoelectric Properties of $(Bi_{0.5}K_{0.5})TiO_3$ Ceramics. *Jpn. J. Appl. Phys. Part 1*, 44(7A):5040–5044, 2005.

[20] A. Sasaki, T. Chiba, Y. Mamiya, and E. Otsuki. Dielectric and Piezoelectric Properties of $(Bi_{0.5}Na_{0.5})TiO_3$-$(Bi_{0.5}K_{0.5})TiO_3$ Systems. *Jpn. J. Appl. Phys. Part 1*, 38(9B):5564–5567, 1999.

[21] Q. Xu, S. Chen, W. Chen, S. Wu, J. Zhou, H. Sun, and Y. Li. Synthesis and piezoelectric and ferroelectric properties of $(Na_{0.5}Bi_{0.5})_{1-x}Ba_xTiO_3$ ceramics. *Mater. Chem. Phys.*, 90(1):111–115, 2005.

[22] H. Yilmaz, G. L. Messing, and S. Trolier-McKinstry. (Reactive) Templated Grain Growth of Textured Sodium Bismuth Titanate $(Na_{1/2}Bi_{1/2}TiO_3$-$BaTiO_3)$ Ceramics - I Processing. *J. Electroceram.*, 11(3):207–215, 2003.

[23] H. Yilmaz, S. Trolier-McKinstry, and G. L. Messing. (Reactive) Templated Grain Growth of Textured Sodium Bismuth Titanate $(Na_{1/2}Bi_{1/2}TiO_3$-$BaTiO_3)$ Ceramics - II Dielectric and Piezoelectric Properties. *J. Electroceram.*, 11(3):217–226, 2003.

[24] H. Nagata, M. Yoshida, Y. Makiuchi, and T. Takenaka. Large Piezoelectric Constant and High Curie Temperature of Lead-Free Piezoelectric Ceramics Ternary System Based on Bismuth Sodium Titanate-Bismuth Potassium Titanate-Barium Titanate near the Morphotropic Phase Boundary. *Jpn. J. Appl. Phys. Part 1*, 42(12):7401–7403, 2003.

[25] D. Lin, D. Xiao, J. Zhu, and P. Yu. Piezoelectric and ferroelectric properties of $[Bi_{0.5}(Na_{1-x-y}K_xLi_y)_{0.5}]TiO_3$ lead-free piezoelectric ceramics. *Appl. Phys. Lett.*, 88(6):062901, 2006.

[26] B. T. Matthias and J. P. Remeika. Dielectric Properties of Sodium and Potassium Niobates. *Phys. Rev.*, 82(5):727–729, 1951.

[27] G. Shirane, R. Newnham, and R. Pepinsky. Dielectric Properties and Phase Transitions of $NaNbO_3$ and $(Na, K)NbO_3$. *Phys. Rev.*, 96(3):581–588, 1954.

[28] K. Nakamura and Y. Kawamura. Orientation Dependance of Electromechanical Coupling Factors in $KNbO_3$. *IEEE Transactions on Ultrasonics, Ferroelectrics, and Frequency Control*, 47(3):750–755, 2000.

[29] S. Wada, A. Seike, and T. Tsurumi. Poling Treatment and Piezoelectric Properties of Potassium Niobate Ferroelectric Single Crystals. *Jpn. J. Appl. Phys. Part 1*, 40(9B):5690–5697, 2001.

[30] K. Nakamura, T. Tokiwa, and Y. Kawamura. Domain structures in $KNbO_3$ crystals and their piezoelectric properties. *J. Appl. Phys.*, 91(11):9272–9276, 2002.

[31] A. Reisman and F. Holtzberg. Phase Equilibria in the System K_2CO_3-Nb_2O_5 by the Method of Differential Thermal Analysis. *J. Am. Chem. Soc.*, 77(8):2115–2119, 1955.

[32] K. Kodaira, J. Shioya, S. Shimada, and T. Matsushita. Sintering and dielectric properties of $KNbO_3$. *J. Mater. Sci. Lett.*, 1(7):277–278, 1982.

[33] P.Vousden. A Study of the Unit-cell Dimensions and Symmetry of certain Ferroelectric Compounds of Niobium and Tantalum at Room Temperature. *Acta Cryst.*, 4(373-376), 1951.

[34] A. Reisman, F. Holtzberg, S. Triebwasser, and M. Berkenblit. Preparation of Pure Potassium Metaniobate. *J. Am. Chem. Soc.*, 78:719–720, 1956.

[35] U. Flückiger, H. Arend, and H. Oswald. Synthesis of $KNbO_3$ Powder. *J. Am. Ceram. Soc.*, 56(6):575–577, 1977.

[36] S.D. Phatak, E.C. Subbarao, and R.C. Srivasta. Elastic-constants of orthorhombic $KNbO_3$ by X-Ray diffuse scattering. *Acta Cryst.*, 28(3):227–231, 1972.

[37] K. Kakimoto, I. Masuda, and H. Ohsato. Solid-Solution Structure and Piezoelectric Property of $KNbO_3$ Ceramics Doped with Small Amounts of Elements. *Jpn. J. Appl. Phys. Part 1*, 43(9B):6706–6710, 2004.

[38] K. Kakimoto, I. Masuda, and H. Ohsato. Lead-free $KNbO_3$ piezoceramics synthesized by pressure-less sintering. *J. Europ. Ceram. Soc.*, 25(12):2719–2722, 2005.

[39] K. Kakimoto, I. Masuda, and H. Ohsato. Ferroelectric and Piezoelectric Properties of $KNbO_3$ Ceramics Containing Small Amounts of $LaFeO_3$. *Jpn. J. Appl. Phys. Part 1*, 42(9B):6102–6105, 2003.

[40] M. Ichiki, L. Zhang, M. Tanaka, and R. Maeda. Electrical properties of piezoelectric sodium-potassium niobate. *J. Europ. Ceram. Soc.*, 24(6):1693–1697, 2004.

[41] A. Reisman and E. Banks. Reactions of the Group VB Pentoxides. VIII. Thermal, Density and X-Ray Studies of the Systems $KNbO_3$-$NaNbO_3$ and $KTaO_3$-$KNbO_3$. *J. Am. Chem. Soc.*, 80(8):1877–1882, 1958.

[42] L. Egerton and D. M. Dillon. Piezoelectric and Dielectric Properties of Ceramics in the System Potassium-Sodium Niobate. *J. Am. Ceram. Soc.*, 42(9):438–442, 1959.

[43] B.-P. Zhang, J.-F. Li, K. Wang, and H. Zhang. Compositional Dependence of Piezoelectric Properties in $Na_xK_{1-x}NbO_3$ Lead-Free Ceramics Prepared by Spark Plasma Sintering. *J. Am. Ceram. Soc.*, 89(5):1605–1609, 2006.

[44] G. Shirane, H. Danner, A. Pavlovic, and R. Pepinsky. Phase Transitions in Ferroelectric $KNbO_3$. *Phys. Rev.*, 93(4):672–673, 1954.

[45] R. E. Jaeger and L. Egerton. Hot Pressing of Potassium-Sodium Niobates. *J. Am. Ceram. Soc.*, 45(5):209–213, 1962.

[46] M. Kosec and D. Kolar. On activated sintering and electrical properties of $NaKNbO_3$. *Mat. Res. Bull.*, 10(5):335–340, 1975.

[47] H. Birol, D. Damjanovic, and N. Setter. Preparation and characterization of $(K_{0.5}Na_{0.5})NbO_3$ ceramics. *J. Europ. Ceram. Soc.*, 26(6):861–866, 2006.

[48] M. Matsubara, T. Yamaguchi, W. Sakamoto, K. Kikuta, T. Yogo, and S.-I. Hirano. Processing and Piezoelectric Properties of Lead-Free $(K,Na)(Nb,Ta)O_3$ Ceramics. *J. Am. Ceram. Soc.*, 88(5):1190–1196, 2005.

[49] Z. S. Ahn and W. A. Schulze. Conventionally Sintered $(Na_{0.5},K_{0.5})NbO_3$ with Barium Additions. *J. Am. Ceram. Soc.*, 70(1):C18–C21, 1987.

[50] S.-H. Park, C.-W. Ahn, S. Nahm, and J.-S. Song. Microstructure and Piezoelectric Properties of ZnO-added $(Na_{0.5}K_{0.5})NbO_3$ Ceramics. *Jpn. J. Appl. Phys. Part 1*, 43(8B):1072–1074, 2004.

[51] B. Malic, J. Bernard, J. Holc, D. Jenko, and M. Kosec. Alkaline-earth doping in $(K,Na)NbO_3$ based piezoceramics. *J. Europ. Ceram. Soc.*, 25(12):2707–2711, 2005.

[52] M. Matsubara, T. Yamaguchi, K. Kikuta, and S. Hirano. Sinterability and Piezoelectric Properties of $(K,Na)NbO_3$ Ceramics with Novel Sintering Aid. *Jpn. J. Appl. Phys. Part 1*, 43(10):7159–7163, 2004.

[53] M. Matsubara and K. Kikuta ans S. Hirano. Sintering and Piezoelectric Properties of Potassium Sodium Niobate Ceramics with Newly Developed Sintering Aid. *Jpn. J. Appl. Phys. Part 1*, 44(1A):258–263, 2005.

[54] G. Feuillard, V. Loyau, L.P. Tran Huu Hue, T. Wurlitzer, E. Ringgaard, W. Wolny, B. Malic, M. Kosec, A. Barzegar, D. Damjanovic, and M. Lethiecq. Comparative performances of new KNN lead-free piezoelectric materials and classical lead-based ceramics for ultrasonic transdicer applications. *IEEE Ultasonics Symposium*, 2:1995–1998, 2003.

[55] Y. Saito, H. Takao, T. Tani, T. Nonoyama, K. Takatori, T. Homma, T. Nagaya, and M. Nakamura. Lead-free piezoceramics. *Nature*, 432(7013):84–87, 2004.

[56] T. Nonoyama, T. Nagaya, Y. Saito, K. Takatori, H. Takao, and T. Homma. Piezoelectric ceramics composition and method of production of same, piezoelectric element, and dielectric element. *United States Patent*, (US 2004/0058797 A1), 2004.

[57] Y. Guo, K. Kakimoto, and H. Ohsato. Phase transitional behavior and piezoelectric properties of $(Na_{0.5}K_{0.5})NbO_3$-$LiNbO_3$ ceramics. *Appl. Phys. Lett.*, 85(15):4121–4123, 2004.

[58] Y. Guo, K. Kakimoto, and H. Ohsato. $(Na_{0.5}K_{0.5})NbO_3$-$LiTaO_3$ lead-free piezoelectric ceramics. *Mater. Lett.*, 59(2-3):241–244, 2005.

[59] G.-Z. Zang, J.-F. Wang, H.-C. Chen, W.-B. Su, C.-M. Wang, P. Qi, B.-Q. Ming, J. Du, and L.-M. Zheng. Perovskite $(Na_{0.5}K_{0.5})_{1-x}(LiSb)_xNb_{1-x}O_3$ lead-free piezoceramics. *Appl. Phys. Lett.*, 88(21), 2006.

[60] S.J. Zhang, R. Xia, T. R. Shrout, G.Z. Zang, and J.F. Wang. Piezoelectric properties in perovskite $0.948(K_{0.5}Na_{0.5})NbO_3$-$0.052LiSbO_3$ lead-free ceramics. *J. Appl. Phys.*, 100(10):104108, 2006.

[61] Y. Guo, K. Kakimoto, and H. Ohsato. Structure and Electrical Properties of Lead-Free $(Na_{0.5}K_{0.5})NbO_3$-$BaTiO_3$ Ceramics. *Jpn. J. Appl. Phys. Part 1*, 43(9B):6662–6666, 2004.

[62] V. Bobnar, J. Bernard, and M. Kosec. Relaxorlike dielectric properties and history-dependent effects in the lead-free $K_{0.5}Na_{0.5}NbO_3$ -$SrTiO_3$ ceramic system. *Appl. Phys. Lett.*, 85(6):994–996, 2004.

[63] Y. Guo, K. Kakimoto, and H. Ohsato. Dielectric and piezoelectric properties of lead-free $(Na_{0.5}K_{0.5})NbO_3$-$SrTiO_3$ ceramics. *Solid State Commun.*, 129(5):279–284, 2004.

[64] M. Kosec, V. Bobnar, M. Hrovat, J. Bernard, B. Malic, and J. Holc. New lead-free relaxors based on the $K_{0.5}Na_{0.5}NbO_3$-$SrTiO_3$ solid solution. *J. Mater. Res*, 19(6):1849–1854, 2004.

[65] R. Wang, R.-J. Xie, K. Hanada, K. Matsusaki, H. Bando, and M. Itoh. Phase diagram and enhanced piezoelectricity in the strontium titanate doped potassium-sodium niobate solid solution. *Phys. Stat. Sol*, 202(6):R57–R59, 2005.

[66] M. Matsubara, K. Kikuta, and S. Hirano. Piezoelectric properties of $(K_{0.5}Na_{0.5})(Nb_{1-x}Ta_x)O_3$-$K_{5.4}CuTa_{10}O_9$ ceramics. *J. Appl. Phys.*, 97(11):114105, 2005.

[67] M. Matsubara, T. Yamaguchi, K. Kikuta, and S. Hirano. Synthesis and characterization of (K0.5Na0.5)(Nb0.7Ta0.3)O-3 piezoelectric ceramics sintered with sintering aid K5.4Cu1.3Ta10O29. *Jpn. J. Appl. Phys. Part 1*, 44(9A):6618–6623, 2005.

[68] Lithium carbonate, International Chemical Safety Card, 1999.

[69] *http://www.answers.com/topic/tantalum.*

[70] P. Bowen. Particle Size Distribution Measurement from Millimeters to Nanometers an from Rod to Platelets. *J. Dispersion Sci. Technol.*, 23(5):631–662, 2002.

[71] *http://www.malvern.co.uk/LabEng/products/Mastersizer/.*

[72] *Handbook of Chemistry and Physics, 75th Edition.* CRC Press, 1995.

[73] C. F. Bohren and D. R. Huffman. *Absorption and Scattering of Light by Small Particles.* Wiley, New York, 1983.

[74] Y. Xu. *Ferroelectric Materials and Their Applications.* North-Holland, Elsevier Science Publishers B.V., 1991.

[75] J.F. Nye. *Physical Properties of Crystals.* Clarendon Press, Oxford, 1992.

[76] A. Barzegar, D. Damjanovic, and N. Setter. The Effect of Boundary Conditions and Sample Aspect Ratio on Apparent d_{33} Piezoelectric Coefficient Determined by Direct Quasistatic Method. *IEEE Transactions on Ultrasonics, Ferroelectrics, and Frequency Control,* 51(3):262–270, 2004.

[77] M. Davis. *Phase transitions, anisotropy and domain engineering: the piezoelectric properties of relaxor-ferroelectric single crystals.* PhD thesis, Ecole Polytechnique Fédérale de Lausanne, 2006.

[78] *IEEE Standard on Piezoelectricity.* The Institute of Electrical and Electronics Engineers, New York, 1988.

[79] A. Barzegar, D. Damjanovic, and N. Setter. Study of size (aspect ratio) effect on longitudinal piezoelectric coefficient measured by quasistatic technique. *Ultasonics Symposium, 2002 Proceedings,* 2:1185–1188, 2002.

[80] P. Vousden. A Study of the Unit-cell Dimensions and Symmetry of certain Ferroelectric Compounds of Niobium and Tantalum at Room Temperature. *Acta Cryst.,* 4(4):373–376, 1951.

[81] M. M. Schwartz. *Handbook of structural ceramics.* McGraw-Hill, Inc, 1991.

[82] J. S. Reed. *Principles of Ceramics Processing, Second Edition.* Wiley, New York, 1995.

[83] M. Matsubara, T. Yamaguchi, K. Kikuta, and S. Hirano. Effect of Li Substitution on the Piezoelectric Properties of Potassium Sodium Niobate Ceramics. *Jpn. J. Appl. Phys. Part 1,* 44(8):6136–6142, 2005.

[84] V.J. Tennery and K.W. Hang. Thermal and X-Ray Diffraction Studies of the $NaNbO_3$-$KNbO_3$ System. *J. Appl. Phys.,* 39(10):4749–4753, 1968.

[85] Y. Saito and H. Takao. High Performance Lead-free Piezoelectric Ceramics in the $(K,Na)NbO_3$-$LiTaO_3$ Solid Solution System. *Ferroelectrics,* 338:17–32, 2006.

[86] E. Hollenstein, M. Davis, D. Damjanovic, and N. Setter. Piezoelectric properties of Li- and Ta-modified $(K_{0.5}Na_{0.5})NbO_3$ ceramics. *Appl. Phys. Lett.,* 87(18), 2005.

[87] T.R. Gururaja and R.K. Panda. Current status and future trends in ultrasonic transducers for medical imaging applications. *Proceedings of the Eleventh IEEE International Symposium on Applications of Ferroelectrics,* pages 223–228, 1988.

[88] K. Nakamura and Y. Kawamura. Electromechanical coupling factor of $KNbO_3$ single crystal. *Processing of the Ultrasonic Symposium*, 2:013–1018, 1999.

[89] V. Lingwal, B.S. Semwal, and N.S. Panwar. Dielectric properties of $Na_{1-x}K_xNbO_3$ in orthorhombic phase. *Bull. Mater. Sci.*, 26(6):619–625, 2003.

[90] H. Birol, D. Damjanovic, and N. Setter. Preparation and Characterization of $KNbO_3$ Ceramics. *J. Am. Ceram. Soc.*, 88(7):1754–1759, 2005.

[91] B. Sundarakannan, K. Kakimoto, and H. Ohsato. Frequency and temperature dependent dielectric and conductivity behavior of $KNbO_3$ ceramics. *J. Appl. Phys.*, 94(8):5182–5187, 2003.

[92] P. Dubernet and J. Ravez. Dielectric study of $KNbO_3$ ceramics over a large range of frequency (100Hz-1GHz) and temperature (300-800 °K). *Ferroelectrics*, 211(1-4):51–66, 1998.

[93] N.M. Kari, T.A. Ritter, S.E. Park, T.R. Shrout, and K.K. Shung. Investigation of potassium niobate as an ultrasonic transducer material. *IEEE Ultasonics Symposium*, 2:1065–1068, 2000.

[94] M. Demartin and D. Damjanovic. Dependance of the direct piezoelectric effect in coarse and fine grain barium titanate ceramics on dynamic and static stress. *Appl. Phys. Lett.*, 68(21):3046–3048, 1996.

[95] Z. Yang, Y. Chang, and L. Wei. Phase transitional behavior and electrical properties of lead-free $(K_{0.44}Na_{0.52}Li_{0.04})(Nb_{0.96-x}Ta_xSb_{0.04})O_3$ piezoelectric ceramics. *Appl. Phys. Lett.*, 90(4):042911, 2007.

[96] A.K. Jonscher. *Dielectric relaxation in solids.* Chelsea Dielectrics Press, London, 1983.

[97] M. Morozov. *Softening and Hardening Transitions in Ferroelectric Pb(Zr,Ti)O₃ Ceramics.* PhD thesis, Ecole Polytechnique Fédérale de Lausanne, 2005.

[98] Z. Yang, Y. Chang, B. Liu, and L. Wei. Effects of composition on phase structure, microstructure and electrical properties of $(K_{0.5}Na_{0.5})NbO_3$-$LiSbO_3$ ceramics. *Mater. Sci. Eng., A*, 432(1-2):292–298, 2006.

[99] K. Singh, S.C. Bhatt V. Lingwal, and N.S. Panwar. Dielectric properties of potassium niobate mixed system. *Mater. Res. Bull.*, 36:2365–2374, 2001.

[100] K. Singh, V. Lingwal, S.C. Bhatt, and N.S. Panwar. Dielectric properties of potassium sodium niobate mixed system. *Mater. Res. Bull.*, 36(13-14):2365–2374, 2001.

[101] W.P. Mason. Aging of the Properties of Barium Titanate and Related Ferroelectric Ceramics. *J. Acoust. Soc. Am.*, 27(1):73–85, 1955.

[102] Y. Xu. *Ferroelectric and Piezoelectric Materials.* Science Press, Beijing, 1978.

[103] H.X. Fu and R.E. Cohen. Polarization rotation mechanism for ultrahigh electromechanical response in single-crystal piezoelectrics. *Nature*, 403(6767):281–283, 2000.

[104] D. Damjanovic. Contributions to the Piezoelectric Effect in Ferroelectric Single Crystals and Ceramics. *J. Am. Ceram. Soc.*, 88(10):2663–2676, 2005.

[105] D.E. Cox, B. Noheda, G. Shirane, Y. Uesu, K. Fujishiro, and Y. Yamada. Universal phase diagram for high-piezoelectric perovskite systems. *Appl. Phys. Lett.*, 79(3):400–402, 2001.

[106] S. Wada, S. Suzuki, T. Noma, T. Suzuki, M. Osada, M. Kakihana, S.E. Park, L.E. Cross, and T.R. Shrout. Enhanced Piezoelectric Property of Barium Titanate Single Crystals with Engineered Domain Configuration. *Jpn. J. Appl. Phys. Part 1*, 38(9B):5505–551, 1999.

[107] D. Damjanovic, F. Brem, and N. Setter. Crystal orientation dependance of the piezoelectric d_{33} coefficient in tetragonal BaTiO$_3$ as a function of temperature. *Appl. Phys. Lett.*, 80(4):652–654, 2002.

[108] D. Damjanovic. Ferroelectric, dielectric and piezoelectric properties of ferroelectric thin films and ceramics. *Rep. Prog. Phys.*, 61(9):1267–1324, 1998.

[109] M. Budimir, D. Damjanovic, and N. Setter. Piezoelectric anisotropy-phase transition relations in perovskite single crystals. *J. Appl. Phys.*, 94(10):6753–6761, 2003.

[110] Y. Ishibashi and M. Iwata. Morphotropic Phase Boundary in Solid Solution Systems of Perovskite-Type Oxide Ferroelectrics. *Jpn. J. Appl. Phys. Part 2*, 37(8B):L985–L987, 1998.

[111] M. Iwata and Y. Ishibashi. Theory of Morphotropic Phase Boundary in Solid Solution Systems of Perovskite-Type Oxide Ferroelectrics p-e Hysteresis Loop. *Jpn. J. Appl. Phys. Part 1*, 38(9B):5670–5673, 1999.

[112] T. Yamamoto. Ferroelectric Properties of the PbZrO$_3$-PbTiO$_3$ System. *Jpn. J. Appl. Phys. Part 1*, 35(9B):5104–5108, 1996.

[113] S. Triebwasser. Behavior of Ferroelectric KNbO$_3$ in the Vicinity of the Cubic-Tetragonal Transition. *Phys. Rev.*, 101(3):993–998, 1956.

[114] H.H. Wieder. Electrical Bahavior of Barium Titanate Single Crystals at Low Temperatures. *Phys. Rev.*, 99(4):1161–1165, 1955.

[115] W.J. Merz. Double Hysteresis Loop of BaTiO$_3$ at the Curie Point. *Phys. Rev.*, 91(3):513–517, 1953.

[116] N. Klein, E. Hollenstein, D. Damjanovic, H.J. Trodahl, N. Setter, and M. Kuball. Phase diagram of (K,Na,Li)NbO$_3$ determined by dielectric and piezoelectric measurements, and Raman spectroscopy. *J. Appl. Phys.*, submitted, 2007.

[117] D.E. Dausch. Ferroelectric Polarization Fatigue in PZT-Based RAINBOWs and Bulk Ceramics. *J. Am. Ceram. Soc.*, 80(9):2355–2360, 1997.

[118] A. Levstik, V. Bobnar, Z. Kutnjak, and M. Kosec. Fatigue and piezoelectric properties of lead lanthanum zirconate titanate ceramics. *J. Phys. D: Appl. Phys.*, 31(20):2894–2897, 1998.

[119] M. Davis, N. Klein, D. Damjanovic, N. Setter, A. Gross, V. Wesemann, S. Vernay, and D. Rytz. Large and stable thickness coupling coefficients of $[001]_c$-oriented $KNbO_3$ and Li-modified $(K,Na)NbO_3$ single crystals. *Appl. Phys. Lett.*, 90(6):062904, 2007.

[120] D. Damjanovic. Stress and frequency dependance of the direct piezoelectric effect in ferroelectric ceramics. *J. Appl. Phys.*, 82(4):1788–1797, 1997.

[121] Q.M. Zhang, H. Wang, N. Kim, and L.E. Cross. Direct evaluation of domain-wall and intrinsic contributions to the dielectric and piezoelectric response and their temperature dependance on lead zirconate-titanate ceramics. *J. Appl. Phys.*, 75(1):454–459, 1994.

[122] E.I. Bondarenko, V.Y. topolov, and A.V. Turik. The role of 90 degree domain wall displacement in forming physical properties of perovskite ferroelectric ceramics. *Ferroelectr. Lett.*, 13:13–19, 1991.

[123] S. Li, W. Cao, and L.E. Cross. The extrinsic nature of nonlinear behavior observed in lead zirconate titanate ferroelectric ceramic. *J. Appl. Phys.*, 69(10):7219–7224, 1991.

[124] Q.M. Zhang, W.Y. Pan, S.J. Jang, and L.E. Cross. Domain wall excitations and their contributions to the weak-signal response of doped lead zirconate titanate ceramics. *J. Appl. Phys.*, 64(11):6445–6451, 1988.

[125] G. Arlt and A. Pertsev. Force constant and effective mass of 90 degrees domain walls in ferroelectric ceramics. *J. Appl. Phys.*, 70(4):2283–2289, 1991.

[126] V. Mueller and Q.M. Zhang. Nonlinearity and scaling behavior in donor-doped lead zirconate titanate piezoceramic. *Appl. Phys. Lett.*, 72(21):2692–2694, 1998.

[127] D. Damjanovic and M. Demartin. The Rayleigh law in piezoelectric ceramics. *J. Phys. D: Appl. Phys.*, 29(7):2057–2060, 1996.

[128] M. Davis, D. Damjanovic, and N. Setter. Temperature dependance of the direct piezoelectric effect in relaxor-ferroelectric single crystals: Intrinsic and extrinsic contributions. *J. Appl. Phys.*, 100(8):084103, 2006.

[129] D. Damjanovic and M. Demartin. Contribution of the irreversible displacement of domain walls to the piezoelectric effect in barium titanate and lead zirconate titanate ceramics. *J. Phys. Condens. Matter.*, 9(23):4943–4953, 1997.

[130] D. Damjanovic and G. Robert. Piezoelectric Nonlinearity and Hysteresis in Ferroelectric Materials. Piezoelectric materials for the end user (Conference Notes).

[131] D. Damjanovic. Logarithmic frequency dependance of the piezoelectric effect due to pinning of ferroelectric-ferroelastic domain walls. *Phys. Rev. B: Condens. Matter*, 55(2):R649–R652, 1997.

[132] D. Damjanovic, S.S.N. Bharadwaja, and N. Setter. Toward a unified description of nonlinearity and frequency dispersion of piezoelectric and dielectric responses in $Pb(Zr,Ti)O_3$. *Mater. Sci. Eng., B*, 120(1-3):170–174, 2005.

[133] D. Damjanovic, M. Demartin, F. Chu, and N. Setter. Practical consequences of the extrinsic contributions to the properties of piezoelectric sensors and actuators. *Proceedings of the Tenth IEEE International Symposium on Applications of Ferroelectrics*, 1:251 – 257, 1996.

[134] D. Damjanovic, M. D. Maeder, P. D. Martin, C. Voisard, and N. Setter. Maxwell-Wagner piezoelectric relaxation in ferroelectric heterostructures. *J. Appl. Phys.*, 90(11):5708–5712, 2001.

Curriculum Vitae

Name	Evelyn Hollenstein
Date of birth	18th July 1979
Nationality	Swiss

Education

- Since May 2003: Thesis work on "Dielectric and piezoelectric properties of potassium sodium niobate ceramics" under the direction of Dr. D.Damjanovic and Prof. N. Setter (Ceramics laboratory, EPFL).

- 2002-2003: Diploma work on "Properties of high performance piezoelectric crystals for ultrasonic medical imaging probes", under the direction of Dr. D.Damjanovic and Prof. N. Setter (Ceramics laboratory, EPFL).

- 1998-2003: Studies in material sciences at Swiss Federal Institute of Technology in Lausanne (EPFL).

Languages

Bilingual in German and French. Fluent in written and spoken English.

Training courses

2002: 2 months course at Unaxis, Display Division in Palaiseau, France (Characterisation of PECVD deposited films with BHF etching).